COMMUNICATIONS OF THE GEOLOGICAL SURVEY OF NAMIBIA

VOLUME 11
1996

MINISTRY OF MINES AND ENERGY

Front cover: Tight to near isoclinal northeast vergent folds of upper Vendian quartzites and shales (lower Schwarzrand Subgroup) within the uppermost of three stacked thrust sheets on Swartkloofberg in southwestern Namibia. This folding and thrusting reflects Cambrian deformation of the Nama Group foreland basin in the eastern frontal zone of the Gariep Belt (see Saylor and Grotzinger, this volume).

photograph: K.H. Hoffman

MINISTRY OF MINES AND ENERGY

Director: Geological Survey G.I.C. Schneider

COMMUNICATIONS OF THE GEOLOGICAL SURVEY OF NAMIBIA

VOLUME 11
1996

Editor: P. B. Groenewald

Obtainable from the Geological Survey
P.O. Box 2168, Windhoek, Namibia

ISSN 0256-1697

Communs geol. Surv. Namibia, ***11*** *(1996), 1-12*

Reconstruction of important Proterozoic-Cambrian boundary exposures through the recognition of thrust deformation in the Nama Group of southern Namibia

Beverly Z. Saylor[*] and John P. Grotzinger

Department of Earth, Atmospheric and Planetary Sciences, Massachusetts Institute of Technology, Cambridge, MAO2139, USA

[8]present address: Department of Geology and Geophysics, University of Wisconsin, 1215 W. Dayton St., Madison, W153706, USA

Northwest-southeast striking northeast-vergent thrust faults divide the exposures of the Kuibis and Schwarzrand Subgroups along the western margin of the Nama basin in southern Namibia into an autochthon and three allochthonous thrust plates. Broad wavelength basement-involved cross-folds create significant structural relief, exposing deep structural levels where the thrust faults merge and pass into basement. These thrust faults are considered to represent late-stage deformation along the leading edge of the Gariep deformational belt.

The Proterozoic-Cambrian boundary, contained within a major unconformity near the top of the Schwarzrand Subgroup, is exposed in each of three thrust plates in the study area. In the lowermost thrust plate, the unconformity lies above a 500 m thick section of the Spitkopf Member, comprising shelf limestone and siliciclastic rocks. Exposures of the Spitkopf Member in the middle and uppermost thrust plates consist of slope facies, are a maximum of 60 m thick and locally are completely eroded by the overlying Proterozoic-Cambrian boundary unconformity. Exposures of the Spitkopf Member in each of the thrust plates are interpreted as geographically widely separated facies on a slope-to-basin transition which is telescoped by the thrust faults into a relatively small area. The total relief along the top of the Spitkopf Member, more than 500 m, is a combination of depositional thinning across the shelf-to-basin transition and erosional incision along the Proterozoic-Cambrian boundary unconformity.

Introduction

This paper describes structural and stratigraphic relationships involving the Vendian to Cambrian Nama Group on Nord Witputs 22, Swartkloofberg 95 and Swartpunt 74 farms in southwestern Namibia (Fig. 1). Exposures of the Nama Group in this area span the Proterozoic-Cambrian boundary. Although the boundary is contained within a major erosional unconformity, U-Pb zircon geochronology on volcanic ash beds, combined with global correlations based on biostratigraphy and carbonisotope chemostratigraphy indicate that the Vendian part of the section extends to within 1 m.y. of the Cambrian System and contains, near its top, some of the youngest known Ediacaran-type fossils (Fig. 2; Grotzinger *et al.*, 1995). Thus, the stratigraphic succession forms an important Proterozoic-Cambrian boundary reference section.

Exposures of the Nama Group in the study area straddle the eastern margin of the contemporaneous Gariep deformational belt (Davies and Coward, 1982; von Veh, 1988). Compressional structures cross-cut the area, resulting in the repetition of stratigraphic units. Fortuitously, the Proterozoic-Cambrian boundary is repeated in three different thrust plates (Fig. 2) which telescope exposures of spatially separate paleogeographic domains into a relatively small and easily accessible region. Here we report results of stratigraphic and structural studies aimed at reconstructing the original succession across the Proterozoic-Cambrian boundary.

General geology

The Nama Group consists of, in ascending order, the Kuibis, Schwarzrand and Fish River Subgroups (Germs, 1983). It was deposited in a foreland basin that subsided in response to convergence along the Damara and Gariep compressional belts (Germs, 1983; Germs and Gresse, 1991) and is deformed along its northern and western margins by compressional structures related to these belts (Martin, 1965; Martin, 1974; Coward, 1983; Miller, 1983). In southwestern Namibia, mixed siliciclastic and carbonate rocks of the Kuibis and Schwarzrand Subgroups thicken southwestward toward the Gariep belt, reaching their maximum thickness (more than 2000 m) in the study area (Figs. 1 & 2).

The Proterozoic-Cambrian boundary, as recognized on the basis of biostratigraphy and carbon-isotope chemostratigraphy, is contained within a regionally extensive erosional unconformity near the top of the Schwarzrand Subgroup (Grotzinger *et al.*, 1995). Ediacaran-type fossils have been discovered in the study area less than 60 m below the unconformity (Grotzinger *et al.*, 1995). In addition, carbon-isotope data from the same Ediacaran fossil bearing section resemble carbon-isotope profiles from terminal Proterozoic sections in Siberia (Pelechaty *et al.*, 1996), arctic Canada (Narbonne *et al.*, 1994), and other areas, reinforcing the terminal Proterozoic age inferred from the biostratigraphy (Fig. 2; Grotzinger *et al.*, 1995). Since typical latest Proterozoic isotope values extend up to the unconformity, with no evidence of the negative isotope excursion which underlies the boundary in other Proterozoic-Cambrian boundary sections, and since the overlying Nomtsas Formation contains Cambrian trace fossils (Germs, 1983; Grotzinger *et al.*, 1995), the Proterozoic-Cambrian boundary is inferred to be contained within the unconformity.

A U-Pb zircon age of 543.3±1 Ma for a volcanic ash bed located 130 m below the Proterozoic-Cambrian boundary unconformity and 90 m below the Ediacaran-type fossils (Fig. 3) is a maximum for the age of the Proterozoic-Cambrian boundary in the study area

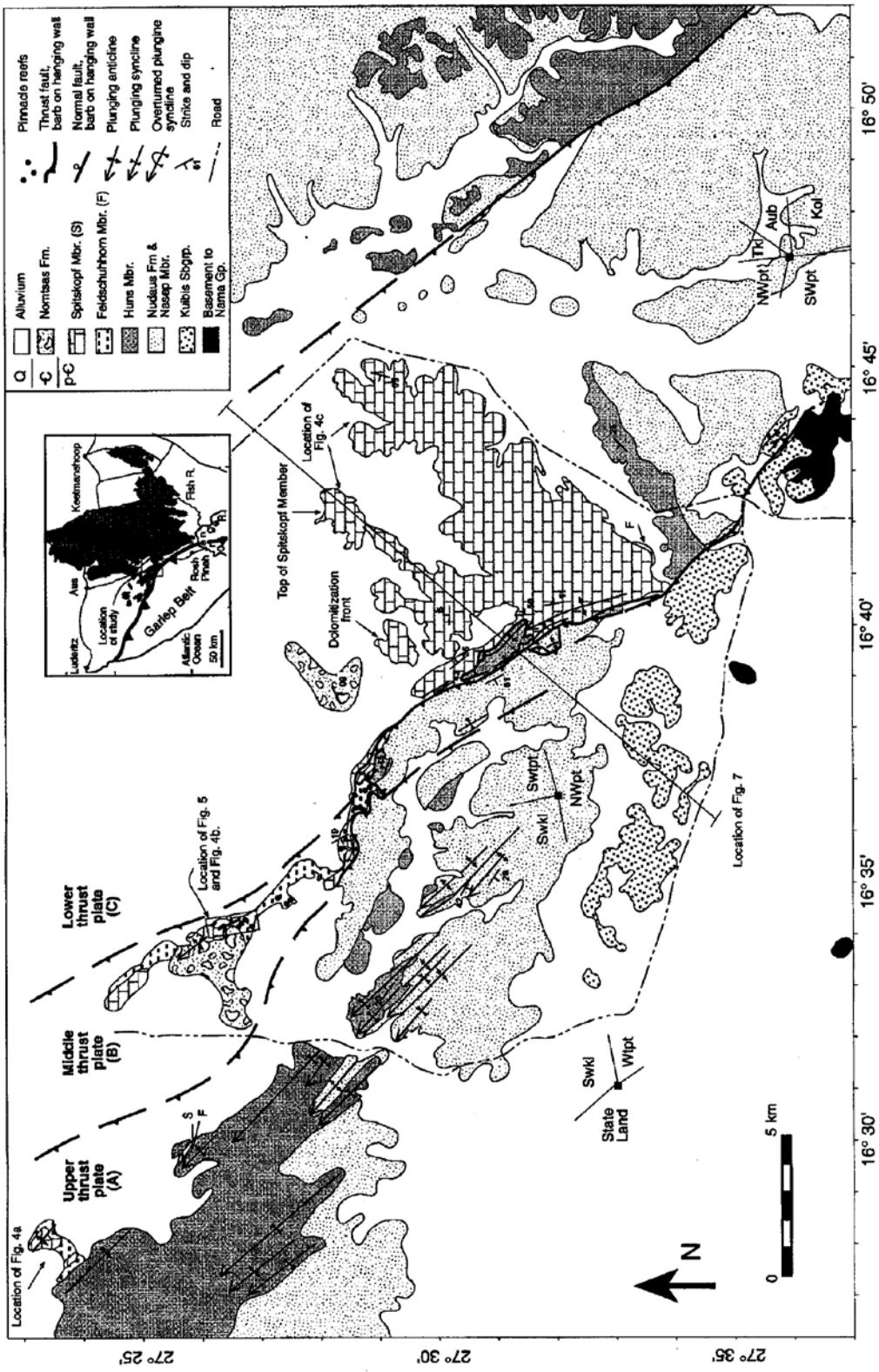

Figure 1: Geological map of the farms Swartkloofberg (Swkl), Swartpunt (Swtpt) and NordWitputs (NWpt). Inset shows location of map area in southwestern Namibia relative to exposures of the Kuibis and Schwarzrand Subgroups (shaded). SWpt: South Witputs; Tkl: Tierkloof; Kol: Kolke

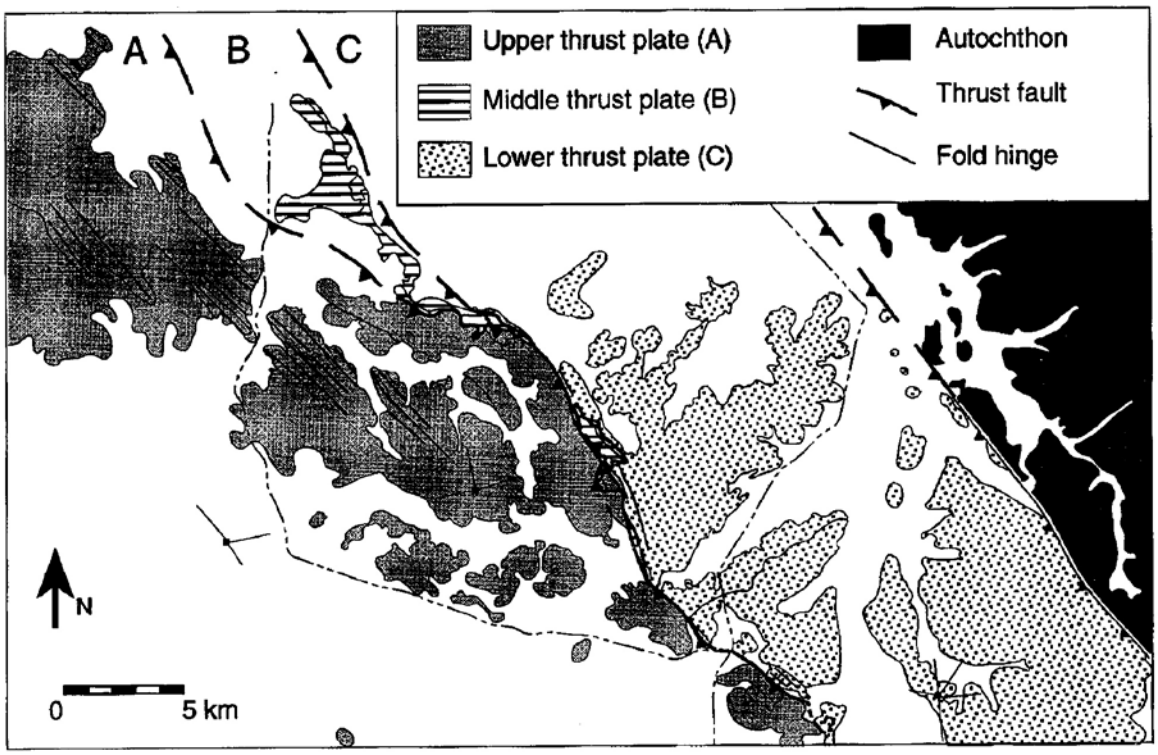

Figure 2: Tectonic map of the study area showing the autochthon and the three thrust plates.

(Grotzinger *et al.*, 1995). This age is the same, within the limits of analytical error, as the age of lower most Cambrian rocks (543.8+5.1/-1.3) in Siberia (Bowring *et al.*, 1993), making the Ediacaran fossils in the study area some of the youngest known representatives of their kind (Grotzinger *et al.*, 1995). An U-Pb zircon age of 538.8 ± 1 Ma for a volcanic ash bed just above the unconformity is a minimum for the age of the Proterozoic-Cambrian boundary in Namibia and constrains the duration of the unconformity to less than 5 m.y. (Grotzinger *et al.*, 1995).

Stratigraphy

The sedimentology and stratigraphy of the Kuibis and Schwarzrand Subgroups have been described and interpreted elsewhere (Germs, 1983; Saylor, 1993; Saylor *et al.*, 1995), and specifics of the stratigraphy in the study area are only briefly described here. This paper focuses on stratigraphic units near the Proterozoic-Cambrian boundary in the study area and how these units change across each of three thrust plates.

Kuibis Subgroup

Exposures of the Kuibis Subgroup are restricted to the southwestern part of the map area where they form part of the lower and upper thrust plates (Fig. 1). The Kuibis Subgroup overlies local outcrops of unnamed stratigraphic units consisting of older diamictite and cream-coloured dolostone, or non-conformably overlies crystalline basement. It is almost 300 m thick and comprises two units of coarse sandstone (Kanies and Kliphoek Members), and two units of dominantly fine-grained carbonate (Mara and Mooifontein Members) (Saylor, 1993; Saylor *et al.* 1995). The siliciclastic dominated units are interpreted to have formed in fluvial to marine margin environments and the carbonate dominated units in shallow subtidal settings (Germs, 1983; Saylor *et al.*, 1995).

Lower Schwarzrand Subgroup

The lower Schwarzrand Subgroup, comprising the Nudaus Formation and the Nasep Member of the Urusis Formation, crops out across much of the map area (Fig. 1). It is 400 m thick and is dominated by siliciclastic mudstone and sandstone, interpreted to have formed in mid-shelf to nearshore and deltaic environments (Germs, 1983; Saylor, 1995). The Nudaus Formation is 150 m thick and consists of sandier-upward parasequences comprising green mudstone with intercalated thin- to medium-bedded sandstone. The upper Nudaus Formation and the lower Nasep Member form a 60 m interval comprising 5 to 20 m-thick units of medium-bedded sandstone, shale and grainstone. The middle 100 m of the Nasep Member consist of green shale, and the upper 60 m consist of cross-bedded and planar lami-

nated, locally slumped, fine sandstone.

Upper Schwarzrand Subgroup

The middle part of the Schwarzrand Subgroup, comprising the Huns, Feldschuhhorn and Spitkopf Members of the Urusis Formation, is interpreted as a carbonate ramp succession (Saylor *et al.*, 1995). It reaches a total thickness in the study area of nearly a kilometre. The Proterozoic-Cambrian boundary unconformity lies at the top of the Spitkopf Member and cuts down section, so that the overlying Cambrian Nomtsas Formation rests on progressively lower strata of the Spitkopf, Feldschuhhorn and Huns Members. The details of this erosional incision and facies and thickness changes in the underlying carbonate platform are pieced together here from structurally and geographically isolated outcrops in each of the three thrust plates.

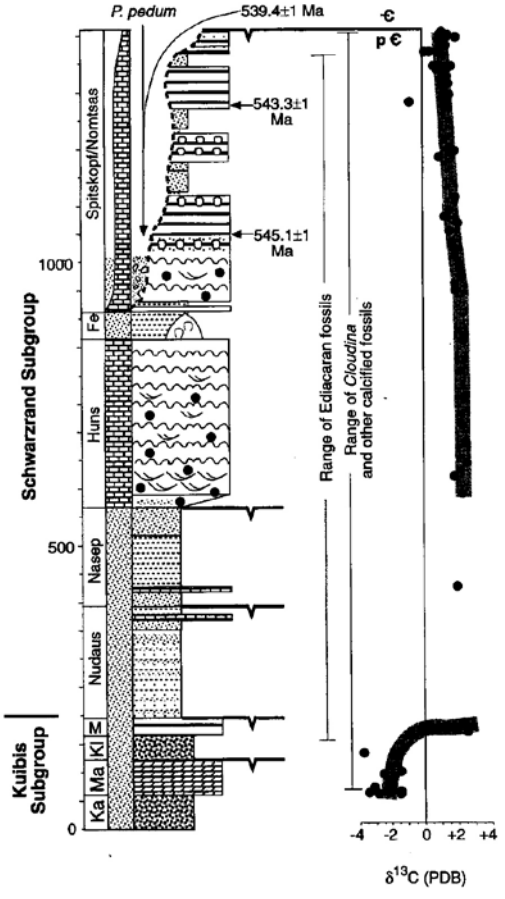

Figure 3: General stratigraphic column for the Kuibis and Schwarzrand Subgroups in the study area showing U-Pb zircon ages and carbon-isotope variations (isotope data from Saylor *et al.* in press; radiometric ages from Grotzinger *et al.*, 1995). See Figure 4 for key. Ka: Kanies Member; Ma: Mara Member; Kl: Kliphoek Member; M: Mooifontein Member.

Huns Member

The Huns Member is a nearly 300 m thick unit consisting predominantly of limestone. The basal 40 m of the Huns Member is recessive, comprising shale with limestone and sandstone interbeds. The remainder consists of metre-scale, upward-shallowing cycles. The few siliciclastic units correlatable across the study area never exceed a few metres in thickness. The carbonate cycles comprise elongate, dolomitized columnar stromatolites overlain by upward-coarsening cross-stratified pellet and intraclast grainstone and commonly are capped by karst-surfaces. They are interpreted to have formed in a high-energy, wave-swept shoal area strongly influenced by high frequency relative sea-level oscillations (Saylor *et al.*, 1995). A unit of pink lime mudstone, with metre high thrombolitic and stromatolitic columns and domes, and intercalated green shale forms the top of the Huns Member. This distinctive unit is recognizable and correlatable across the map area (Fig. 4).

Reefs

Exhumed pinnacle reefs are preserved in the middle thrust plate (Figs. 1, 3 and 4). Initially these reefs were interpreted as part of the Cambrian Nomtsas Formation and were thought to have grown in an erosional valley that incised through the Spitkopf Member (Germs, 1983). However, they lie above light-coloured stromatolitic limestone similar to that at the top of the Huns Member and locally lie below dark, thin-bedded Spitkopf limestone. Consequently, they have been reinterpreted as part of the Huns Member (Figs. 3 & 4; Saylor, 1993; Saylor *et al.*, 1995)

In one location (Fig. 5; see Fig. 1 for location) two pinnacle reefs are enveloped in shale and conglomerate of the Cambrian Nomtsas Formation. They appear to project from a layer of stromatolitic limestone, which itself appears to abut Spitkopf limestone along the steep wall of an incised valley. However, the juxtaposition against the valley wall is not stratigraphic. Instead, it is the result of a small normal fault with only a few metres of offset. The distinctive stromatolitic layer can be recognized on both sides of the normal fault and can be traced laterally in the hanging wall to where it is enveloped in siliciclastic mudstone of the Feldschuhhorn Member and underlies dark limestone of the Spitkopf Member. The surface layer of the pinnacle reefs at this level resembles the stromatolitic layer suggesting that mantling of the lower pinnacles by the stromatolitic layer can account for what appears to be two different reef horizons. Much like their present exposure, the reefs most likely formed resistant structures that were exhumed from surrounding shale during canyon incision. The reefs were covered again with conglomerate as the canyon filled with Nomtsas Formation.

In summary, nowhere do the stratigraphic relationships require that any of the pinnacle reefs lie within the Nomtsas Formation (Saylor *et al.*, 1995). In contrast, they are all considered to have developed from a single

horizon at the top of the Huns Member during a period of reduced carbonate production following flooding and drowning of the platform.

Feldschuhhorn Member

The Feldschuhhorn Member is a 60 m thick green-shale unit. It stratigraphically overlies and envelopes the pink stromatolitic limestone and pinnacle reefs at the top of the Huns Member (Figs. 1, 3, 5). Locally developed, light-coloured stromatolitic limestone is interpreted above to mantle the pinnacle reefs. The upper part of the Feldschuhhorn Member contains interbedded sandstone and grades upward into black, fine-grained limestone of the Spitkopf Member.

Spitkopf Member

The Spitkopf Member in the lower thrust plate has not previously been described in any detail. It is 500 m thick (Fig. 4c) and consists of alternating carbonate and siliciclastic units, each of which is several tens to one hundred or more metres thick. The lower carbonate units consist largely of metre-scale, karst-capped cycles, which, similar to cycles of the Huns Member, are interpreted to have formed in a high-energy wave-swept environment. Higher carbonate units consist of thin-bedded, fine-grained limestone with local development of thrombolitic and stromatolitic domes and the upper carbonate units consist almost entirely of thick-laminated to thin-bedded limestone with rare beds of flat-pebble, intraclast breccia, commonly with mounded tops. With the exception of intraclast breccias, which are interpreted to have formed during occasional storms, which ripped-up and reworked the thinbedded limestone (e.g. Sepkoski, 1982), higher carbonate units show little evidence for the influence of strong waves or currents. They resemble Cambrian "ribbon-rock" and are similarly interpreted to have formed in low-energy, shallow- to deeper-subtidal environments on a carbonate ramp (Demicco, 1983; Cowan and James, 1993). Thick siliciclastic units form coarsening-upward successions, each with green mudstone at the base followed by ripple-laminated or thick-bedded, planar-laminated and hummocky cross-stratified very fine to fine sandstone at the top. These siliciclastic facies are interpreted to have been deposited in outer- to mid-shelf environments.

The Spitkopf Member in the middle and upper thrust plates (Figs 4a, b) is less than 60 m thick. It consists of fine-grained, black, thick-laminated to thin-bedded limestone, breccia and shale. The breccia beds are composed of platy clasts that resemble the surrounding limestone. Breccias range from incipient fracture zones, to fully-developed, matrix-supported, disorganized debrites. The relative proportion of breccia, particularly debrites, and shale increases westward. These sections of the Spitkopf Formation resemble the Cow Head Formation of Newfoundland (e.g. James and Mountjoy, 1983) and are interpreted to have formed by slope failure and mass-wasting on a carbonate slope.

The combination of ramp- and slope-type facies that constitutes the Spitkopf Member is characteristic of distally steepened ramps (Read, 1985). Exposures of the Spitkopf Member in the study area are interpreted as representative sections along a ramp to basin transition, extending from outer ramp to slope positions (e.g. James and Mountjoy, 1983), which have been structurally telescoped into a relatively small area.

Nomtsas Formation

Exposures of the Nomtsas Formation are restricted to the northern part of the map area. They overlie and form the fill of erosional canyons incised through the Spitkopf Member.

Outcrops of this Formation in the lower thrust plate are inferred to overlie the Spitkopf Member, but the contact is covered. Exposures of the stratigraphically underlying Spitkopf Member near the covered zone are dolomitized and brecciated. The dolomitization and brecciation are local features, however, and this horizon can be traced laterally to undeformed limestone approximately 120 m below the top of the SpitkopfMember (see Fig. 1). It is unclear whether the Nomtsas Formation lies directly on this dolomitized horizon, or if the remaining 120 m of the section are buried beneath intervening Quaternary alluvium. However, based on the similarity of this horizon to a dolomitized and brecciated unit which directly underlies exposures of the Nomtsas Formation in the middle thrust plate, we suggest that it may correspond to the Spitkopf-Nomtsas contact and that the basal erosion surface of the Nomtsas Formation in the lower thrust plate may have cut down into as much as 120 m of the Spitkopf Member (Fig. 4c).

In the middle structural unit, the Nomtsas Formation overlies a 60 m thick section of the Spitkopf Member and locally the basal erosion surface has cut entirely through the Member down to the level of pinnacle reefs at the top of the Huns Member (Fig. 4b). Stromatolitic and thrombolitic carbonate at the top of the Spitkopf exposures and immediately underlying the Nomtsas Formation is dolomitized and characterized by extensive development of fitted breccias.

Nomtsas rocks in the middle and upper thrust plate are lithologically and stratigraphically similar comprising matrix- and clast-supported conglomerate, overlain by shale-rich diamictite, followed by clast-free mudstone with interbedded sandstone. Disorganized and locally inverse-stratified boulder and pebble conglomerate in a sandy matrix and shale-rich diamictite with outsized clasts as large as 3 m across are interpreted to have formed by debris-flow and slump processes (Saylor, 1993; Saylor *et al.*, 1995). Conglomerate clasts, which include limestone, dolostone, sandstone and volcanic ash, are lithologically similar to stratigraphically lower units and are interpreted as debris shed from the flanks of incised valleys (Saylor, 1993; Saylor *et al.*, 1995). Clasts similar to the dolomitized unconformity

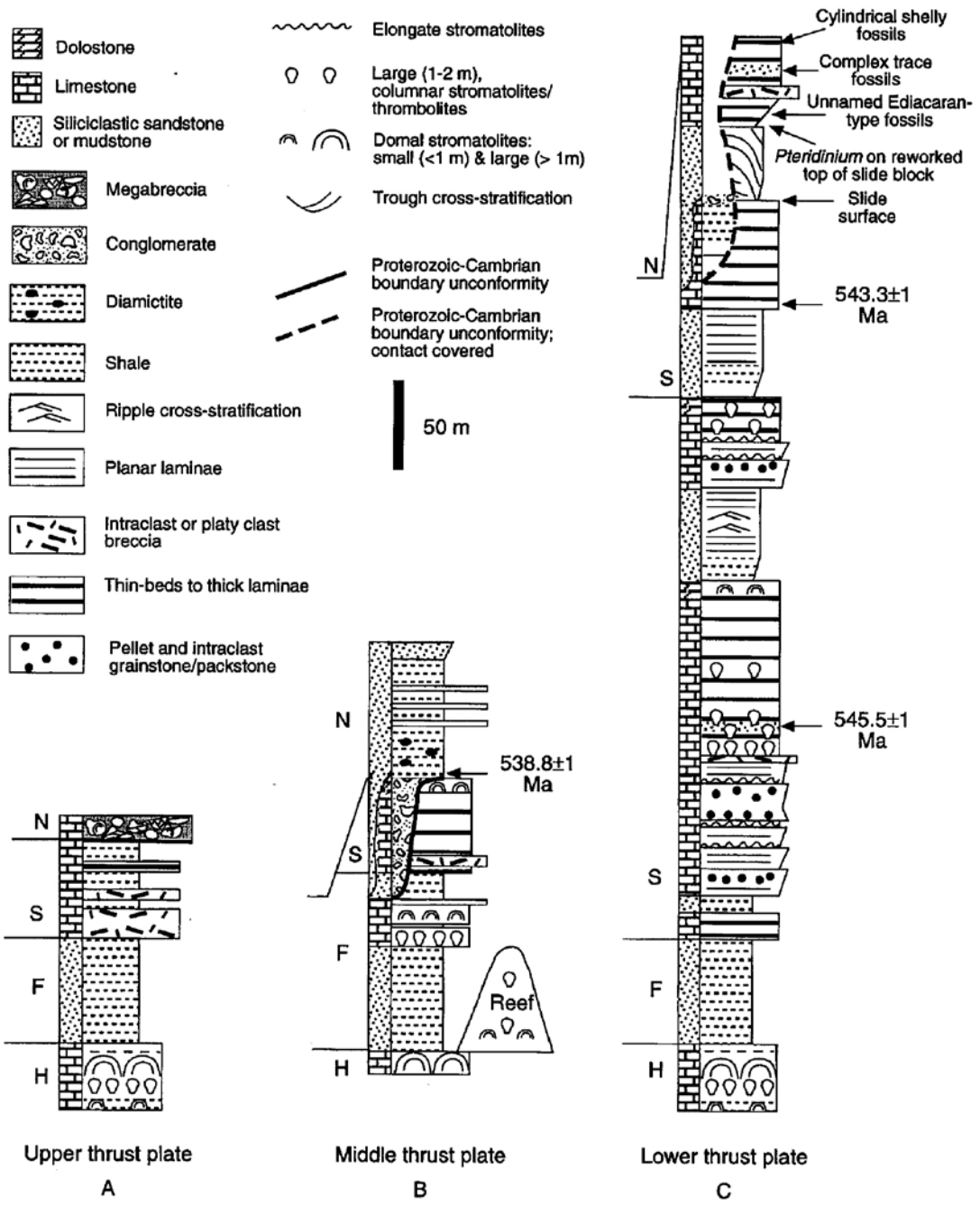

Figure 4: Measured sections from the top of the Huns Member (a distinctive pink stromatolitic unit) up to the Nomtsas Formation for the lower, middle and upper thust plates. See Fig. 1 for locations of sections. H: Huns Member; F: Feldschuhhorn Member; S: Spitkopf Member: N: Nomtsas Formation.

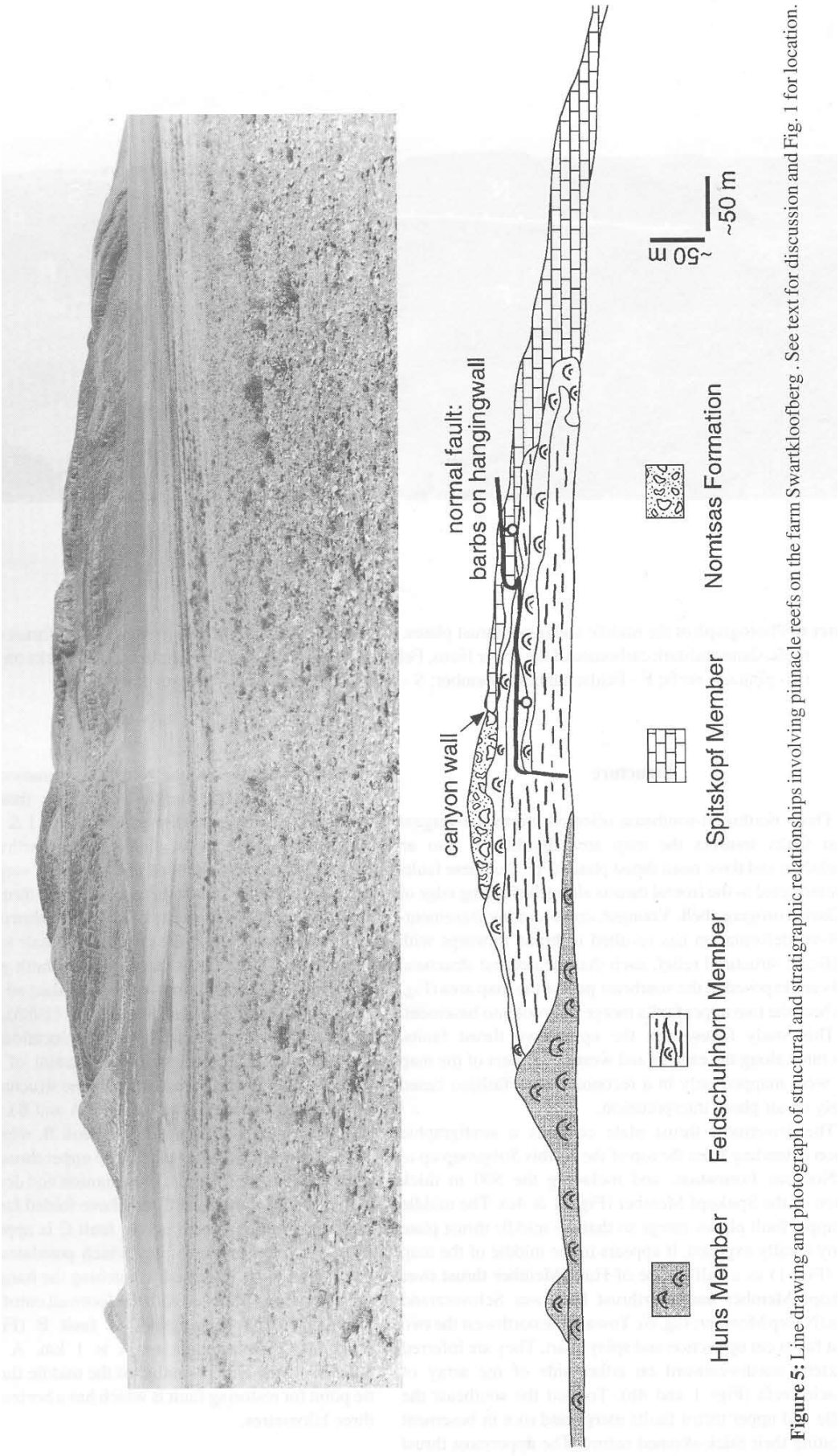

Figure 5: Line drawing and photograph of structural and stratigraphic relationships involving pinnacle reefs on the farm Swartkloofberg . See text for discussion and Fig. 1 for location.

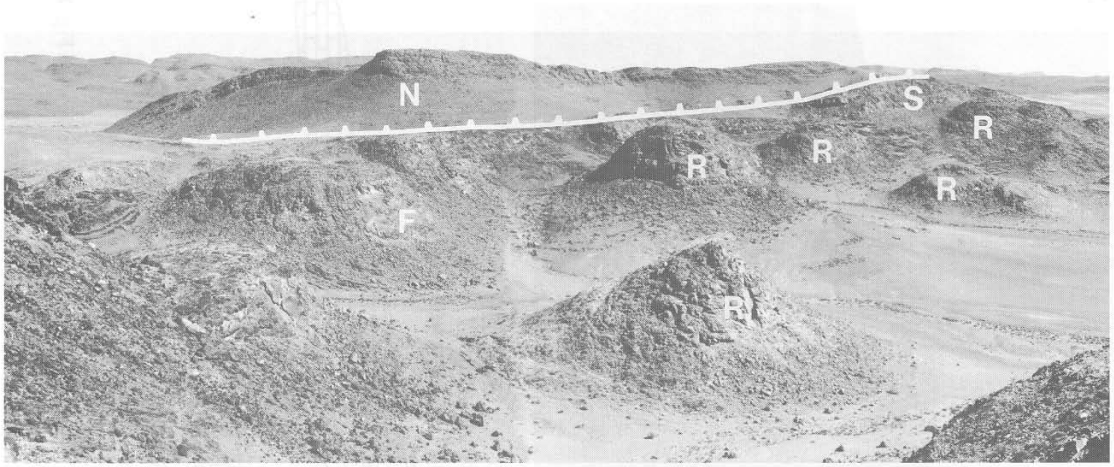

Figure 6: Photograph of the middle and upper thrust plates. Siliciclastic rocks of the Nasep Member are thrust over pinnacle reefs, shale and dark carbonate of the upper Huns, Feldschuhhorn and Spitskop Members. Tick marks on hangingwall. (R - pinnacle reefs; F - Feldschuhhorn Member; S - Spitskop Member; N - Nudaus Formation)

surface may indicate that dolomitization preceded valley infilling.

In the western part of the map area the surface corresponding to the sub-Nomtsas unconformity may be represented by an abrupt change in conglomerate facies from SpitkopfMember slope breccia, composed of platey clasts of deep water slope-facies limestone, to megabreccia with large (up to 3 m) boulders of stromatolitic, thrombolitic and massive fine-grained dolostone and limestone similar to the more shallow-water ramp facies (Fig. 4a). Slope breccias on distally steepened ramps such as the Spitkopf Member generally consist entirely of deep-water clasts (James and Mountjoy, 1983). Thus, although the megabreccia has no sand in the matrix and differs from other exposures of the Nomtsas Formation conglomerate, the change to more shallow-water clasts probably records shelf-edge exposure and erosion (e.g. Hiscott and James, 1984) during relative sea-level fall and the initial development of the up-dip, sub-Nomtsas unconformity.

Structure

Three northwest-southeast oriented, northeast - vergent thrust faults transect the map area dividing it into an autochthon and three main thrust plates (Fig. 2). These faults are interpreted as the frontal thrusts along the leading edge of the Gariep orogenic belt. Younger, cross-cutting, basement-involved deformation has resulted in broad upwarps with significant structural relief, such that the deepest structural levels are exposed in the southeast part of the map area (Fig. 1), where the two upper faults merge and root into basement.

This study focuses on the upper two thrust faults. Structures along the eastern and western borders of the map area were mapped only in a reconnaissance fashion based largely on air photo interpretation.

The lower most thrust plate contains a stratigraphic section extending from the top of the Kuibis Subgroup up to the Nomtsas Formation, and including the 500 m thick section of the Spitkopf Member (Figs. 1 & 4c). The middle and upper fault planes merge so that the middle thrust plate is only locally exposed. It appears in the middle of the map area (Fig. 1) as a half-klippe of Huns Member thrust over Spitkopf Member and overthrust by lower Schwarzrand rocks (Nasep Member; Fig. 6). Toward the northwest the two thrust faults cut up section and splay apart. They are inferred to extend northwestward on either side of the array of pinnacle reefs (Figs. 1 and 4b). Toward the southeast the middle and upper thrust faults merge and root in basement indicating their thick-skinned nature. The uppermost thrust plate contains a complete stratigraphic section extending from basement up into the Nomtsas Formation (Fig. 4a).

Rocks in the middle and upper thrust plate are deformed by numerous linked folds (Figs. 1 & 2). The folds parallel the thrust faults, plunge to the northwest, and are generally open, but inclined and northeast-vergent. Locally the folds are isoclinal or are cut by minor thrust faults with displacement of a few metres. The middle thrust fault itself is folded. Deformation in the lower thrust plate is less intense. Near the bounding faults there are a few fault-parallel folds.

Figure 7 shows a cross-section, balanced according to the principles of explained by Suppe (1983), through the middle of the map area (see figure 1 for location). This cross-section meets the stratigraphic constraint of

successively more distal exposures westward and the structural constraint of merging, basement rooted faults (A and B).

The oldest fault in the area is fault B, which forms the base of the middle thrust plate. The upper thrust plate lies in a splay (fault A) of fault B. Later motion and development of a thrust ramp along fault C may have folded faults A and B. Horizontal displacement across fault C is approximately 1 km. Since fault A is a splay which postdates fault B, the offset along A is restored by matching the hanging wall cut-off of the Huns Member with the footwall cutoff of the Huns Member in the hanging wall of fault B (Fig. 7b). The horizontal displacement on A is 1 km. A hanging wall anticline in the Huns Member of the middle thrust plate is a tie point for restoring fault B which has a horizontal offset of three kilometres.

Paleogeographic restoration

The stratigraphic succession from the Kuibis Subgroup up through the Huns Member of the Schwarzrand Subgroup shows little change across the three thrust plates. Thicknesses remain approximately the same and distinct beds and marker horizons can be recognized across the map area. The SpitkopfMember, however, changes significantly. In the lower thrust plate it is 500 m thick, but in the middle and upper thrust plates it is 0 to 60 m thick. In the lower thrust plate the Spitkopf Member consists of outer ramp limestone and deltaic sandstone, and in the upper two thrust plates it consists of deeper-water limestone, breccia and shale on a distally steepened ramp.

These substantial differences are not the result of modern erosion patterns because in all thrust plates contacts with the underlying Feldschuhhorn Member and the overlying Nomtsas Formation are preserved. Instead, these differences reflect some combination of stratigraphic thinning and facies change, across the distal ramp and erosional truncation on a basin ward-dipping unconformity beneath the Nomtsas Formation (Fig. 8). The pattern of erosional modification of original depositional relief is similar to relationships described from the shelf margin of the Permian Grayburg Formation in west Texas (Franseen, 1989).

The total amount of relief along the top of the Spitkopf Member, 500 m over a palinspastically restored distance of 8 km, is similar in scale to, although somewhat greater than the relief across the Grayburg shelf margin (350 mover 4.5 km). Over a distance of 5 km in the lower thrust plate there may be as much as 130 m of erosional incision on the sub-Nomtsas unconformity. In the middle thrust plate, there is at least 60 m of incision expressed by the steep walls of the unconformity surface (Fig. 4 b, c). Consequently, the remaining 310m of relief must be accounted for over the distance (3 km) represented by the horizontal displacement of the lower thrust fault.

There is essentially no depositional thinning in the upper thrust plate and most of the shelf-to-basin tran-

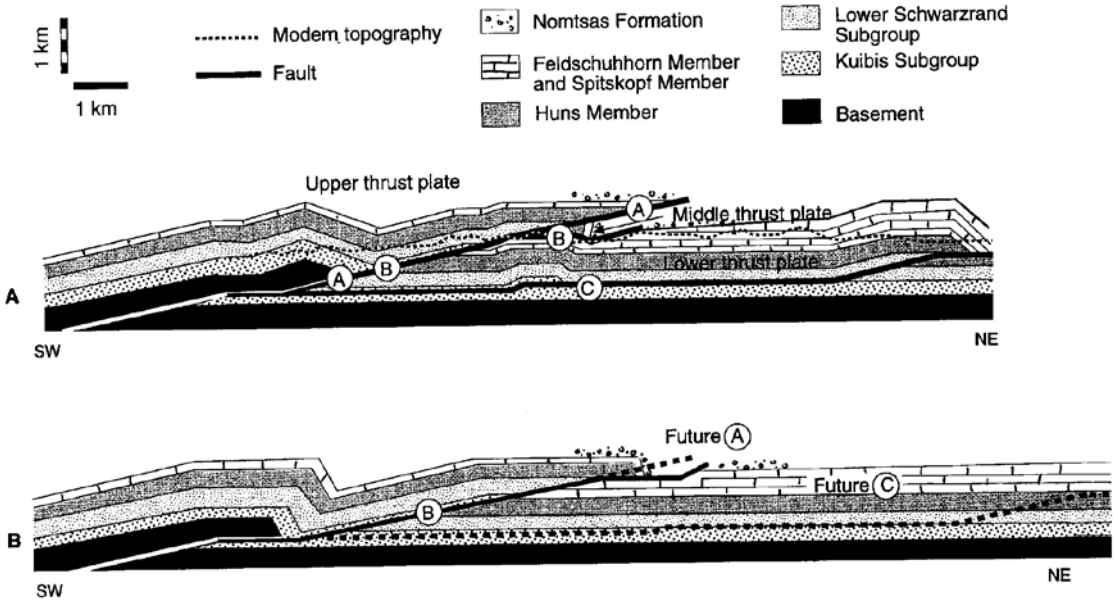

Figure 7: a. Cross-section showing the lower, middle and upper thrust plates. Location of cross-section shown in figure 1. **b.** Partially restored cross-section showing geometry prior to movement along fault C and splay A. Note that the lower Schwarzrand Subgroup includes the Nudaus Formation and the Nasep Member.

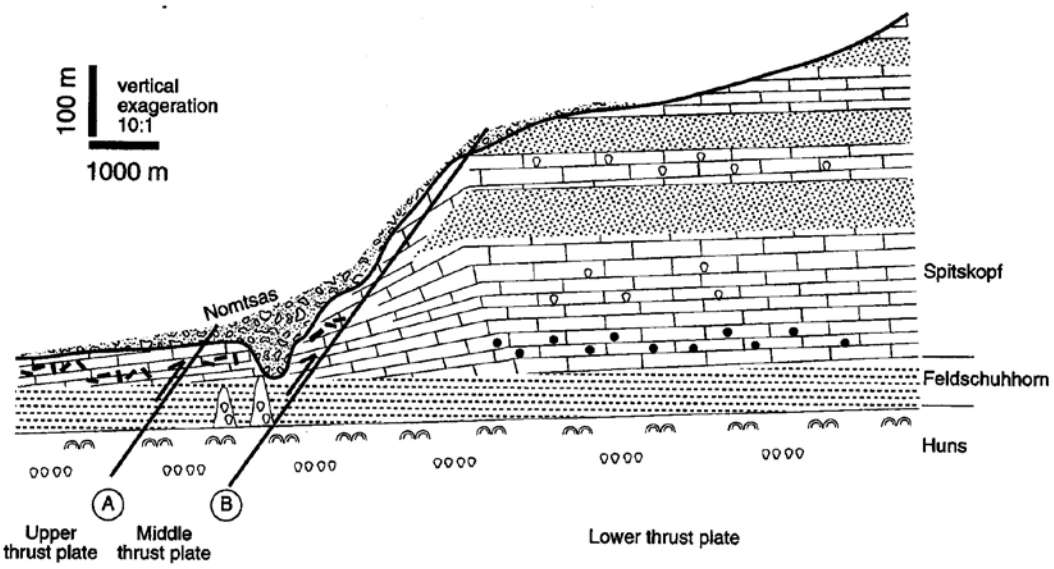

Figure 8: Schematic cross-section through the shelf-to-basin transition of the Spitskopf Member. The total relief along the Precambrian-Cambrian boundary, which is shown by the thick, solid line, is a combination of depositional thinning and erosional truncation of a distally steepened ramp Key in Fig. 1.

sition has been cut out along the middle thrust fault. Since no marker horizons in the Spitkopf Member can be correlated across this fault, the proportion of the 310m of relief which is represented by pre-erosion depositional thinning across the shelf-to-basin transition is unknown. The calculated depositional slope for the maximum possible amount of depositional thinning, (310 m across the palinspastically restored distance of 3.5) is 6°. Although somewhat high, 6° is reasonable for the distally steepened part of a ramp and is consistent with the abundance of breccias in the slope sections (Read, 1985). The original depositional profile may have been much less steeply inclined, however, because slopes of only 2° are sufficient to cause slope failure. Since erosional incision affected both ramp exposures in the lower thrust plate and slope exposures in the middle thrust plate, incision and the relief along the erosional escarpment probably modified the depositional ramp profile substantially.

It is uncertain whether the erosional relief across the distally steepend ramp developed everywhere by sub-aerial exposure and fluvial incision or, if, like the Grayburg escarpment, some parts, particularly those down-dip, developed by submarine erosion and mass wasting. The unconformity surface is recognized 100 km east (cratonward) of the study area where it is associated with incised canyons a few tens of metres deep. There, the canyons are partially infilled by planar-stratified conglomerate and trough cross-stratified sandstone (unpublished data), facies which record strong current influence. The great lateral extent of erosional topography developed along this unconformity surface and the evidence for strong currents are hard to account for by mass wasting in an exclusively sub-marine environment, so the more proximal canyons are tentatively interpreted to have formed by fluvial incision. A striking similarity between facies of the Nomtsas Formation in each of the thrust plates, with no apparent change in environment, is suggestive of deposition during diachronous transgression and back -filling of the escarpment, following a large relative sea-level drop. The coarse conglomerate and diamictite facies consists of debris derived from the escarpment and deposited by sediment gravity flows, probably in a deeper marine environment consistent with the preceding slope setting. Fine conglomerate and sandstone facies may have been introduced by mass wasting of facies derived from up-slope estuarine environments (Saylor *et al.*, 1995). Dolomitization fronts and mantling breccias associated with the unconformity in both the lower and middle thrust plates in the study area may have been formed by mixing of meteoric and marine waters following exposure and karst weathering (e.g. Badiozamani, 1973; James and Choquette, 1987), but may also have been formed much later by fluids that travelled through the porous Nomtsas Formation (e.g. Mussman *et al.*, 1987). Support for early (pre-Nomtsas) dolomitization is provided by the presence of dolomitized clasts within the Nomtsas Formation.

The Proterozoic-Cambrian boundary unconformity is therefore interpreted to record a major fall in relative sealevel. A minimum estimate for drop in relative sea-

level is a few tens of metres, sufficient to expose and incise up-dip portions of the unconformity. If dolomitization along down-dip exposures of the unconformity surface is related to karst processes, relative sea-level fall might have been 500 m or more.

The Nama basin was a tectonically active foreland basin (Germs, 1983) and tectonic uplift associated with thrust deformation may have been an important factor in the development of the erosional unconformity. Stratigraphic patterns throughout the Schwarzrand Subgroup, including westward-thickening stratigraphic units and eastward downcutting erosional unconformities, indicate tectonically driven flexural subsidence of the western part of the basin and slower subsidence and episodic uplift of the eastern part of the basin (Germs and Gresse, 1991; Gresse and Germs, 1993; Saylor *et al.*, 1995). Certainly erosion along the eastern extent of the Proterozoic-Cambrian boundary unconformity surface may be related to uplift of a flexural bulge (Germs and Gresse, 1991). Evidence for rapid subsidence of the western part of the basin, however, indicates that it lies in front of the bulge and that development of the unconformity in the study area cannot be explained by bulge uplift. The coincident development of an erosional unconformity in both the rapidly subsiding western part of the basin and the slowly subsiding eastern part of the basin may best be explained by a eustatic sea-level fall. The recognition of approximately coeval unconformities at the Proterozoic-Cambrian boundary in Siberia (Pelechaty *et al.*, 1996), Canada (Narbonne *et al.*, 1994) and the western United States (Cooper and Fedo, 1995) demonstrates the global nature of this unconformity and provides additional evidence that the sea-level fall may be eustatic in nature (Runnegar *et al.*, 1995).

Conclusions

1) Northwest-southeast striking thrust faults divide exposures of the Kuibis and Schwarzrand Subgroups on the farms Swartkloofberg, Swartpunt, Nord Witputs, Tierkloof and Aub into an autochthon and three thrust plates. The thrust faults root into base-ment and are interpreted as the leading edge of the Gariep deformational belt. The Proterozoic-Cambrian boundary, contained within a major unconformity in the upper part of the Schwarzrand Subgroup, is exposed in each of the thrust plates.
2) The lower thrust plate contains a nearly complete stratigraphic section extending from the top of the Kuibis Subgroup up to the Cambrian Nomtsas Formation at the top of the Schwarzrand Subgroup. The unconformity at the base of the Nomtsas formation lies above a 500 m thick section of the Spitkopf Member and has erosional relief of more than 130 m.
3) The middle thrust plate contains only the middle and upper part of the Schwarzrand Subgroup. Pinnacle reefs are restricted to the middle thrust plate. The reefs lie structurally above the upper Spitkopf Member and were originally misinterpreted as part of the Nomtsas Formation, but have been reinterpreted to lie stratigraphically at the top of the Huns Member. Exposures of the Spitkopf Member above the pinnacle reefs in the middle structural level are a maximum of 60m thick and locally the Proterozoic-Cambrian unconformity cuts down to the level of the reefs.
4) The upper thrust plate contains a complete section from basement up to conglomerate thought to correlate with the sub-Nomtsas unconformity. The SpitkopfMember is a maximum of 60 m thick and consists of toe of slope facies.
5) The character of the SpitkopfMember changes across the structural levels from distal ramp to slope facies. These facies formed along a ramp-to-basin transition which was dissected by thrust faults and telescoped into a relatively small area. The total relief along the Proterozoic-Cambrian unconformity, more than 500 m, is a combination of depositional thinning and erosional incision across this transition.
6) The Proterozoic-Cambrian boundary unconformity in Namibia developed during a major fall in relative sealevel. Development of significant erosional topography along the down-dip exposures of the unconformity surface, well in front of the flexural bulge, may be explained best by a eustatic sea-level fall. This interpretation is strongly supported by Runnegar *et al.*'s (1995) suggestion that approximately coeval falls in relative sea-level in Siberia, Canada and the western United States indicate a eustatic sea level event at this time.

Acknowledgements

This research was supported by NSF grants EAR 9205479 and EAR-9058199, the Geological Survey of Namibia and Geological Society of America student grants awarded to BZS. We thank M. Coyne, A. Fitzgerald, A. Khetani, P. Myrow, B. Smith, J. Southard, F. Urban, F. Vandenbergh and members of the IGCP 220 field trip to Namibia for assistance and lively discussions in the field. We thank K. Hodges for instruction on balancing cross-sections and P. Gresse and K.H. Hoffmann for thorough reviews of the manuscript.

References

Badiozamani, K. 1973. The Dorag dolomitization model - application to the Middle Ordovician of Wisconsin. *J. sedim. Petrol.*, 43, 965-984.

Bowring, S. A., Grotzinger, J.P., Isachsen, C.E., Knoll, A.H., Pelechaty, S.M. and Kolosov, P. 1993. Calibrating rates of Early Cambrian evolution. *Science*,

261, 1293-1298.

Cooper, J.D. and Fedo, C.M. 1995. Base of the Sauk sequence in the southern Great Basin and eastern Mojave desert. *Geol. Soc. Am., Abstracts with Programs*, **27**, A-331.

Cowan, C.A. and James, N.P. 1993. The interactions of sealevel change, terrigenous-sediment influx and carbonate productivity as controls on Upper Cambrian Grand Cycles of western Newfoundland, Canada. *Bull. geol. Soc. Am*., **105**, 1576-1590.

Coward, M.P. 1983. The tectonic history of the Damara belt, *In*: R. McG. Miller (ed.) *Evolution of the Damara Orogen of South West Africa/Namibia*. Spec. Publ. geol. Soc. S. Afr., **11**, 409-423.

Davies, C.J. and Coward, M.P. 1982. The structural evolution of the Gariep Arc in southern Namibia (South-West Africa). *Precambr. Res.*, **17**, 173-198.

Demicco, R.V. 1983. Wavy and lenticular-bedded carbonate ribbon rocks of the upper Cambrian Conococheague Limestone, central Appalachians. *J. sedim. Petrol.*, **53**, 1121-1132.

Franseen, E.K. 1989. Evolution and destruction of carbonate bank at the shelf margin: Grayburg Formation (Permian), western escarpment, Guadalupe Mountains, Texas. *In*: P.D., Crevello, J.L., Wilson, J.F., Sarg and J.F., Read (eds.) *Controls on carbonate platform and basin development*, 289-304.

Germs, G.J.B. 1983. Implications of a sedimentary facies and depositional environmental analysis of the Nama Group in South West Africa/Namibia. *In*: R.McG. Miller (ed.), *Evolution of the Damara Orogen of South West Africa/Namibia*, Spec. Publ. Geol. Soc. S. Afr., **11**, 89-114.

Germs, G.J.B. and Gresse, P.G. 1991. The foreland basin of the Damara and Gariep orogens in Namaqualand and southern Namibia: stratigraphic correlations and basin dynamics. *S. Afr. J. Geol.*, **94**, 159-169.

Gresse, P.G. and Germs, G.J.B. 1993. The Nama foreland basin; sedimentation, major unconformity bounded sequences and multisided active margin advance. *Precambr. Res.*, **63**, 247-272.

Grotzinger, J.P., Bowring, S.A., Saylor, B.Z. and Kaufman, A.J. 1995. Biostratigraphic and geochronologic constraints on early animal evolution. *Science*, **270**, 598-604.

Hiscott, R.N. and James, N.P. 1984. Carbonate debris flows, Cow Head Group, western Newfoundland. *J. sedim. Petrol.*, **55**, 735-745.

James, N.P. and Choquette, P.W. 1987. *Paleokarst*. Berlin: Springer-Verlag, 416 p.

James, N.P. and Mountjoy, E.W. 1983. Shelf-slope break in fossil carbonate platforms: an overview. *In*: D.J. Stanley and G.T. Moore (eds.), *The Shelf Break: Critical Interface on Continental Margins*. Soc. Econ. Paleont. Mineral., Spec. Pub., **33**, 189-206.

Martin, H. 1965. *The Precambrian geology of South West Africa and Namaqualand*. Precambr. Res. Unit, Univ. Cape Town, 159 pp.

Martin, H. 1974. Damara rocks as nappes on the Naukluft Mountains, South West Africa. *Bull. Precamb. Res. Unit, Univ. Cape Town*, **15**, 153-165.

Miller, R.McG. 1983. The Pan-African Damara Orogen of South West Africa/Namibia. *In*: R.McG. Miller (ed.) *Evolution of the Damara Orogen of South West Africa/Namibia*. Spec. Publ. Geol. Soc. S. Afr., **11**, 431-515.

Mussman, W.J., Montanez, I.P. and Read, J.F. 1987. Ordovician Knox paleokarst unconformity, Appalachians. *In*: N.P. James and P.W. Choquette (eds.) *Paleokarst*. Berlin: Springer-Verlag, 211-228.

Narbonne, G.M., Kaufman, A.J. and Knoll, A.H. 1994. Integrated chemostratigraphy and biostratigraphy of the Windermere Supergroup, northwestern Canada: implications for Proterozoic correlations and the early evolution of animals. *Bull. geol. Soc. Am*., **106**, 1281-1292.

Pelechaty, S.M., Grotzinger, J.P. and Kaufman, A.J. 1996. Evaluation of $\partial^{13}C$ chemostratigraphy for intrabasinal correlation: Vendian strata of northeast iberia. *Bull. geol. Soc. Am*., **108**, 992-1003.

Read, J.F. 1985. Carbonate platform models. *Am. Ass. Petrol. Geol.*, **69**, 1-21.

Runnegar, B., Gehling, J.G., Horodyski, R.J., Jensen, S. and Knauth, L.P. 1995. Base of the Sauk sequence is a global eustatic event that lies just above the Precambrian-Cambrian boundary. *Geol. Soc. Am., Abstracts with Progams*, **270**, A-330.

Saylor, B.Z. 1993. Progress report on the sedimentology and stratigraphy of Kuibis and Schwarzrand Subgroups, Witputs area, southwestern Namibia. *Communs. geol. Surv. Namibia*, **8**, 127-135.

Saylor, B.Z., Grotzinger, J.P., Germs, G.J.B. 1995. Sequence stratigraphy and sedimentology of the Neoproterozoic Kuibis and Schwarzrand Subgroups (Nama Group), southwestern Namibia. *Precambr. Res.*, **73**, 153-171.

Sepkoski, J.J. 1982. Flat pebble conglomerates, storm deposits and the Cambrian bottom fauna. *In*: G. Einsele and A. Seilacher (eds.), *Cyclic and Event Stratification*. Berlin: Springer-Verlag, 371-385.

Suppe, J. 1983. Geometry and kinematics of fault-bend folding. *Am. J. Sci.*, **283**, 684-721.

von Veh, M.W. 1988. *The stratigraphic and structural evolution of the Late Proterozoic Gariep Belt in the Sendelingsdrif-Annisfontein area, northwestern Cape Province*. Ph.D. thesis (unpublished), Univ. Cape Town, 174 pp.

Communs geol. Surv. Namibia, ***11*** *(1996), 13-21*

Alkaline rocks in the Kuboos-Bremen Igneous Province, southern Namibia: the Grootpenseiland and Marinkas Kwela Complexes

R.H. Smithies and J.S. Marsh
Department of Geology, Rhodes University, Grahamstown, 6140, South Africa

The early Cambrian Kuboos-Bremen Igneous Province, of northwestern South Africa and southern Namibia, comprises a series of intrusive bodies that collectively encompass virtually the entire range of alkaline rock types. Two of these bodies, the Grootpenseiland and Marinkas Kwela Complexes, lie immediately north of the Orange River and are amongst the few that show this wide lithological range on a local scale. The rocks of both complexes are overwhelmingly felsic in composition. The oldest are nepheline-bearing syenites, which form the southwestern most intrusive phases. The sequence of intrusion in both complexes is to the northeast and to more siliceous rocks. Large granitic stocks form the youngest and most northeasterly intrusive phases. The same lithological range and intrusive sequence also occurs at Kanabeam, approximately 5 km to the northeast of Marinkas Kwela, indicating a close commonality in the origin and geological evolution of complexes in that region.

Introduction

First described by Söhnge and de Villiers (1948), the Kuboos-Bremen Igneous Province consists of a number of discrete intrusive complexes which are located with a remarkably high degree of linearity (Fig. 1). The province extends in a north-easterly direction for at least 270 km from the western Richtersveld region of South Africa to the Great Karas Mountains in southern Namibia. Equally remarkable is the range of igneous rock types that the province incorporates. Rocks of felsic composition predominate; mafic rocks comprise less than about 5% of the province and include medium- to coarse-grained gabbroic rocks found as xenoliths within later felsic rocks. Granites and Si-oversaturated syenites dominate to the southwest, forming the Swartbank, Kuboos and Tatasberg plutons. Si-undersaturated rocks, including nepheline-(sodalite) syenite and phonolite, become proportionally more important to the northeast. Carbonatite occurs approximately 20 km northeast of the Orange River, forming the Marinkas Kwela Carbonatite Complex. Radiometric age determinations show the province to be the result of Pan African magmatism, active in that region between at least 514 Ma and 529 Ma (Allsopp *et al.*, 1979; Smithies, 1992).

Intrusive phases of the Kuboos-Bremen Igneous Province were emplaced into a wide range of Precambrian crustal elements. From southwest to northeast these include the sediments of the Gariep Group and, respectively, calc-alkaline igneous rocks and gneisses of the Richtersveld and Gordonia Subprovinces of the Namaqua Metamorphic Province. Sporadically outcropping throughout the region, the Nama Group is a platform sequence that is partly complementary to the Gariep Group and lies unconformably on the rocks of the Namaqua Metamorphic Province.

Some aspects of the geology of the Kuboos-Bremen Igneous Province have been covered in regional studies by Söhnge and de Villiers (1948), Kröner (1975), Kröner and Blignault (1976) and Blignault (1977). Only two of the complexes, however, have so far received detailed attention in the literature - the Younger Bremen Complex (Middlemost, 1967) towards the northeastern end of the province, and the Kanabeam Complex (Reid, 1991). Reid (*pers. comm.*) recognized that, in the central portion of the province, the intrusive sequence, from Si-undersaturated in the southwest to Si-oversaturated in the northeast, is repeated along three loci of intrusion. One of these is at Kanabeam (Reid, 1991). The other two form one continuous outcrop between the Orange River and Kanabeam; northeast from the Orange River, the sequence from Si-undersaturated to Si-oversaturated is evident over the first 5 km and manifests itself again over the next 10 km. This repetition is the basis for recognizing the presence of two discrete intrusive complexes, called, respectively, the Grootpenseiland and Marinkas Kwela Complexes. We have completed a detailed geological study of both complexes. For logistical reasons, our study has been confined to the rocks on the north side of the Orange River. Alkali granite crops out to the south of the river. It apparently forms a continuation of the Grootpenseiland Complex, however, its relationship to the Si-undersaturated rocks to the north of the river could not be investigated. It is possible that the granite relates more to the large granitic bodies that comprise the southern portion of the Kuboos-Bremen Igneous Province. For the purpose of this study, the term 'Grootpenseiland Complex' refers only to the rocks to the north of the Orange River.

Field relationships and some detailed petrographic observations are presented here. This contribution will be followed by a more detailed discussion of the geochemistry and petrogenesis of the complexes (Smithies and Marsh, in prep.).

Geological Setting

All of the rocks of the Grootpenseiland Complex and most rocks of the Marinkas Kwela Complex intrude granitoids belonging to the Vioolsdrif Suite of the Richtersveld Subprovince. The far northern part of the Marinkas Kwela Complex also intrudes across the tec-

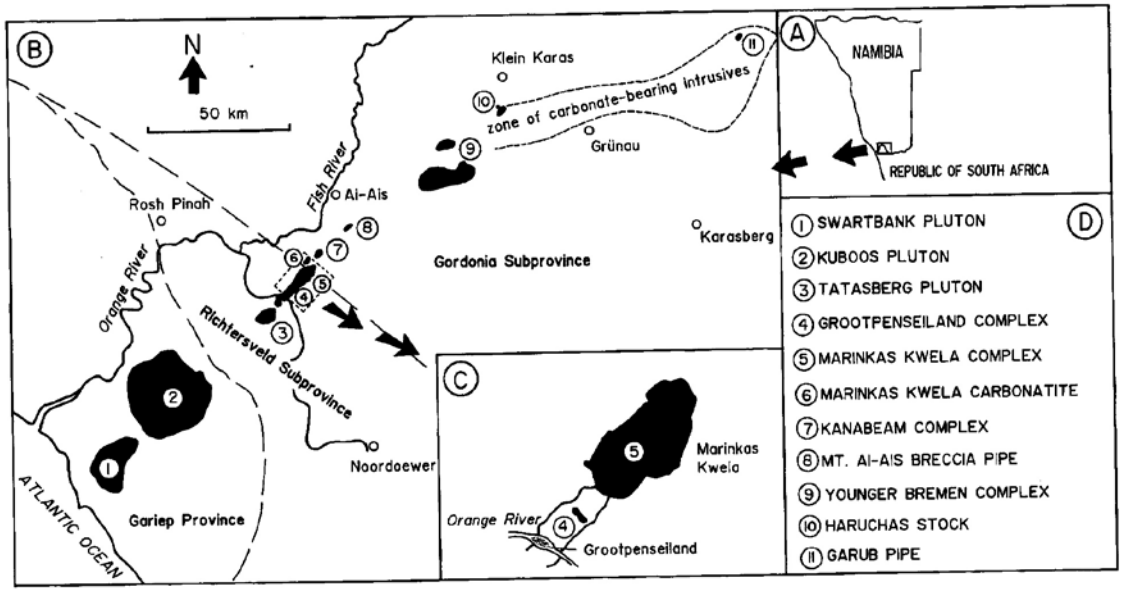

Figure 1: Regional locality map showing linear distribution of the intrusive complexes in the Kuboos-Bremen Igneous Province, with more detail (C) of the complexes that are the focus of this study. Modified after Reid (1991).

tonic transition zone separating the Richtersveld Subprovince from the quartzo-feldspathic gneisses of the Gordonia Subprovince. Intrusive contacts are commonly sharp and chilled margins are rare, although many contacts are obscured by scree.

In both complexes, field relations clearly show that the sequence of intrusion is from south to north. Rock types also trend to a more Si-oversaturated composition with decreasing intrusive age (Table 1). Thus, in each complex the sequence of intrusion is as follows:

1) Si-undersaturated rocks (nepheline syenites) crop out in the southwest;

2) outcrops of rocks that are critically saturated with respect to silica (syenite) are more or less centrally located;

3) Si-oversaturated rocks crop out in the northeast and include a large granite stock in each complex (the Grootpenseiland granite and the Marinkas Kwela granite respectively).

Inspection of figure 2 indicates that at present levels of outcrop the two complexes impinge on each other with the Grootpenseiland granite intruding the Si-undersaturated rocks of the Marinkas Kwela Complex. The intrusive age (Rb-Sr whole-rock) of the oldest phase of the Grootpenseiland Complex (529 ± 24 Ma) and the youngest phase of the Marinkas Kwela Complex (514 ± 26 Ma) are within error of each other (Smithies, 1992), and it seems likely that the two complexes developed synchronously.

A Note on Nomenclature

The rocks described here have been broadly subdivided into those having quartz as a minor or major mineral and that are generally *Q*-normative, those having only accessory, or no, quartz and that are only marginally *Q*- or *ne*-normative, and those having feldspathoids as a minor or major mineral and that are generally *ne*-normative. These will simply be referred to in general terms as granitoid (***G***), syenite (***S***) and *ne*-normative rocks (***NS***) respectively. More detailed classifications will be offered where appropriate. Within the classification 'nepheline syenite' (s.l.) fall two nepheline syenites (s.s.), one showing intergranular textures and the other showing hypidiomorphic granular textures. As a means of distinguishing clearly between them, the former is called 'foyaite' and the latter 'nepheline syenite'.

Where systematic variations in mineralogy and chemistry have been noted, the rocks are grouped into 'series'. Representative analyses and CIPW norms of the rock types found in the Grootpenseiland and Marinkas Kwela Complexes are in Table 2 while Table 3 presents average clinopyroxene and amphibole compositions.

Rock Types

ne-normative Rocks

This heading includes two rock series and a further two rock types ($\boldsymbol{NS}_{1\text{-}4}$) whose distribution is shown in figure 2.

NS_1 (*monzodiorite*)

A medium-grained and melanocratic monzodiorite is found in the southwest of the Grootpenseiland Complex where it forms small contorted inclusions of about 0.5

TABLE 1 : Relative proportions, and sequence of intrusion, of components within the Grootpenseiland and Marinkas Kwela Complexes.

Rock Type	Code	Relative proportion and intrusive age in the Grootpenseiland complex		Relative proportion and intrusive age in the Marinkas Kwela complex	
		oldest (southwest)	*youngest (northeast)*	*oldest (southwest)*	*youngest (northeast)*
Si-undersaturated rocks	**NS**				
Monzodiorite	NS_1	xx			
nepheline-bearing syenite	NS_2	xxxxx			
Alkali-melasyenite - nepheline syenite	NS_3			xxx	
Foyaite	NS_4			xxxxx	
Syenites	**S**				
Alkali-syenite	S_1	xxxxxxxxx		xxx	
Alkali-feldspar syenite	S_2	xxxxxxxx			
Granitoids	**G**				
Monzonite - granite	G_1		xxxxx	xxxxxxx	
Alkali-granite	G_{2a}			xxxxxxxx	
	G_{2b}		xx		xx

m in length within leucocratic nepheline syenites, and a discontinuous elongate body of about 700 m by 20 m within syenites. The monzodiorite shows no chilled margins and is probably xenolithic. Although up to 6 wt% *ne*-normative, the rock contains no modal feldspathoids. It consists essentially of subhedral to euhedral phenocrysts of plagioclase and diopside (clinopyroxene terminology after Morimoto *et al.*, 1988) in a groundmass of plagioclase, alkali-feldspar, diopside ($Wo_{47}En_{46}Fs_7$ to $Wo_{47}En_{25}Fs_{28}$), biotite, ferroan pargasite (amphibole terminology after Leake, 1978) and accessory sphene and apatite. Plagioclase phenocrysts are up to 1.2 cm in size and are distinctly more calcic (An_{80-58}) than groundmass plagioclase (An_{20-05}), Ferrokaersutite and biotite are rare phenocrystic phases.

NS_2 (*nepheline-bearing syenite series*)

Leucocratic rocks form a series that evolves from medium-grained and biotite-rich in the south, to coarse-grained and amphibole-rich in the north. The series forms a thin, irregular outcrop in the far southwest of the Grootpenseiland complex and is intruded by small dykes of the syenite that surrounds it.

Rocks in this series exhibit hypidiomorphic granular textures. The dominant felsic constituent is microperthite. Plagioclase (An_{56-10}) occurs only in the biotite-rich rocks, mostly as cores to microperthite. Nepheline occurs mainly in the amphibole-rich rocks where it lies interstitially between feldspar laths. Amphibole (ferroan pargasite to hastingsite) often rims biotite, particularly in the biotite-rich rocks, although both minerals also occur as discrete subhedral to euhedral grains. Clinopyroxene, mostly diopside but ranging to hedenbergite ($Wo_{45}En_{39}Fs_{16}$ to $Wo_{46}En_{16}Fs_{38}$), is commonly subhedral and sometimes rimmed by amphibole. Accessory phases include sphene, apatite, magnetite, zircon and fluorite.

NS_3 (*Alkali-melasyenite-nepheline syenite (s.s) series*)

This series occurs in the southwest of the Marinkas Kwela Complex, where it forms a northwest oriented band measuring about 2 km by 200 m, surrounded by foyaite (*NS_4*). The southern margin of the band is of fine-grained alkali-melasyenite.A mineralogical gradation occurs northwards into coarse-grained and leucocratic nepheline syenite (s.s.) and compositional planes more or less parallel the steeply dipping southern contact with the foyaite. Close to that contact, alkali-melasyenite xe-

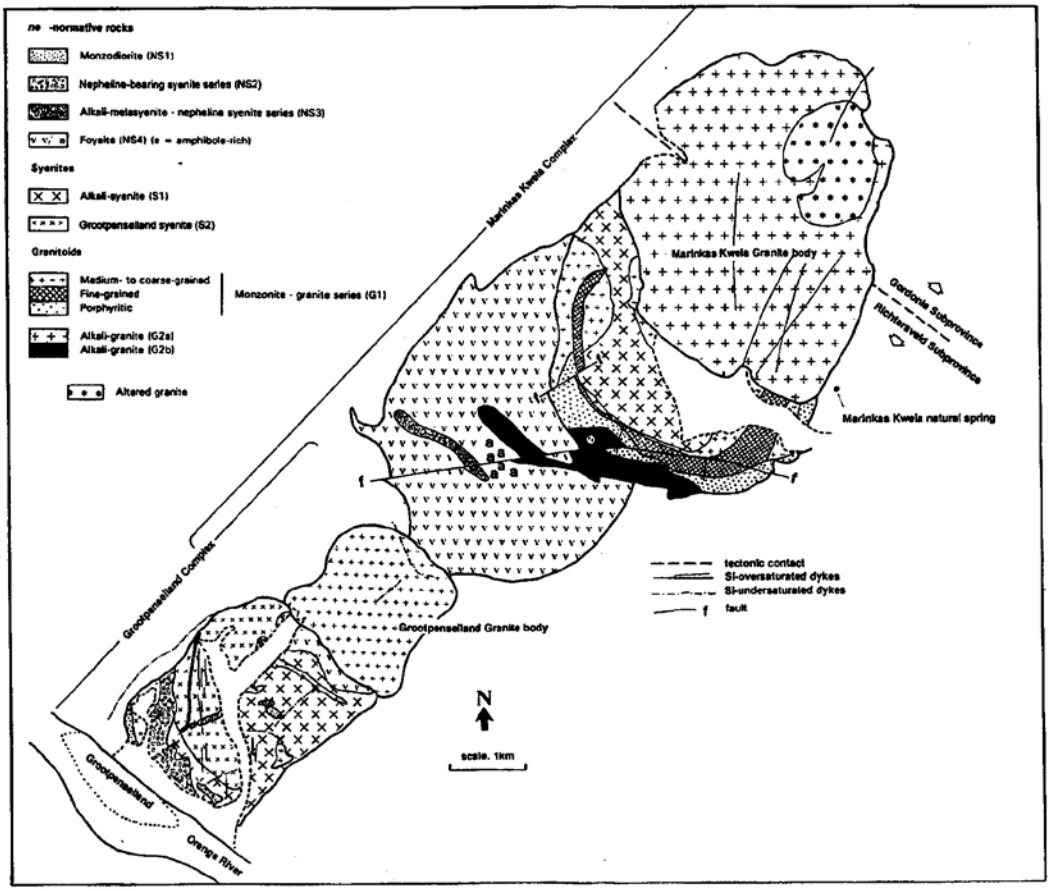

Figure 2: Geological map of the Grootpenseiland and Marinkas Kwela Complexes

noliths up to 1m in diameter lie in the foyaite.

The more mafic rocks have a mottled, intergranular appearance produced by mafic aggregates, poikilitically enclosed by large grains of intergranular nepheline, and together lying in a coarse-grained framework of coarsely perthitic alkali-feldspar. Plagioclase (An_{12-5}) is rare. Ferroan pargasite is the dominant mafic phase but in some cases has cores of diopside ($Wo_{48}En_{39}Fs_{13}$) to hedenbergite ($Wo_{47}En_{20}Fs_{33}$) or biotite, and contains inclusions of magnetite. Apatite, sphene and zircon are accessories associated with the mafic phases.

The nepheline syenite (s.s.) has a hypidiomorphic granular texture. In the most leucocratic samples, sodian hedenbergite (Ac_{35}) is abundant and commonly rims amphibole. The gradation from alkali-melasyenite to nepheline syenite is marked by an increase in the proportion of modal nepheline and a decrease in that of plagioclase and mafic phases.

NS_4 (*Foyaite*)

Foyaite crops out extensively in the southwestern third of the Marinkas Kwela Complex. It is predominantly coarse-grained and highly leucocratic and can be subdivided into clinopyroxene-rich and amphibole-rich varieties. The former are more common. They occur mainly to the northeast of the Grootpenseiland granite, but a small outlier also occurs to the southwest of that granite. The amphibole-rich variety is found only in the central part of the foyaite outcrop and in small, late-stage dykes which intrude that outcrop.

The foyaites show intergranular textures characterized by a network of tabular perthite grains that are randomly oriented or show slight preferential alignment, and in this way are distinct from the nepheline syenite (NS_3). In the clinopyroxene-rich variety, hedenbergite ($Wo_{46}En_{27}Fs_{27}$ to $Wo_{43}En_{7}Fs_{50}$) to sodian hedenbergite (Ac_{35}) is commonly the sole mafic phase, but is sometimes extensively rimmed by amphibole. In the amphibole-rich variety, hastingsite to taramite is commonly the sole mafic phase; biotite may occur as very minor inclusions in the amphibole or as late-stage reaction rims around magnetite. Late-stage aegirine-augite commonly rims amphibole in the amphibole-rich foyaite but is rare in the clinopyroxene-rich foyaite.

Braid-microperthite is the dominant felsic constituent of both varieties of foyaite. Nepheline ranges from minor to major modal proportions and lies interstitially to feldspar, except in some specimens of sodalite-bearing foyaite where subhedral to euhedral nepheline occurs. Where present, sodalite also lies interstitially to feldspar, and sometimes represents a reaction product of nephe-ine. Both feldspathoids may show partial to

TABLE 2: Representative major-element compositions and CIPW norms (wt%) for major rock types of the Grootpenseiland (GI) and Marinkas Kwela (MK) Complexes. All Fe is expressed as FeO. CIPW norms calculated assuming Fe^{2+}/Fe^{3+} = 2 (molecular)

Sample:	NS_1	NS_2 (biot)	NS_2 (amph)	NS_3 (mel)	NS_3 (ne-sy)	NS_4	S_1	S_2	G_1 (monz)	G_1 (gran)	G_{2a}	G_{2b}
Complex:	GI	GI	GI	MK	MK	MK	GI	GI	MK	GI	MK	GI
SiO_2	49.76	58.70	60.05	53.74	59.58	58.14	62.40	62.67	59.61	66.86	76.75	74.86
TiO_2	1.80	1.20	0.59	1.46	0.41	0.27	0.10	0.88	0.85	0.25	0.04	0.04
Al_2O_3	16.77	18.47	18.79	17.39	19.24	21.01	17.86	18.71	18.51	14.99	12.18	12.72
FeO	8.54	5.29	4.42	8.17	3.67	3.69	5.68	3.41	3.99	3.49	1.64	1.30
MnO	0.21	0.16	0.16	0.23	0.17	0.13	0.21	0.09	0.11	0.09	0.08	0.05
MgO	4.42	1.91	0.63	3.34	0.65	0.48	0.02	0.67	1.23	0.33	0.09	0.04
CaO	8.32	4.11	2.19	6.09	1.92	1.57	1.07	1.72	3.82	0.99	0.42	0.36
Na_2O	4.03	4.99	6.30	5.16	7.79	8.50	6.34	5.46	5.44	5.48	4.31	5.75
K_2O	2.84	4.19	4.96	3.25	4.86	6.13	5.33	5.30	4.84	5.10	4.39	4.41
P_2O_5	1.30	0.78	0.26	1.00	0.16	0.16	0.08	0.21	0.53	0.09	0.07	0.07
H_2O-	0.15	0.11	0.14	0.23	0.23	0.19	0.13	0.10	0.16	0.12	0.13	0.10
LOI	1.31	0.71	0.73	0.84	1.17	0.92	0.46	0.61	0.39	0.68	0.36	0.32
Total	**99.45**	**100.62**	**99.22**	**100.90**	**99.85**	**101.19**	**99.68**	**99.83**	**99.48**	**98.47**	**100.46**	**100.02**
q		2.74					0.60	5.70	0.60	12.43	33.48	27.37
c		0.12										
or	16.78	24.76	29.31	19.21	28.72	36.22	31.50	31.32	28.60	30.14	25.94	26.06
ab	30.29	42.22	51.82	39.92	47.17	32.34	53.65	46.20	46.03	46.37	36.47	40.88
an	19.28	15.29	8.34	14.69	3.18	1.07	4.53	7.16	11.79	1.24	0.92	
ne	2.06		0.81	2.03	10.16	21.45						1.39
ac												1.44
ns												
di	10.92		0.70	7.34	4.48	4.85	0.23		3.04	2.65	0.61	1.17
hy		7.94					5.38	3.51	4.03	2.40	1.48	1.11
ol	7.96		3.43	7.48	1.77	1.43						
mt	4.60	2.84	2.38	4.39	1.97	1.99	3.04	1.83	2.15	1.87	0.88	
il	3.42	2.28	1.12	2.77	0.78	0.51	0.19	1.67	1.61	0.47	0.08	0.08
ap	3.08	1.85	0.62	2.37	0.38	0.38	0.19	0.50	1.26	0.21	0.17	0.17

complete alteration to natrolite. Sphene, apatite and fluorite are accessory phases of both foyaites.

Syenites

S_1 (*Alkali-syenite*)

This rock type comprises a large portion of the Grootpenseiland Complex, also cropping out in a small, centrally located area of the Marinkas Kwela complex (Fig. 2). The highly leucocratic rock is inhomogeneous in texture, sometimes ranging from fine-grained to very coarse-grained across a single metre-scale outcrop. Very coarse-grained granular varieties occur in topographically higher parts of the central and northeastern portions of the Grootpenseiland Complex. The rock may demonstrate discontinuous and contorted banding on a scale of up to 30 cm. The bands alternate from highly felsic and coarse-grained to less felsic and fine-grained.

The rock contains up to 95% subhedral to euhedral microperthite. Amphibole (hasting site to katophorite) is the dominant mafic constituent, followed by biotite > aegirine-augite ($Di_6Hd_{68}Ac_{25}$)> magnetite, with accessory zircon, fluorite and allanite. It is the presence of alkali mafic minerals (katophorite and aegirine-augite) that distinguishes these rocks from other syenites (S_2).

S_2 (*Grootpenseiland syenite*)

This syenite is a medium- to coarse-grained and leucocratic rock forming poor outcrops in the central portion of the Grootpenseiland Complex. Turbid and commonly sericitized microperthite is the dominant phase. Biotite, commonly forming clusters of large radiating plates, is the main mafic mineral in rocks near the southwest margin of the complex, but in the central portion of the complex, amphibole is more abundant. Clinopyroxene (diopside to augite) ($Wo_{43}En_{32}Fs_{25}$ to $Wo_{45}En_{25}Fs_{28}$) is ubiquitous in minor proportions and quartz is an interstitial accessory phase in some rocks.

Sphene, apatite, fluorite and zircon form very rare accessories.

Granitoids

Granitoids comprise nearly half the outcrop of the Grootpenseiland Complex and an even greater portion of the Marinkas Kwela Complex (Fig. 2).

G_1 (*monzonite - granite series*)

The compositional range of granitoids of this series is wider in the Marinkas Kwela Complex than it is in the Grootpenseiland Complex. It extends from mesocratic monzonite through quartz syenite and granite to highly leucocratic alkali-feldspar granite. The rocks occur in a sequence of circular dykes that overlap to form a wide ringdyke in which the most evolved rock type - alkali-feldspar granite - forms a discontinuous outer envelope. The absence of chilled margins suggests only limited cooling in between successive intrusions.

The rocks are mostly medium- to coarse-grained and hypidiomorphic granular, but fine-grained and porphyritic varieties also occur. In the hypidiomorphic variety, microperthite occurs both as subhedral to euhedral grains, and as extensive rims around plagioclase. The latter exhibits compositional zoning from calcic cores (An_{40}) to sodic (An_8) rims. Quartz lies interstitially to feldspar and ranges from accessory proportions in the monzonite to 30% in the alkali-feldspar granite. Amphibole (ferro-tschermarkite to ferro-edenite) is usually the most abundant mafic phase. It is commonly subhedral and may contain cores of altered diopside. Biotite is common and occurs either as inclusions within amphibole, or as discrete subhedral to euhedral grains which are partially rimmed by magnetite. Sphene and apatite are abundant accessories only in the less evolved rocks whereas zircon and allanite are abundant accessories only in the more evolved rocks.

G_2 (*Alkali-granites*)

Leucocratic and medium- to coarse-grained alkali-granite makes up the remainder of both Complexes and can be subdivided into two types.

The Marinkas Kwela granite (***G_{2a}***) forms a stock in the far north of Marinkas Kwela Complex and shows

TABLE 3: Average clinopyroxene and amphibole analyses. Fe^{2+}/Fe^{3+} ratios calculated after Droop (1987)

Clinopyroxene								
	NS1	NS2	NS3	NS4	S1	S22	G1	G2
n=	48	96	34	59	12	11	24	11
SiO_2	51.4	51.6	50.6	50.3	50.8	52.3	50.4	49.5
TiO_2	0.5	0.3	0.4	0.3	0.2	0.4	0.3	0.2
Al_2O_3	2.3	1.1	2.2	1.4	1.1	1.0	1.1	0.2
Cr_2O_3	0.0	0.0	0.0	0.0	0.0	0.0	0.0	0.0
Fe_2O_3	5.2	3.3	5.6	8.9	16.6	0.3	3.4	6.0
FeO	4.0	9.2	6.7	10.2	11.0	11.2	10.2	20.6
MnO	0.4	0.9	0.7	1.2	1.3	0.9	0.7	1.5
MgO	12.9	10.4	10.9	5.5	0.5	11.9	9.5	1.2
CaO	23.0	22.1	21.6	18.5	10.6	20.9	23.1	15.5
Na_2O	1.1	1.1	1.4	3.3	7.3	0.6	0.7	3.3
Total	**100.7**	**100.0**	**100.0**	**99.6**	**99.5**	**99.5**	**99.3**	**97.6**
Amphibole								
	NS1	NS2	NS3	NS4	S1	S22	G1	
n=	28	58	83	90	30	4	107	
SiO_2	39.4	39.0	38.8	39.1	39.6	43.4	40.9	
TiO_2	3.4	3.0	2.7	1.9	1.1	1.8	2.2	
Al_2O_3	11.8	10.6	10.6	9.3	7.7	6.8	8.3	
Cr_2O_3	2.2	1.8	2.6	5.9	7.5	6.3	5.4	
Fe_2O_3	18.2	22.7	20.9	21.9	26.4	18.3	21.0	
FeO	0.4	0.9	0.9	1.3	1.4	0.9	0.7	
MnO	8.0	5.1	5.6	3.8	0.5	7.1	5.4	
MgO	10.4	10.6	10.2	8.8	7.5	10.4	10.4	
CaO	2.8	3.0	3.2	3.8	4.3	2.0	2.3	
Na_2O	2.0	1.5	1.4	1.5	1.4	0.8	1.1	
Total	**98.5**	**98.2**	**96.8**	**97.2**	**97.5**	**97.9**	**97.5**	

sharp contacts with all the rocks it intrudes. It is made up mostly of hypidiomorphic granular aegirine-augite alkali-granite. Quartz-feldspar porphyries also occur, found in topographically higher parts of the granite body where they are virtually devoid of mafic minerals and associated with hypidiomorphic granular varieties that are similarly leucocratic. Additionally, in the north-east corner of the body an ovoid depression of about 2 km^2 marks a zone of intense alteration characterized by a pervasive assemblage of quartz-sericite-pyrite.

Aegirine-augite alkali-granite ($\boldsymbol{G_{2b}}$) occurs in both Complexes. In the Grootpenseiland Complex it is found in plugs and northerly-trending dykes, which cross-cut earlier Si-undersaturated rocks, and is the youngest intrusive phase of that Complex. In the Marinkas Kwela Complex, G_{2b} crops out in the central part of the Complex and shows sharp intrusive contacts against the G_1 ring-dyke and the foyaites (NS_4).

Both types of alkali-granite have hypidiomorphic granular textures. They are hypersolvus granites; the microperthite being of the patch and braid variety in G_{2a} and G_{2b} respectively. Quartz forms clusters of subhedral to anhedral grains. Mafic phases crystallize interstitially to feldspar. Aegirine-augite is most common and is accompanied by arfvedsonite in G_{2a} and ferrowinchite in G_{2b}.

Comparison With the Kanabeam Complex

There appear numerous similarities, in rock type and relative spatial and temporal arrangement of rock types, between the Grootpenseiland and Marinkas Kwela Complexes and the Kanabeam Complex. According to Reid (1991), a series of ring-dykes comprising at least six varieties of nepheline syenite form a sub-complex that is the oldest, and most southerly, component at Kanabeam. Four of these rock types are recognized in either the Grootpenseiland Complex (north of the Orange River) and the Marinkas Kwela Complex (Table 4), like wise forming the first and most southerly intrusive phase of each complex.

Intruding the nepheline syenites at Kanabeam, is a central plug of quartz syenite with a swarm of microsyenite dykes and plugs to the north. The quartz syenite has no close analogy recognized in the two Complexes to the south, although it shows some similarities to the Grootpenseiland syenite (S_2). The micro syenite contains neither quartz nor nepheline, is critically saturated, and closely resembles syenites found in the central portions of the Grootpenseiland and Marinkas Kwela Complexes.

In the northeast of the Kanabeam Complex, Si-oversaturated rocks comprise the youngest intrusive phases, beginning with granite, granite porphyry and, finally, microgranite (Reid, 1991). The first two of these phases bear mineralogical similarities to rocks of the monzonite - granite series (G_1) of the Grootpenseiland and Marinkas Kwela Complexes, whereas the microgranite shows similarities to hydrothermally altered portions of alkali-granite at Marinkas Kwela (G_{2a}).

Consequently, a remarkable feature of the central portion of the Kuboos-Bremen igneous province is that within a distance of less than 30km there occur three discrete intrusive alkali complexes, including Kanabeam, that are almost identical in terms of their range of rock types, and in terms of the spatial and temporal sequence in which individual rock types were emplaced. These similarities suggest that all three complexes derived

TABLE 4: Correlation between major rock types at Kanabeam (Reid, 1991) and at Grootpenseiland-Marinkas Kwela. In lists A and B, the order of intrusion, and sequences of intrusion (from southwest to northeast), is from top to bottom. NF = no similar rock type found at Grootpenseiland-Marinkas Kwela.

A: Kanabeam complex			B: Grootpenseiland and Marinkas Kwela complexes	
	normative *Q* or *ne* (average wt%)			normative *Q* or *ne* (average wt%)
Nepheline syenite (ns)			Si-undersaturated rocks	
	ns1 -	NF	NS_1	4% *ne*
	ns2 -		NS_2	1% *ne*
(monzonite)	ns3 6% *ne*		NS_3	8% *ne*
	ns4 6% *ne*		NS_4	18% *ne*
(foyaite)	ns5 18% *ne*			
(melasyenite)	ns6 10% *ne*		Syenite	
			S_1	1% *Q*
Quartz syenite	15% *Q*	NF?	S_2	3% *Q*
Microsyenite				
Granite	20% *Q*		Granitoids	
Granite (porphyry)	15% *Q*		G_1	7% *Q*
Microgranite	37% *Q*		G_{2a}	32% *Q*
			G_{2b}	16% *Q*

from parental magmas of similar compositions and underwent similar subsequent compositional evolution.

Evolution of the Complexes

In the Grootpenseiland and Marinkas Kwela Complexes, field relationships clearly show that intrusive ages decrease from south to north. An accompanying progression in rock type also occurs, trending to more Si-oversaturated composition with decreasing intrusive age; from nepheline syenites in the southwest, through rocks that are critically saturated with respect to silica (syenite) in the middle, to ring-dykes and stocks of granitoids in the northeast. The close spatial relationships observed between Si-undersaturated and Si-oversaturated rocks of these two Complexes are also features of many other alkaline complexes (Pankhurst *et al.*, 1976; Upton and Thomas, 1980; Fletcher and Beddoe-Stephens, 1987; Woolley and Jones, 1987; Henderson *et al*., 1988; Reid, 1991). It has been proposed - for example by Foland and Henderson (1976) and Eby (1987) - that in such situations the two magma types may be genetically related to each other. Reid (1991), tentatively put forward an alternative suggestion regarding the Kanabeam Complex, whereby the Si-undersaturated rocks relate to a basanitic parental magma, magmas parental to the Si-oversaturated rocks are anatectic melts of silicic crust, and the intermediate rock types form through the interaction of those two melt lineages.

Smithies (1991) and Smithies and Marsh (in prep.) found that the most primitive nepheline-bearing syenite (NS_2) at Grootpenseiland and the most primitive monzonite (G_1) at both Grootpenseiland and Marinkas Kwela are mineralogically and geochemically almost identical to each other, although they clearly relate to different rock series in the field. According to Smithies (1991), Si-undersaturated rocks and the rocks of the monzonite -granite series (G_1) have very similar Sr and Nd isotopic compositions (respectively, initial Sr ratio 0.7048 and 0.7047; epsilon Nd + 1.0 and +3.5) which reflect derivation primarily from a mantle source. Oxygen isotopes, however, suggest a greater crustal input within the monzonite granite series (Smithies, 1991). The close compositional similarity between the least fractionated Si-undersaturated and Si-oversaturated rocks, and the isotopic evidence, led Smithies (1991) and Smithies and Marsh (in prep.) to suggest that the two rock types may, in fact, be derived from a common Si-undersaturated parental melt, but that the diverging compositional trends shown by the respective rock series were caused through the interaction of this melt with crustal material. Where little interaction occurred, the melts fractionated towards successively more foyaitic or phonolitic residuals. Incorporation of a 'granitic' component, however, resulted in critically saturated or Si-oversaturated trends. In this way it is possible to relate all intrusive phases of each complex to a common parental melt.

Nevertheless, the rocks found in both complexes are overwhelmingly felsic and far removed from parental compositions, the nature of which can only be guessed at. The least evolved rock in either complex is the monzodiorite (NS_1) of the Grootpenseiland Complex (48.13 - 49.78 wt% SiO_2), which is up to 6.00 wt% *ne*-normative and contains feldspar phenocrysts with extremely calcic cores (An_{80}). In the Kanabeam Complex, Reid (1991) reports the occurrence, in phonolite breccia pipes, of rounded xenoliths of olivine (Fo_{78}) and calcic plagioclase (An_{76}) bearing gabbro. These rocks have lower silica (45.20 wt%) and are more *ne*-normative (15.69 wt%) than any rock found in the other two Complexes and have compositions that approximate basanite. They may closely approach the 'composition of mantle melts envisaged to be parental to all three complexes.

Acknowledgments

We acknowledge the financial support of GENMIN and the useful reviews by Franco Pirajno, Dave Reid and Anton Ie Roex.

References

Allsopp, H.L., Kostlin, E.O., Welke, H.J., Burger, A.J., Kröner, A. and Blignault, H.J. 1979. Rb-Sr and U-Pb geochronology of late Precambrian - early Palaeozoic igneous activity in the Richtersveld (South Africa) and southern South West Africa. *Trans. geol. Soc. S. Afr.*, **82**, 185-204.

Blignault, H.J. 1977. *Structural-metamorphic imprint on part of the Namaqua Mobile Belt in South West Africa*. PhD thesis (unpubl.), Univ. Cape Town, 197 pp.

Droop, G.R.T. 1987. A general equation for estimating Fe^{3+} concentrations in ferromagnesian silicates and oxides from microprobe analyses, using stoichiometric criteria. *Min. Mag.*, **51**, 431-435.

Eby, G.N. 1987. The Monteregian Hills and White Mountains alkaline igneous province, eastern North America. *In*: Fitton, J.G. and Upton, B.G.J. (eds). *Alkaline Igneous Rocks*. Geological Society Special Publication, **30**, 433-447.

Fletcher, C.J.N. and Beddoe-Stephens, B. 1987. The petrology, chemistry and crystallization history of the Velasco alkaline province, eastern Bolivia. *In*: Fitton, J.G. and Upton, B.G.J. (eds.) *Alkaline Igneous Rocks*. Geological Society Special Publication, **30**, 403-413.

Foland, K.A. and Henderson, G.M.B. 1976. Application of age and Sr isotope data to the petrogenesis of the Marangudzi Ring Complex, Rhodesia. *Earth. Planet. Sci. Lett.*, **29**, 291-301.

Henderson, C.M.B., Pandlebury, K. and Foland, K.A 1989. Mineralogy and Petrology of the Red Hill Alkaline Igneous Complex, New Hampshire, U.S.A. *J. Petrol.*, **30**, 627-666.

Kröner, A. 1975. Late Precambrian formations in the western Richtersveld, northern Cape Province. *Roy. Soc. S. Afr. Trans.*, **41**, 375-437.

Kröner, A. and Blignault, H.J. 1976. Towards a definition of some tectonic and igneous provinces in western South Africa and southern South West Africa. *Trans. geol. Soc. S. Afr.*, **79**, 232-238.

Leake, B.E. 1978. Nomenclature of amphiboles. *Min. Mag.*, **42**, 533-563.

Middlemost, E. 1967. Petrology of the Bremen Granite - Syenite Complex, South West Africa. *Trans. geol. Soc. S. Afr.*, **70**, 117-134.

Morimoto, N., Fabrics, J., Ferguson, AK., Ginzburg, I.V., Ross, M., Seifert, F.A, Zussman, J., Aoki, K. and Gottardi, G. 1988. Nomenclature of pyroxenes. *Am. Mineral.*, **73**, 1123-1133.

Pankhurst, R.J, Beckinsale, R.D. and Brooks, C.K. 1976. Strontium and Oxygen Isotopic Evidence Relating to the Petrogenesis of the Kangerdlugssuaq Alkaline Intrusion, East Greenland. *Contrib. Mineral. Petrol.*, **54**, 17-42.

Reid, D.L. 1991. Alkaline rocks in the Kuboos-Bremen igneous province, southern Namibia: The Kanabeam multiple ring complex. *Communs. geol. Surv. Namibia*, **7**, 3-13.

Smithies, R.H. 1992. *The geochemical evolution of three alkaline complexes in the Kuboos-Bremen igneous province, southern Namibia*. PhD thesis (unpubl.), Rhodes Univ. Grahamstown, 197 pp.

Söhnge, P.G. and de Villiers, J. 1948. The Kuboos pluton and its associated line of intrusives. *Trans. geol. Soc. S. Afr.*, **51**, 1-31.

Upton, B.G.J. and Thomas, J.E. 1980. The Tugtutoq Younger Giant Dyke Complex, South Greenland: Fractional Crystallization of Transitional Olivine Basalt Magma. *J. Petrol.*, **21**, 167-198.

Woolley, A.R. and Jones, G.C. 1987. The petrochemistry of the northern part of the Chilwa alkaline province, Malawi. *In*: Fitton, J.G. and Upton, B.G.I. (eds.) *Alkaline Igneous Rocks*. Geological Society Special Publication, **30**, 335-355.

Communs geol. Surv. Namibia, ***11*** *(1996), 23-31*

Scapolitization in the Kuiseb Formation of the Damara Orogen: geochemical and sTable 1sotope evidence for fluid infiltration along deep crustal shear zones

A. Dombrowski[1], S. Hoernes[2] and M. Okrusch[1]

[1]*Mineralogisches lnstitut, Universität Würzburg, Am Hubland, 97074 Würzburg, Germany*

[2]*Mineralogisch-Petrologisches lnstitut, Poppelsdorfer Schloß, 53115 Bonn, Germany*

In the Pan-African Damara Orogen, an unusual scapolitization occurs within metaturbidites of the Kuiseb Formation in the Khomas Hochland, central Namibia. Geochemical investigations exclude an evaporitic precursor for the scapolite-bearing Kuiseb schists. Carbon isotope data indicate a local sedimentary source of fluids which reacted with pre-existing plagioclase in the Kuiseb schists to form the scapolite.

Introduction

Scapolite formation in amphibolite facies meta-sedimentary rocks may be attributed to either evaporites as protoliths (Mora and Valley, 1989; Gómez-Pugnaire *et al.*, 1994; Behr *et al.*, 1983), or interaction with externally derived chlorine- and/or CO_2-rich fluids during metamor-phism (Oliver *et al.*, 1992). Deciphering an evaporitic nature for the scapolite-forming process is difficult because clear evidence such as pseudomorphs after evaporite minerals (e.g. halite) are generally lacking.

We present a case study within rocks of the Pan-African Kuiseb Formation in central Namibia where two horizons of scapolite-bearing schists are traceable for more than one hundred kilometres along strike (Kukla, P.A., 1990, 1992; Kukla, C., 1993), raising the question of whether or not this represents a possible primary sedimentary feature. Geochemical analyses of bulk rock compositions, rare earth element (REE) patterns, as well as sTable 1sotope compositions of carbon in scapolite and calcite will be used to address this question.

Geological setting

The study area is located in the northern part of the Khomas Hochland, central Namibia (Fig. 1). This part of the Pan-African Damara Orogen is made up by rocks of the Kuiseb Formation, which consists of a monotonous sequence of schistose pelitic and psammitic meta-

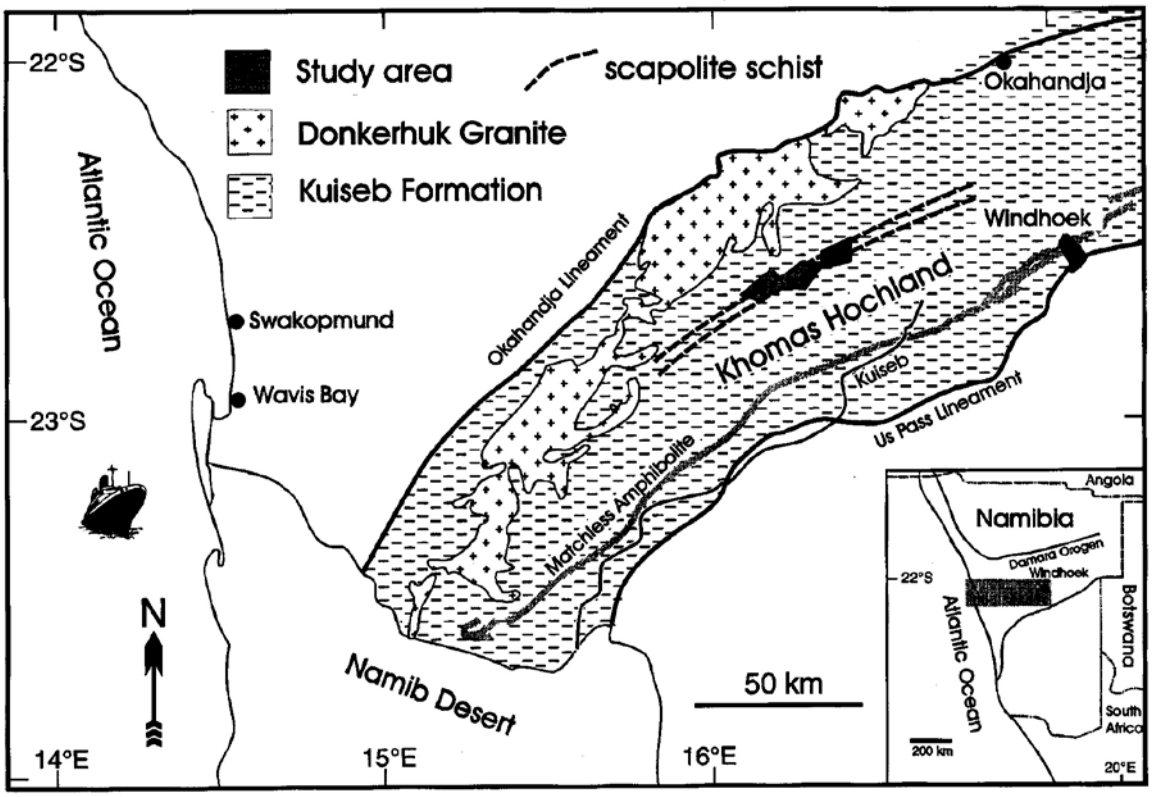

Figure 1: Map showing the location and simplified regional geological setting of the study area.

turbidites with intercalations of graphitic schist, calc-silicate rocks, marble, tremolite schist, scapolite schist and the Matchless amphibolite. Metamorphic conditions were of amphibolite facies grade with a progressive northward increase in peak temperatures reaching anatectic conditions in the northern Khomas Hochland near the syn-orogenic Donkerhoek granite (e.g. Hartmann *et al.*, 1983; Kukla, P.A., 1992; Kukla, C., 1993; Bühn *et al.*, 1994). Most textural evidence for the polyphase deformation history has been overprinted by post-tectonic growth of the minerals. For the geotectonic evolution of the Khomas Hochland, Kukla and Stanistreet (1991) established a tectono-sedimentary model comprising the evolution of an accretionary prism within a convergent continental margin setting. According to Kukla (1992), the scapolite-bearing assemblages are associated with two of the major high strain zones that subdivide the Khomas Trough in the form of structural discontinuities. Kukla (1990, 1992), therefore, interpreted scapolitization as a product of fluid movement along these zones of tectonic weakness which led to an interaction of the Kuiseb schists with saline brines either from early rift-related sequences or pore fluids which were being expelled from the accretionary prism.

Analytical procedures

Major and trace elements as well as Cl concentrations were determined from fused discs by conventional XRF methods using a Philips PW1410 spectrometer. Lithium was analysed by atomic absorption using a Perkin Elmer 300. CO_2 was determined volumetrically.

The REE contents were analysed, using the facilities of the GeoForschungsZentrum Pots dam, by ICP-AES, after decomposing the samples in HF-$HClO_4$ and separating the REE in chromatographic columns (Zuleger and Erzinger, 1988). Chondri tic normalizing factors are taken from Evenson *et al.* (1978). Subscript *N* in the text indicates chondrite normalized values.

STable 1sotope analyses were carried out at the Mineralogical Institute of the Bonn University using a Prism I by VG Instruments. The finely ground sample powders were treated with 100% H_3PO_4 at different temperatures. Reaction at 25°C for one hour was sufficient to dissolve nearly completely the usually small contents of calcite. The liberated CO_2 was collected and measured in the mass spectrometer. The small amount of gas produced during a further two hours of reaction at 25°C was pumped away. Extraction of CO_2 from the scapolite structure occurred at 75°C over at least 12 hours of reaction. The temperature was maintained by placing the reaction vessel in a dry heat box, simultaneously cooling the stopcocks by a stream of air at room temperature. To test the results of the scapolite analysis, the samples were immersed in dilute HCI to remove any calcite and then reacted with 100 % H_3PO_4 in the described manner (cf. Moecher *et al.*, 1994). The results of both methods agree within analytical error. Analytical precision for ∂-values from scapolite is in the range of ± 0.15-0.2‰. Values of $\partial^{13}C$ are reported in the standard per mil notation relative to PDB.

Figure 2: Spheroidal scapolite porphyroblasts (white) in scapolite schist of the Kuiseb Formation.

Sample description

The scapolite-bearing Kuiseb schists are characterized in the field by a dark grey colour when fresh, but their behaviour during weathering gives them a typically speckled appearance (Fig. 2). The extent of scapolitization is very variable in the investigated samples with scapolite contents of up to 60 vol. % of the rock.

The occurrence of scapolitization under static conditions is shown by the presence of large postkinematic poikiloblasts, up to several millimetres in diameter. These are of mizzonitic composition, with an average formula of $Na_{1.5}Ca_{2.5}Al_{4.6}Si_{7.4}O_{24}Cl_{0.3}(CO_3)_{0.7}$ (Table 1), and rest in a matrix of biotite and quartz with various minor phases such as epidote, calcite, Ca-amphibole and titanite. In contrast to the adjacent metaturbidites, primary sedimentary features and deformation structures are largely obliterated. The scapolite-free Kuiseb metasedimentary rocks are characterized by the equilibrium assemblage staurolite + garnet + biotite ± muscovite ± sillimanite + quartz ± plagioclase reflecting metamorphic conditions of the lower amphibolite facies, with temperatures of 550 - 650°C and pressures of 2.5-5.5 kb (Kukla, 1992; Bühn *et al.*, 1994).

Major and trace element geochemistry

Recognition of metamorphosed evaporites in metasedimentary series is difficult and relies mainly on indirect evidence, because of the major changes in mineral content and bulk rock composition possible during metamorphism. The increasing solubility of NaCl in water with increasing temperature, for example, is responsible for the complete disappearance of halite crystals during diagenesis and early stages of metamorphism. Since pseudomorphs after evaporite minerals in metamorphic rocks are scarce, former evaporites are often assumed when minerals such as scapolite, lazurite or tourmaline occur, or highly saline fluid inclusions are found. Such interpretations are, however, rarely unequivocal.

Comparison between the geochemical characteristics of evaporitic sediments and their metamorphosed equivalents is problematic since metamorphism generally leads to the removal of volatile components and changes in bulk rock chemistry are common. Moine *et al.* (1981) developed some discriminating criteria based on elements believed to be relatively inert during metamorphic processes. They found Mg, Al, Fe, Ca and Li to be the least affected elements and that these reveal characteristic differences between evaporitic and non-evaporitic sediments. The scapolite-bearing Kuiseb schists are distinctly different from (meta-) evaporitic sediments (Table 2), according to the discriminating criteria of Moine *et al.* (1981). The position of the Kuiseb schists, whether scapolite-bearing or not, in the triangular plot Ca-Mg-Al (Fig. 3) is identical to that of common platform sediments and modem turbidites, implying that derivation of these scapolite-bearing assemblages from an evaporitic precursor is unlikely. Compared to the scapolite-free Kuiseb schists, the scapolite schists are characterized by a shift towards the Ca apex of the plot. In general, a distinctly higher Ca content of the scapolite schists is the major and significant differ-

Table 1: Representative microprobe analyses of scapolite from the Kuiseb Formation.

	AD93-35	AD93-35	AD93-8	AD93-8	AD93-9	AD93-9
wt.%						
SiO_2	49.23	47.80	48.77	48.54	47.71	47.66
Al_2O_3	26.17	26.46	25.96	26.18	25.90	25.94
CaO	15.00	15.54	15.52	15.21	15.32	15.18
Na_2O	4.80	4.48	4.63	4.69	4.56	4.71
K_2O	0.78	0.62	0.71	0.80	0.49	0.51
SO_3	0.06	0.00	0.03	0.03	0.02	0.00
Cl	1.22	1.08	1.16	1.17	0.97	1.20
Total	97.26	95.98	96.78	96.62	94.97	95.20
Atomic proportions based on 12 <Si+Al>						
Si	7.38	7.26	7.37	7.34	7.32	7.31
Al	4.62	4.74	4.63	4.66	4.68	4.69
Total	12.00	12.00	12.00	12.00	12.00	12.00
Ca	2.41	2.53	2.51	2.46	2.52	2.49
Na	1.40	1.32	1.36	1.37	1.36	1.40
K	0.15	0.12	0.14	0.15	0.10	0.10
Total	3.96	3.97	4.01	3.98	3.98	3.99
%Mej[a]	61.02	63.78	62.88	61.86	63.55	62.67
Eq.An[b]	54.07	57.95	54.19	55.44	56.08	56.32

[a]= (Ca/(Ca+Na+K)) * 100 (Shaw, 1960)
[b]= 100(Al-3)/3 (Orville, 1975)
Fe, Ti, Mg and Mn are below detection limit.
The whole data set is available on request.

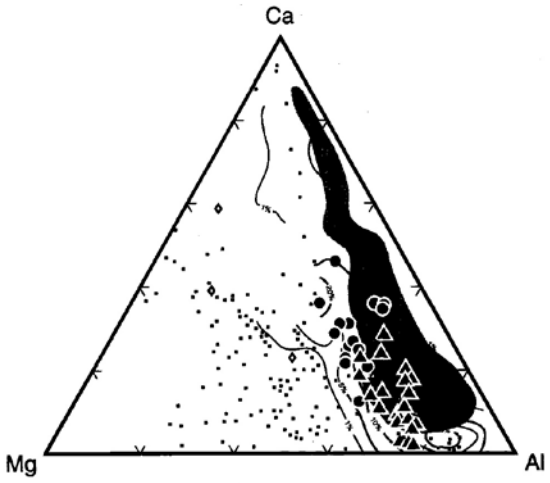

Figure 3: Triangular plot Ca-Mg-Al after Moine *et al.* (1981). Contour lines = density lines of the reference set of common platform sediments, shaded field = 69 analyses from modern turbidites from McLennan *et al.* (1990) where the darker area represents 50% of the data points; ● = scapolite-bearing schists and ▲ = scapolite-free metasedimentary rocks of the Kuiseb Formation; • = evaporites and ◊ = NaCl-bearing evaporites, from Moine *et al.* (1981; Table 2).

Table 2: Geochemical characteristics of scapolite - bearing Kuiseb schists in comparison with those of evaporites and meta-evaporites documented by Moine et al. (1981).

	Evaporites	Meta-evaporites	Scapolite schists
MgO	high 7-17%*	high 4-20%	medium 5-11%
$Fe_2O_3^{tot}$	3-5%	2-4.5%	3-9%
Li	high 100-300 ppm		low 18-88 ppm
Mg/Al	high 0.8-1.6	0.42-1.68	low 0.14-0.53
Mg/Fe	high 1.5-3.1	1.48-3.81	low 0.39-1.02
K/Al	0.1-0.6	0.17-0.74	0.21-0.54
Na/Al	0.01-0.09	0.02-0.19	0.09-0.28

* - weight %

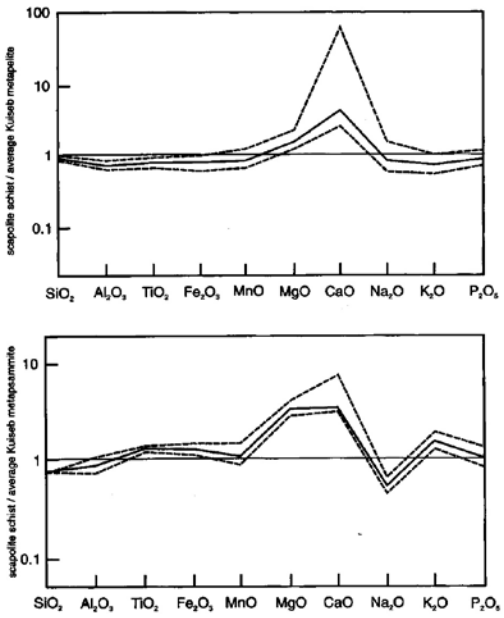

Figure 4: Major element geochemistry of the scapolite schists normalized to average Kuiseb schist compositions after Kukla (1992), dashed lines represent the standard deviation (1 σ).

ence between the scapolite-bearing and scapolite-free parageneses within the Kuiseb Formation (Fig. 4, see also Table 3).

REE geochemistry

In order to obtain additional constraints on the character of the protolith, REE analyses were carried out on four samples of scapolite schist and five samples of scapolite-free Kuiseb metasedimentary rocks (Table 4). Their chondrite-normalized patterns are depicted in figure 5. All samples show light REE (LREE) enrichment and flat heavy REE (HREE) patterns; La_N/Lu_N ranges from 6.1 to 9.2. All show a significant negative Eu-anomaly with Eu/Eu* in the range 0.57 to 0.63 (except for sample AD 93-21 with Eu/Eu* of 0.49). Total REE abundances vary between 159 and 244 ppm in the scapolite schists whilst the scapolite-free meta-sedimentary rocks reveal more uniform contents of 204 to 242 ppm. The following conclusions can be drawn from the REE patterns of the investigated samples:

1) All analysed samples of the Kuiseb Formation show identical REE patterns which means that scapolite-bearing and scapolite-free parageneses have an uniform sedimentary precursor. Virtually the same patterns were found by Hawkesworth *et al.* (1981) and Häussinger *et al.* (1993) for Kuiseb schist samples from different occurrences;
2) Sediments deposited through evaporation would have a distinctly different REE signature because chemical sediments should reflect the composition of the seawater from which they were precipitated. Thus, total concentrations of REE in (meta)-evaporites are expected to be very low (< 10 ppm; Ronov *et al.*, 1974) because of the exceedingly low REE contents of ocean waters (Goldberg *et al.*, 1963; McLennan, 1989). Furthermore, the chondrite-normalized REE patterns of seawater (Goldberg *et al.*, 1963; Høgdahl *et al.*, 1968) usually show a large depletion of Ce and a relative enrichment in HREE (Wedepohl, 1970; Piper, 1974) which is not found in the REE patterns of the Kuiseb schists.
3) The REE patterns of the scapolite-free and scapolite-bearing Kuiseb schists do not deviate significantly from the average of 23 post-Archaean shales (PAAS), reflecting the composition of the upper continental crust (Fig. 6). The Eu/Eu* values are slightly greater than that of PAAS (0.66) and the average La_N/Yb_N ratio of 7.56 suggests somewhat less fractionation than the PAAS value of 9.2.
4) In hydrothermal fluids, the REE are transported as complexes, which are more distinct for each REE than the corresponding ionic compounds (Mineyev, 1963). Thus, the different susceptibilities of the HREE and LREE to complexing, and the different stabilities of the respective complexes, should cause different fractionation within the REE of the scapolite schists -which is not the case. We therefore assume that fluid/rock interaction did not greatly affect the REE contents of the Kuiseb schists;
5) The somewhat lower contents in total REE of the scapolite-bearing samples probably represent a dilution effect caused by the higher density of the scapolite-bearing rocks.

Carbon isotope analyses

STable 1sotope investigations were carried out to shed some light on the origin of the carbon in scapolite and calcite. Evaporation processes strongly affect the isotopic composition of carbon and thus, former evaporitic sediments should be characterized by their heavy $\partial^{13}C$ values (Rothe and Hoefs, 1977). If the scapolitization was caused by externally derived fluids, carbon

Table 3: Bulk rock geochemistry of the Kuiseb metasediments. Rocktypes *pe* = metapelite, *ps* = metapsammite, *scp* = scapolite schist; n.d. = not determined, b.d. = below detection limit, H_2O = LOI-CO_2.

sample numbers: AD93-	1	2A	3	4C	5	6	7	8	9	10	11	12	13	14	15	16	17	18	19	20
wt %	*pe*	*scp*	*scp*	*scp*	*pe*	*pe*	*pe*	*scp*	*scp*	*scp*	*scp*	*scp*	*scp*	*scp*	*ps*	*ps*	*ps*	*scp*	*scp*	*ps*
SiO_2	58.32	52.08	49.61	52.31	56.30	54.19	57.43	50.72	53.75	50.60	54.37	53.22	46.99	68.47	69.25	73.95	73.93	48.94	70.32	74.28
TiO_2	0.72	0.71	0.86	0.70	0.86	0.89	0.80	0.82	0.69	0.78	0.69	0.77	0.63	0.54	0.84	0.57	0.66	1.03	0.55	0.78
Al_2O_3	17.23	16.44	18.68	14.61	18.07	18.83	17.73	18.22	16.21	17.92	15.54	17.33	14.91	11.83	13.54	11.82	11.73	21.15	12.02	11.27
Fe_2O_3	1.88	1.18	2.20	1.50	4.07	4.00	3.50	2.08	0.62	1.41	1.94	2.09	1.60	0.91	1.40	1.18	1.29	4.52	0.89	1.00
FeO	5.5	5.15	5.9	4.2	3.55	4.0	3.85	6.1	6.0	5.9	4.5	5.4	4.3	2.75	4.2	2.3	2.3	4.4	2.3	3.0
MnO	0.06	0.08	0.08	0.09	0.11	0.11	0.08	0.10	0.14	0.10	0.09	0.07	0.09	0.11	0.08	0.05	0.05	0.11	0.07	0.08
MgO	5.44	6.08	7.18	6.74	4.96	5.63	5.24	6.85	5.29	5.83	6.24	5.99	5.04	2.22	2.31	1.52	1.55	5.89	1.44	1.69
CaO	4.23	7.81	6.18	9.33	4.99	5.00	3.05	5.71	7.83	6.94	6.83	6.31	13.16	5.45	1.03	2.67	2.22	5.65	5.76	2.13
Na_2O	1.23	1.54	1.36	1.46	2.01	1.58	1.71	1.39	1.79	2.08	1.28	0.98	0.93	1.96	2.04	2.08	2.15	1.95	1.85	2.45
K_2O	4.25	4.16	4.88	3.38	3.33	3.82	4.51	4.98	3.49	4.27	4.04	4.51	3.53	1.97	3.30	2.20	2.80	4.07	1.61	2.13
P_2O_5	0.17	0.19	0.21	0.19	0.24	0.21	0.21	0.20	0.17	0.20	0.16	0.19	0.17	0.15	0.25	0.27	0.21	0.26	0.16	0.22
H_2O	1.52	1.59	1.71	1.63	1.43	1.57	1.75	1.92	1.82	2.07	1.59	1.55	0.75	1.33	1.61	0.68	0.75	1.43	1.27	0.93
CO_2	n.d.	1.45	0.19	2.35	n.d.	n.d.	n.d.	0.33	1.16	0.73	2.22	0.51	7.24	1.07	n.d.	0.26	n.d.	0.47	0.50	n.d.
Cl	n.d.	0.3	0.4	0.4	n.d.	n.d.	n.d.	0.4	0.4	0.5	0.0	0.2	0.3	0.5	n.d.	b.d.	n.d.	b.d.	0.4	n.d.
total	100.6	98.7	99.5	98.8	99.9	99.8	99.9	99.8	99.4	99.4	99.5	99.1	99.6	99.2	99.9	99.6	99.6	99.9	99.1	100.0
ppm																				
V	137	133	137	100	135	140	115	143	128	133	115	136	113	70	103	72	72	158	69	71
Cr	104	98	96	73	83	86	69	100	106	128	87	120	130	40	72	37	41	102	45	44
Co	37	27	24	19	27	32	21	31	32	21	32	42	29	79	48	56	57	26	45	22
Ni	42	36	42	30	43	47	49	46	34	41	32	38	30	14	31	13	13	53	12	23
Zn	152	82	89	144	121	150	164	77	186	117	140	104	138	54	98	30	53	170	54	75
Ga	29	1	27	25	29	27	28	24	23	27	23	32	26	11	20	17	19	34	21	15
Rb	207	199	240	151	170	194	208	249	182	244	187	214	157	99	130	112	122	204	99	123
Sr	135	210	221	241	173	162	118	191	202	198	155	227	287	200	127	246	247	192	214	187
Y	27	40	38	38	39	44	37	34	33	30	32	29	34	30	36	32	39	48	39	49
Zr	136	142	168	160	173	178	167	155	134	143	129	142	123	181	247	238	336	215	229	436
Nb	15	15	16	14	15	16	18	15	14	14	13	13	11	10	13	10	14	17	12	15
Ba	372	561	567	623	426	517	541	574	500	508	530	736	508	702	701	599	830	523	219	341
Pb	8	<5	<5	6	34	36	24	<5	9	<5	15	9	8	<5	19	<5	<5	37	11	28
Th	8	14	15	7	18	16	14	11	10	11	11	13	11	12	9	12	16	26	15	21
Li	75	75	63	63	56	82	88	63	44	63	88	75	56	25	50	31	37	88	25	31

Table 3: *continued*

sample numbers: AD93-	21	22	23	24	25	26	27	28	29	30	31	32	33	34	35	36	37	38	39	40
wt. %	*scp*	*pe*	*scp*	*pe*	*pe*	*pe*	*ps*	*pe*	*pe*	*pe*	*pe*	*pe*	*pe*	*scp*	*scp*	*scp*	*pe*	*ps*	*pe*	*ps*
SiO2	73.11	56.25	71.19	58.50	62.79	55.57	71.42	46.46	63.77	58.99	56.93	42.50	58.07	46.97	54.10	71.77	57.26	73.11	40.90	69.87
TiO2	0.75	0.75	0.56	0.81	0.96	0.93	0.70	0.96	0.95	0.95	0.78	1.08	0.77	0.95	0.77	0.54	0.84	0.58	1.21	0.70
Al2O3	10.35	20.02	11.07	17.37	15.52	18.85	12.41	21.36	15.72	18.35	17.69	24.38	19.07	19.94	18.13	11.17	18.30	11.72	26.59	13.72
Fe2O3	0.80	1.86	1.64	2.05	1.87	2.37	1.58	1.95	1.85	1.75	1.60	2.83	2.02	8.24	2.19	0.77	1.92	1.92	2.65	1.06
FeO	2.7	6.2	2.2	5.5	5.3	7.1	3.55	7.0	5.1	4.1	5.3	7.1	5.7	1.35	5.3	2.75	6.1	1.9	8.1	3.8
MnO	0.10	0.06	0.06	0.13	0.10	0.11	0.07	0.07	0.08	0.04	0.08	0.07	0.06	0.06	0.08	0.11	0.10	0.14	0.33	0.06
MgO	1.46	3.71	1.78	4.50	3.48	4.03	2.32	6.30	3.81	4.25	5.36	6.79	3.85	7.26	5.49	1.79	3.63	1.95	5.37	2.31
CaO	4.81	1.28	5.59	3.14	1.63	0.64	1.09	6.03	0.58	1.63	5.38	3.17	0.52	3.16	5.94	5.11	2.28	4.32	8.07	2.17
Na2O	2.07	1.81	1.64	1.82	3.73	1.44	2.41	1.08	0.90	2.35	0.92	1.15	0.47	1.22	1.15	1.27	2.05	0.73	0.74	2.96
K2O	1.71	4.99	1.46	4.29	2.74	5.29	2.74	5.11	4.05	3.98	3.99	7.83	5.72	6.90	4.32	1.56	4.37	1.83	4.59	2.33
P2O5	0.20	0.17	0.16	0.18	0.23	0.25	0.18	0.23	0.24	0.21	0.19	0.24	0.18	0.22	0.19	0.15	0.20	0.16	0.23	0.19
H2O	0.83	3.19	1.12	1.67	1.77	3.21	1.35	2.40	2.94	1.95	1.60	3.69	3.38	1.33	2.08	1.01	2.15	1.17	2.25	1.12
CO2	0.36	n.d.	0.12	n.d.	n.d.	n.d.	n.d.	0.41	n.d.	0.12	n.d.	n.d.	n.d.	1.83	0.18	0.82	n.d.	0.72	n.d.	n.d.
Cl	0.2	n.d.	0.3	n.d.	n.d.	n.d.	n.d.	n.d.	n.d.	0.1	n.d.	n.d.	n.d.	0.1	0.3	0.2	n.d.	n.d.	n.d.	n.d.
total	99.5	100.3	98.9	100.0	100.1	99.8	99.8	99.4	100.0	98.7	99.8	100.8	99.8	99.6	100.2	99.0	99.2	100.3	101.0	100.3
ppm																				
V	71	168	69	129	124	153	85	156	115	130	131	141	155	112	111	63	147	71	231	91
Cr	47	108	43	84	90	96	63	119	83	89	98	163	94	100	114	48	97	45	153	60
Co	25	28	35	24	36	36	12	28	22	27	28	26	28	16	29	46	25	36	29	34
Ni	13	49	13	46	41	53	29	43	43	42	34	66	44	43	40	18	46	20	68	26
Zn	54	173	45	155	100	107	73	86	112	43	165	60	127	71	138	92	177	92	238	104
Ga	10	33	16	28	19	24	17	29	24	26	27	37	33	37	37	20	31	14	45	21
Rb	75	241	93	199	147	233	122	299	163	208	183	416	225	365	247	97	228	122	294	140
Sr	258	117	182	253	202	88	138	322	199	344	393	167	57	137	179	187	136	214	249	149
Y	50	40	36	39	45	41	27	38	38	38	25	27	38	34	29	30	44	33	56	40
Zr	461	140	228	166	264	196	209	180	227	219	150	198	143	199	143	203	170	211	245	244
Nb	15	14	11	15	15	14	11	18	16	15	14	19	14	18	16	10	17	12	22	15
Ba	643	585	280	660	263	763	639	732	830	682	812	1236	659	838	366	339	475	359	460	480
Pb	9	48	<5	28	31	8	<5	8	<5	8	<5	<5	<5	10	7	19	39	16	44	21
Th	27	11	11	13	13	15	13	17	12	11	16	<5	13	17	10	9	13	10	26	10
Li	18	69	25	69	37	44	31	75	37	44	50	88	44	69	50	31	69	31	101	37

Table 4: Rare earth element (REE) analyses of selected scapolite-bearing (*) and scapolite-free Kuiseb metasedimentary rocks.

Sample numbers: AD93-	5	8*	9*	13*	21*	24	30	32	35*
(ppm)									
La	41	40	33	31	49	41	41	47	37
Ce	91	82	68	62	94	90	82	99	73
Pr	10	10	8.5	7.4	12	10	9.8	11	9.3
Nd	40	39	33	30	46	40	39	46	35
Sm	8.9	7.6	7.3	6.7	9.6	8.6	7.9	9.7	7.0
Eu	1.5	1.3	1.3	1.1	1.4	1.5	1.3	1.7	1.2
Gd	8.1	7.1	6.5	5.9	9.1	7.8	7.0	8.6	6.4
Tb	1.2	1.2	0.96	0.95	1.4	1.2	1.0	1.3	1.0
Dy	7.5	7.0	6.1	5.8	8.7	7.9	6.2	7.6	6.2
Ho	1.5	1.3	1.1	1.2	1.8	1.6	1.3	1.5	1.1
Er	4.3	3.6	3.3	3.4	4.9	4.9	3.6	4.1	3.2
Tm	0.61	0.51	0.49	0.51	0.7	0.67	0.5	0.57	0.47
Yb	4.1	3.0	3.0	3.3	4.8	4.4	3.5	3.5	2.9
Lu	0.64	0.46	0.48	0.52	0.77	0.68	0.57	0.52	0.44
Eu/Eu*	0.58	0.58	0.63	0.58	0.49	0.61	0.57	0.61	0.59
La_N/Yb_N	6.74	8.97	7.4	6.32	6.87	6.26	7.89	9.04	8.57

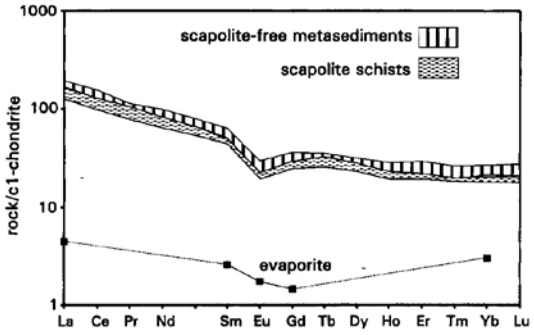

Figure 5: C1-chondrite-normalized REE patterns of the Kuiseb schists.

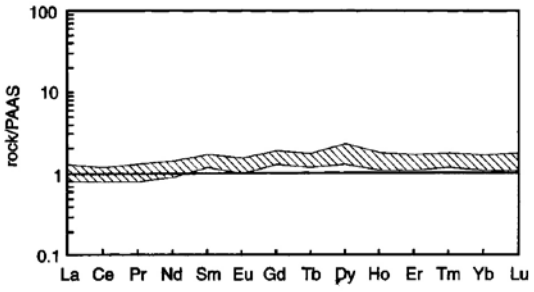

Figure 6: PAAS-normalized REE pattern of the Kuiseb metasedimentary rocks. Values for PAAS-normalization (Post-Archean average Australian shale) are from Nance and Taylor (1976).

should mirror the isotopic characteristics of the fluid phase which interacted with the Kuiseb schists.

The carbon isotopic composition of the investigated scapolite schist samples varies in a narrow range of -8 to -11 ‰ (Table 5, Fig.7) for both scapolite and calcite. A comparison of the data from the scapolite schists in the Khomas Hochland with carbon isotope distributions of the lithosphere and hydrosphere is depicted in Fig.8. In addition, the range of values for the Kuiseb graphite schists and a marble horizon near the Matchless amphibolite in the Khomas Hochland is shown (Kukla, 1992). The average $\Delta_{Scp\text{-}Cc}$ of 0.4 for the scapolite schists of the Kuiseb Formation confirms the assumption of Moecher *et al.* (1994) that fractionation between calcite and scapolite is essentially zero. During evaporation processes an enrichment of the heavier isotope in the remaining sediment occurs. If ocean water with a carbon isotopic composition of around zero is evaporated the resulting $\partial^{13}C$ -values are shifted to higher $^{13}C/^{12}C$ ratios. Thus, evaporation of ocean water is not responsible for the isotopic signature of carbon in the scapolite schists. Another source of CO_2 could be the organic carbon present in the form of graphite schists in the Khomas Hochland, with $\partial^{13}C$ values ranging between -19 and -23 ‰ (Kukla, 1992). Oxidation of this material at lower amphibolite facies temperatures would result in CO_2 with Carbon 9 to 10 ‰ less depleted than the equilibrium graphite (Bottinga, 1969). Thus, the carbon in the scapolites and calcites most likely originated from organic compounds in the sediment pile of the Kuiseb Formation. Derivation of scapolite- and calcite-CO_2 from the marble horizon in the Khomas Hochland by decarbonatization reactions is unlikely. The CO_2-calcite fractionation (Bottinga, 1969) at temperatures of 550-500°C would have required an enrichment of ^{13}C in the scapolite schists by about 2.5-3‰, compared to the marble carbon. We would suggest that this thin marble horizon was invaded by the same CO_2-rich fluid, which caused scapolitization in the siliciclastic rocks.

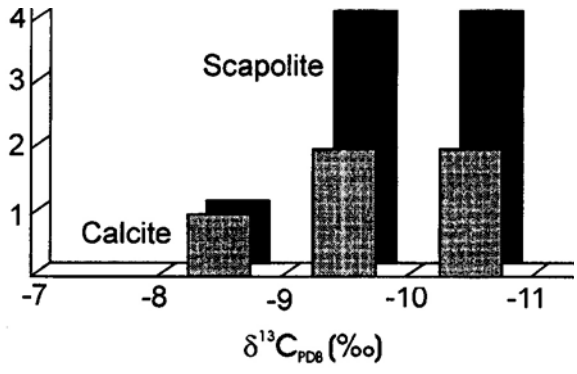

Figure 7: Carbon isotopic composition of CO_2 in sca and calcite of the Kuiseb scapolite schists.

Conclusions

Scapolitization of psammitic and pelitic meta-sedimentary rocks of the Kuiseb Formation gives evidence for the interaction between the metamorphic mineral assemblage and a fluid phase permeating the rocks at the time of metamorphism. On the basis of geochemical data, we exclude an evaporitic origin for the scapolite schists within the Kuiseb Formation. The REE patterns of both scapolite-bearing and scapolite-free Kuiseb schists reveal no evaporitic signature but show a strong similarity to the characteristics of the average upper continental crust represented by PAAS. Furthermore, this interpretation is supported by light $\partial^{13}C$ values of CO_2 in scapolite and calcite, which cannot be the result of evaporation. A conclusive explanation for the light carbon isotopic composition of the scapolite schists in the Kuiseb Formation is derivation from an organic source, probably from graphite within the Kuiseb deposits themselves. This conforms to the uniformity of REE patterns of scapolite-bearing and scapolite-free metasedimentary rocks. If an external fluid input is assumed, changes in the REE contents and fractionation patterns would be expected because chlorine-bearing fluids are favoured complexing ligands for REE. We thus assume a scenario of expulsion of CO_2- and Cl-rich pore fluids from the sediments during progressive deformation leading to the scapolite-forming reaction in the Kuiseb metaturbidites which postdates the D_3 deformation. The fluids concentrated and ascended along shear zones into higher levels of the sediment pile where scapolite formation occurred at the expense of pre-existing plagioclase.

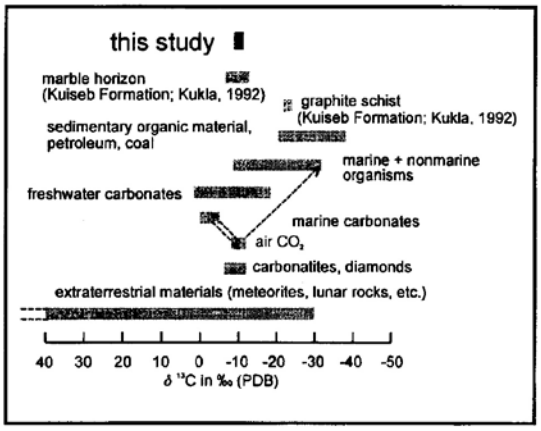

Figure 8: Comparison of $\delta^{13}C$ data from scapolite schists in the Khomas Hochland with carbon isotope distribution of the lithospere and hydrosphere (after Hoefs, 1980). Data for Kuiseb graphite schists and marble in the Khomas Hochland from Kukla (1992).

Table 5: Stable isotope analyses of carbon from scapolite and calcite.

Sample	scapolite $\delta^{13}C_{PDB}$	calcite $\delta^{13}C_{PDB}$
AD93-2	-9.3	-9.2
AD93-3	-9.1	
AD93-4C	-10.2	-10.2
AD93-8	-8.8	
AD93-9	-9.3	-9.1
AD93-13	-10.2	-10.2
AD93-19	-10.6	-8.8
AD93-23	-10.0	
AD93-35	-10.5	

Acknowledgements

This project is funded by the Deutsche Forschungsgesellschaft. Thanks are due to Jorg Erzinger at the GeoForschungsZentrum Potsdam for usefull discussions during sample preparation and REE analyses. We highly appreciate the constructive critisism of this manuscript by Hartwig Frimmel, University of Cape Town, and an anonymous reviewer. The final version benefited much from the review of Nigel Cook which was particularly helpful in improving the English.

References

Behr, H.J., Ahrendt, H., Porada, H., Röhrs, J. and Weber, K. 1983. Upper Proterozoic playa and sabkha deposits in the Damara orogen, SWA/Namibia. *In*: R. McG. Miller (ed.), *Evolution of the Damara Orogen of SouthWest Africa/Namibia*, Spec. Publ. geol. Soc. S. Afr., **11**, 1-20.

Bottinga, Y. 1969. Carbon isotope fractionation between graphite, diamond and carbon dioxide. *Earth & Planet. Sci. Lett.*, **5**, 301-307.

Bühn, B., Häussinger, H., Kramm, U., Kukla, C., Kukla, P.A. and Stanistreet, I.G. 1994. Tectonometamorphic patterns developed during Pan-African continental collision in the Damara Inland Belt, Namibia. *Chem. Erde*, **54**, 329-354.

Evensen, N.M., Hamilton, P.J. and O'Nions, R.K. 1978. Rare-earth abundances in chondri tic meteo-rites. *Geochim. Cosmochim. Acta*, **42**, 1199-1212.

Goldberg, E.D., Koide, M., Schmitt, R.A. and Smith, R.H. 1963. Rare-earth distributions in the marine environment. *J. Geophys. Res.*, **68**, 4209-4217.

Gómez-Pugnaire, M.T., Franz, G. and Sánchez-Vizcaino, V.L. 1994. Retrograde formation of NaCl-scapolite in high pressure metaevaporites from the Cordillera Béticas (Spain). *Contrib. Mineral. Petrol.*, **116**, 448-461.

Häussinger, H., Okrusch, M. and Scheepers, D. 1993. Geochemistry of premetamorphic hydrothennal alteration of metasedimentary rocks associated with the Gorob Massive Sulfide Prospect, Damara Oro-

gen, Namibia. *Econ. Geol.*, **88**, 72-90.

Hartmann, O., Hoffer, E. and Haack, U. 1983. Regional metamorphism in the Damara Orogen: interaction of crustal motion and heat transfer. *In*: R McG. Miller (ed.), *Evolution of the Damara Orogen of SouthWest Africa/Namibia*. Spec. Publ. geol. Soc. S. Afr., **11**, 233-241.

Hawkesworth, C.J., Kramers, J.D. and Miller, RMcG. 1981. Old model Nd ages in Namibian Pan-African rocks. *Nature,* **289**, 278-282.

Hoefs, J. 1980. *STable 1sotope geochemistry*. Springer- Verlag, Berlin, 208 pp.

Høgdahl, O.T., Melson, S. and Bowen, V.T. 1968. Neutron activation analysis of lanthanide elements in seawater. *In*: Baker, RA (ed.), *Trace inorganics in water*. Adv. Chem. Ser., **73**, 308-325.

Kukla, C. 1993. Strontium isotope heterogeneieties in amphibolite facies, banded metasediments - A case study from the Late Proterozoic Kuiseb Formation of the southern Damara Orogen, central Namibia. *Mem. geol. Surv. Namibia*, **15**, 139 pp.

Kukla, P.A. 1990. Unususal scapolitization of Late Proterozoic deep-sea fan sequences in an amphibolite-grade metamorphic terrain, Damara Orogen, Central Namibia. *Eur. J. Mineral. Beih.*, **2**, 145.

Kukla, P.A. 1992. Tectonics and sedimentation of a late Proterozoic Damaran convergent continental margin, Khomas Hochland, Central Namibia. *Mem. geol. Surv. Namibia*, **12**, 95pp.

Kukla, P.A and Stanistreet, I.G. 1991. Record of the Damaran Khomas Hochland accretionary prism in Central Namibia: refutation of an 'ensialic' origin of a Late Proterozoic orogenic belt. *Geology,* **19**, 473-476.

McLennan, S.M. 1989. Rare earth elements in sedimentary rocks: influence of provenance and sedimentary processes. *In*: Lipin, B.R. and McKay, G.A (eds.) *Geochemistry and mineralogy of rare earth elements*. Reviews in Mineralogy, **21**, 169-200.

McLennan, S.M., Taylor, S.R, McCulloch, M.T. and Maynard, J.B. 1990. Geochemical and Sr-Nd isotopic composition of deep-sea turbidites: crustal evolution and plate tectonic association. *Geochim. Cosmochim. Acta*, **54**, 2015-2050.

Mineyev, D.A. 1963. Geochemical differentiation of the rare-earth elements. *Geochemistry,* **12**, 1129-1149.

Moecher, D.P., Valley, J.W. and Essene, E.J. 1994. Extraction and carbon isotope analysis of CO_2 from scapolite in deep crustal granulites and xenoliths. *Geochim. Cosmochim. Acta*, **58**, 959-967.

Moine, B., Sauvan, P. and Jarousse, J. 1981. Geochemistry of evaporite-bearing series, a tentative guide for the identification of meta-evaporites. *Contrib. Mineral. Petrol.*, **76**, 401-412.

Mora, C.L and Valley, J.W. 1989. Halogen-rich scapolite and biotite: implications for metamorphic fluid - rock interaction. *Am. Mineral.*, **74**, 721-737.

Nance, W.B. and Taylor, S.R 1976. Rare earth element patterns and crustal evolution - L Australian post-Archaean sedimentary rocks. *Geochim. Cosmochim. Acta*, **40**, 1539-1551.

Oliver, N.H.S., Wall, V.J. and Cartwright, I. 1992. Internal control of fluid compositions in amphibolite-facies scapolitic calc-silicates, Mary Kathleen, Australia. *Contrib. Mineral. Petrol.*, **111**, 94-112.

Orville, P.M. 1975. Stability of scapolite in the system Ab-An-NaCl-$CaCO_3$ at 4 kb and 750°C. *Geochim. Cosmochim. Acta*, **39**, 1091-1105.

Piper, D.Z. 1974. Rare earth elements in ferromanganese nodules and other marine phases. *Geochim. Cosmochim. Acta*., **52**, 1373-1382.

Ronov, A.B., Balashov, Yu.A, Girln, Yu.P., Bratishko, R.Kh. and Kazakov, G.A. 1974. Regularities ofrare-earth element distribution in the sedimentary shell and in the crust of the earth. *Sedimentology,* **21**, 171-193.

Rothe, P. and Hoefs, J. 1977. Isotopengeochemische Untersuchungen an Karbonaten der Ries-See-Sedimente der Forschungsbohrung Nördlingen. *Geol. Bavaria*, **75**, 59-66.

Shaw, D.M. 1960. The geochemistry of scapolite. Part L previous work and mineralogy. *J. Petrol.*, **1**, 218-260.

Wedepohl, 1970. *Handbook of Geochemistry, Vol. 11/5, Elements La (57) to U (92)*. Springer-Verlag, Berlin.

Zuleger, E. and Erzinger, J. 1988. Determination of the REE and Y in silicate materials with ICP-AES. *Fresenius Z. Anal. Chem*., **332**, 140-143.

Communs geol. Surv. Namibia, ***11*** *(1996), 33-48*

U-Pb and Rb-Sr isotopic data for the Mooirivier Complex, Weener Igneous Suite and Gaub Valley Formation (Rehoboth Sequence) in the Nauchas area and their significance for Paleoproterozoic crustal evolution in Namibia

Thomas Becker, Bent Tauber Hansen, Klaus Weber and Bettina Wiegand

Institut für Geologie und Dynamik der Lithosphäre
Goldschmidtstr. 3, D-37073 Göttingen, Germany

U-Pb zircon ages and Rb-Sr whole rock ages have been obtained for several intrusive and volcanic rocks of the Rehoboth Sequence (Weener Igneous Complex, WIC and Gaub Valley Formation, GVF) and the pre-Rehoboth basement (Mooirivier Complex) in the Nauchas area of Namibia. U-Pb zircon upper discordia intercepts define similar ages for the WIC (~1765 and ~1767 Ma), associated granitoids (~1762 Ma and ~1743 Ma), as well as for the pre-Rehoboth Mooirivier Complex (~1725 Ma) and the Neuhof (Kamasis) Formation (~1784 Ma; Burger and Walraven, 1978). These data suggest that the Rehoboth Sequence and the pre-Rehoboth basement are broadly coeval. Rb-Sr whole rock data define errorchrons of ~1752 Ma with an initial $^{87}Sr/^{86}Sr$ ratio of 0.7034 for the GVF and of ~1620 Ma with an initial ratio of 0.7047 for the WIC. An intense disturbance of this isotopic system during post-emplacement alteration processes is inferred.

In a regional context, comparable ages have been determined in crustal segments extending from southern Brazil through southern Africa to equatorial Africa and constitute a major crust-forming event during late Paleoproterozoic times (Eburnian-Ubendian cycle). Similarities in age and rock association of other inliers in Namibia (i.e. Epupa and Huab Inlier, Abbabis Inlier, Namaqua Metamorphic Complex) suggest that much of the pre-Damara basement was formed during this event, in magmatic arc settings.

Introduction

Various magmatic and sedimentary pre-Damara rocks exposed in several inliers along the southern margin of the Damara orogen have been grouped in the past under the sack terms Rehoboth Magmatic Arc (RMA) (Watters, 1976) or Rehoboth Basement Inlier (RBI) (Ziegler & Stoessel, 1993). According to SACS (1980), the respective suites of rocks are subdivided into: (a) high-grade metamorphic complexes and formations of assumed pre-Rehoboth age (Neuhof & Elim Formations, Mooirivier Complex); (b) the ca. 1800 Ma old Rehoboth Sequence (Marienhof, Billstein and Gaub Valley Formations); and (c) the *ca.* 1200 Ma Sinclair Sequence (Nückopf, Grauwater, Eskadron, Doornpoort and Klein Aub Formations). The stratigraphy and regional extent of these pre-Damara units are presented in Table 1 and Figure 1, respectively. This lithostratigraphy is based mainly on field evidence because geochronological data have been absent. However, since most primary contacts between different formations have been overprinted tectonically by the Damara event or earlier orogenies, this classification is preliminary at present. Table 2 shows geochronological data for the pre-Damara units of Namibia. It is obvious that some of the rocks which have been attributed to the Sinclair Sequence are of Rehoboth age and vice versa (i.e. Nückopf, Marienhof, Gaub Valley and Neuhof Formations, Weener Igneous Complex). This is indicative of great petrographic similarities between rocks of different age and probably different origin. Furthermore, besides some poorly defined Sm-Nd ages varying from 1600 to 2600 Ma (Ziegler & Stoessel, 1993) and two doubtful zircon dates, ages older than 1860 Ma have not been recorded in rocks of magmatic origin in this area. Available ages scatter with a bimodal distribution, in the ranges *ca.* 1000 to 1200 Ma and *ca.* 1700 to 1860 Ma, suggesting two distinct magmatic events rather than the continuous crustal reworking proposed by Ziegler and Stoessel (1993).

The stratigraphic and genetic problems outlined above are particularly significant for the volcaniclastic Gaub Valley Formation (GVF) and the Weener Igneous Complex (WIC). The GVF occurs within the Southern Margin Zone of the Damara Orogen as a long NE-SW extending inlier with a total length of 60 km and a maximum width of 20 km (in the type locality), as well as several smaller isolated inliers (Fig. 1). In the past the GVF has been classified as pre-Damara basement, probably older than 1500 Ma (SACS, 1980; Hill, 1975). However, ages between 1000 and 1200 Mahave been obtained on subvolcanic granites (Pfurr *et al.*, 1991) in one of the smaller inliers (Rostock Inlier). Accordingly, these units have been interpreted as either initial rift volcanic rocks of the Damara Sequence or collision-induced rift volcanic rocks of the Sinclair Sequence (Pfurr, 1990). Similar problems apply to the WIC which is intrusive into the GVF and other units of the Rehoboth Sequence (Table 2).

These problems led to a follow-up study of the GVF and WIC in their type localities south of Gamsberg, involving detailed mapping as well as geochemical and isotopic investigations. The possible co-magmatic evolution of the WIC and GVF within a caldera cycle became evident during field work (Becker *et al.*, 1994), a model which required substantiation with isotopic and geochemical data. Results of the isotopic investigation are presented in this paper.

Analytical procedures

Heavy mineral separates were extracted from samples, 20-40 kg in weight, following procedures outlined by Teufel (1988). Zircon concentrates were separated

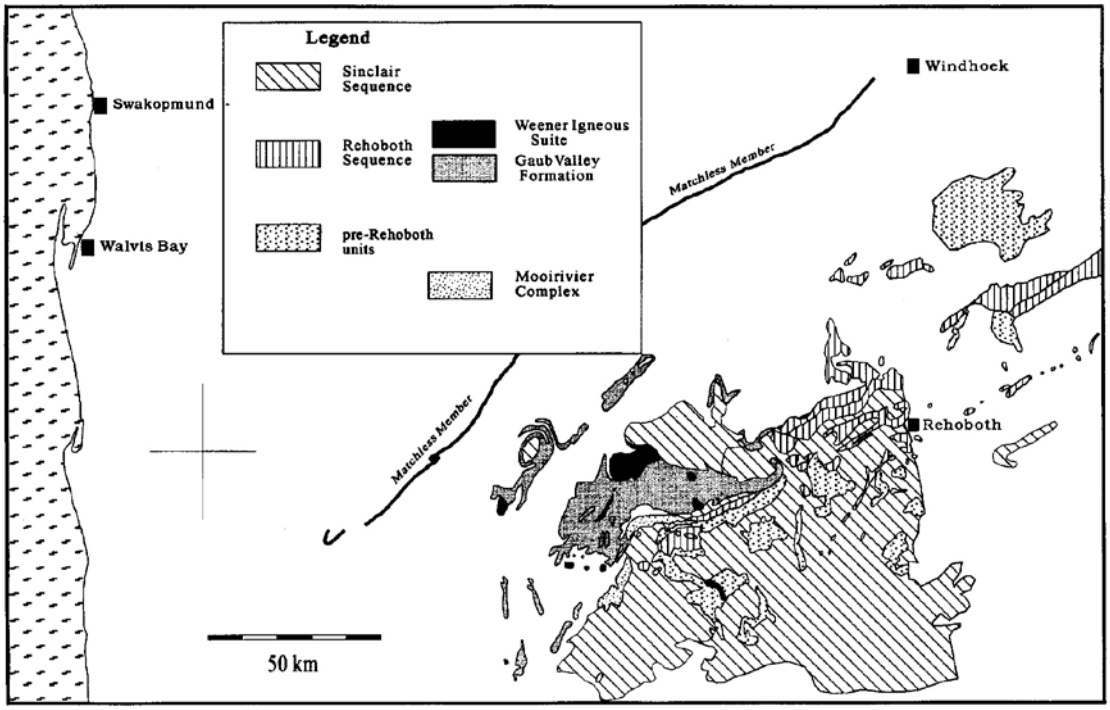

Figure 1: Simplified geological map of the pre-Damara units within the southern Damara Orogen (Matchless Member is shown for orientation)

in fractions of different size and magnetic susceptibility. Only the diamagnetic zircon concentrates were used for further investigation. A selection of 3-5 mg inclusion-poor crystals of each fraction were handpicked for isotope analyses.

The chemical procedures for the zircon analyses followed the method of Krogh (1973). To determine the concentrations of uranium and lead, a highly enriched $^{208}Pb/^{235}U$ mixed spike was added to an aliquot of the zircon solutions. Purification of uranium and lead was carried out on ion exchange microcolumns. Uranium and lead measurements were obtained on a Teledyne 12 inch radius/90° sector mass spectrometer using the rhenium single filament technique. The samples were loaded with Ta_2O_5 (uranium) and H_3PO_4 plus silica gel (lead). Lead isotopic data were corrected for common lead and the analytical blank. The initial lead ratios for the correction of nonradiogenic lead were calculated after the two stage model of Stacey & Kramers (1975) corresponding to an age of 1765 Ma. For age calculations, the constants recommended by IUGS were applied (Steiger & Jäger, 1977). The errors and error correlations in the $^{206}Pb/^{238}U$ and $^{207}Pb/^{235}U$ data were calculated according to Ludwig (1980). They are based on assigned errors of the U-Pb ratio in the spike (0.15%), in the initial ratios $^{207}Pb/^{204}Pb$ and $^{206}Pb/^{204}Pb$ (1 %), in the blank lead (1 %), and its concentration (50%). The correlation factor for initial and blank lead was assigned 0.7. The error ellipses for the data points have been drawn at a confidence level of 95% on the concordia diagrams. A York II regression calculation was used to obtain the ages and errors of intercepts of the best-fit line with the concordia (York, 1969). All errors are given at a 2 σ confidence level.

For Rb-Sr analyses, whole rock aliquots were spiked with a $^{84}Sr/^{87}Rb$ mixed spike prior to dissolution. Separation of Rb and Sr was made by column chemistry using quartz columns filled with cation exchange resin (Bio-Rad* 50 W x 8). The Rb and Sr measurements were made using the tantalum double filament technique

Table 1: Stratigraphy of the pre-Damara units within the southern Damara Orogen (after SACS, 1980).

Sequence	Formation	contact relationship	intrusive unit
Sinclair Sequence	Klein Aub		
		unconformity	
	Doornpoort		
	Eskadron		
		unconformity	
	Grauwater		
	Dordabis		
		disconformity	Gamsberg Granite Suite
	Nückopf		
Rehoboth Sequence	Gaub Valley		Weener Igneous Suite
		unconformity to Marienhof F.	Doornboom Complex
	Billstein	(possibly equivalent to Billstein F.)	Alberta Complex
		unconformity	Swartmodder Granite
	Marienhof		
Pre-Rehoboth units	Elim	correlate of Khoabendus Group	
	Neuhof	closely associated with the Mooirivier C.	Naub Diorite
		unconformity	
	Mooirivier Complex	mainly as xenoliths within the Gamsberg Granite Suite	

for Rb (sample loaded with H_2O^{4*}), and the tantalum single filament technique for Sr (sample loaded with 0.5N $H_3PO_4^{2*}$). Errors based on replicate analyses using standard procedures are 1 % for $^{87}Rb/^{86}Sr$ and 0.01 % for $^{87}Sr/^{86}Sr$. The data for Rb were corrected for mass fractionation compared to standard measurements. For age calculations, the constants recommended by the IUGS (Steiger & Jäger, 1977) were used, with statistical regression calculated according to the method of York (1969). All errors are given at a 2 σ confidence level.

U-Pb zircon ages

Orthogneissic WIC samples have been analysed from the type locality (2), from smaller intrusions within the GVF at distances of 5 and 15 km from the main body (2), and from the Mooirivier Complex (1). Since none of the pyroclastic samples which had been previously collected from the GVF contained zircons, a granitic pebble from the basal clastic-dominated GVF was taken to provide at least a maximum U-Pb zircon age for this formation. The sample positions and their respective U-Pb zircon ages (upper intercept) are shown in figure 2.

Weener Igneous Complex and smaller intrusions within the Gaub Valley Formation

The oval-shaped WIC with dimensions of *ca.* 13 x 7 km is the largest of several tonalitic to granodioritic intrusions in the western part of the Rehoboth area. They are intrusive into the Mooirivier Complex, the Elim and the Gaub Valley Formations, and were in turn crosscut by the Gamsberg and Piksteel Intrusive Suites (Fig. 1, Table 1). Because of similar petrographic characteristics and field relationships, these granitoids were combined as the Weener Igneous Suite by De Waal (1966). However, Rb-Sr age determinations by Reid *et al.* (1988), Seifert (1986) and one U-Pb zircon analysis (one fraction) by Ziegler and Stoessel (1991) on different bodies yielded considerably varying ages of *ca.* 1200 Ma, *ca.* 1870 Ma, and *ca.* 1720 Ma, respectively, probably indicative of several generations of magma genesis.

Two samples were collected from the WIC in its type area south of the Gamsberg. The fine- to medium-grained and variably deformed rocks are clearly of igneous origin, but have been subjected to at least one event of low-grade metamorphism during Pan African (500 Ma) orogeny. Numerous small mafic inclusions and, in some places, large fragments of the country rock

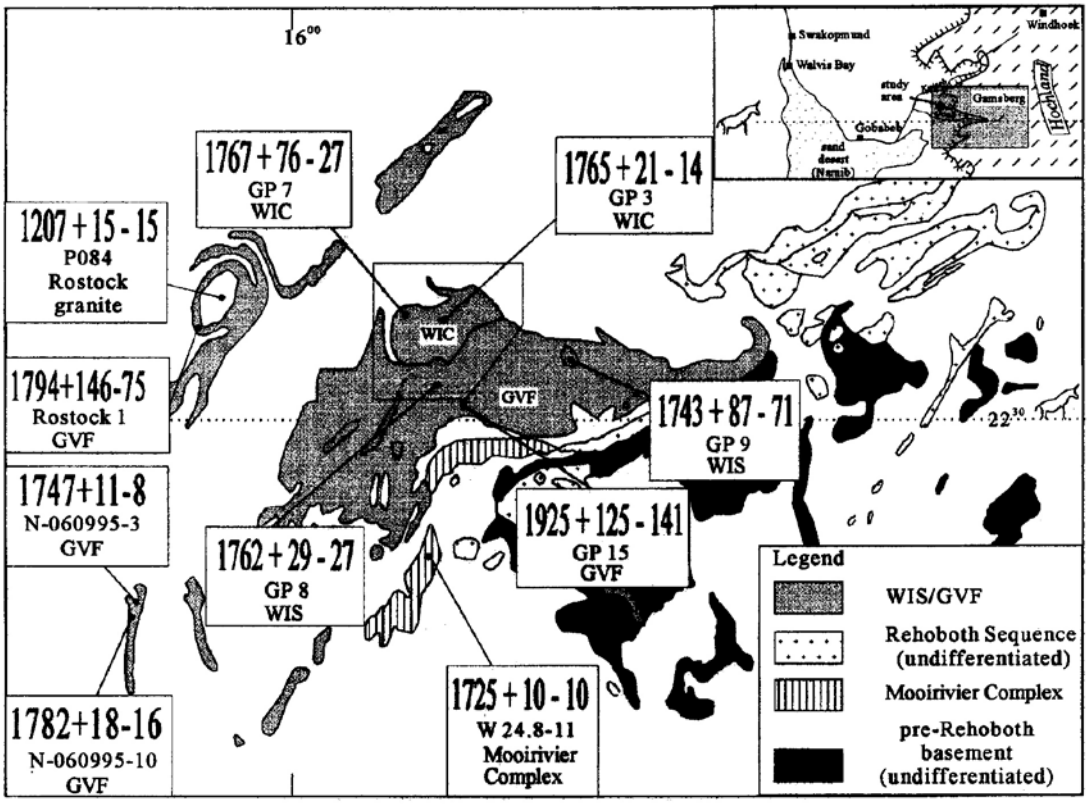

Figure 2: Sample positions and results of the U-Pb isotopic analyses (upper discordia intercepts) of the Weener Igneous Complex, the Gaub Valley Formation and the Mooirivier Complex (ages in Ma). P084 from Pfurr (1990), N-060995 and N-060995-10 from Nagel *et al.* (1996).

are distinctive features. The mineral assemblage comprises quartz, plagioclase and biotite as major components, with varying amounts of hornblende and epidote. Apatite, zircon, chlorite, garnet, muscovite and opaque minerals occur in minor to accessory amounts. Details of the WIC and surrounding lithologies were given by Becker *et al.* (1994) and Becker (1995).

Two samples were taken from smaller granitic intrusions within the GVF (GP8, GP9). Their modal composition is characterized by quartz, two feldspars, biotite and muscovite as major constituents and chlorite, zircon, apatite and ilmenite as minor to accessory phases. The rocks are nearly undeformed and the original magmatic texture is largely preserved. Metamorphism is represented only by grain size reduction of the quartz and the development of high angle grain boundaries. From field evidence it is impossible to attribute these intrusions to the 1200 Ma old Gamsberg Suite or to the older Weener Igneous Suite.

Zircons separated from the two samples of the WIC are homogeneous in typology and composition (Fig. 3). Euhedral prismatic to long prismatic crystals with simple crystal faces are dominant, although many show evidence of magmatic corrosion. In the classification diagram of Pupin (1980), the population covers fields characteristic for zircons derived from mantle magmas, with incipient crystallization temperatures exceeding 900°C. The zircons are light red to colourless and commonly contain inclusions of small randomly oriented crystallites (rounded and euhedral), fluid inclusions and biotite inclusions. In most grains, cathodoluminescence revealed rims with an oscillatory zoning oriented parallel to the c-axis and often small euhedral cores (Fig. 4). These features probably reflect a change in magma composition during growth and a possible inherited component.

Zircon typologies from the granitic intrusions are more variable in comparison to the zircon population of the WIC. In addition to the types described above, there is an important second group characterised by a smaller length/width ratio and a higher degree of metamictisation and corrosion. Inclusion trails and corroded surfaces are attributed to magmatism. Cathodoluminescence revealed the presence of small euhedral dark cores and oscillatory zoning. No metamorphic overgrowths were recognized. .

Results of the isotope analyses are presented in Table 3 and conventional $^{206}Pb/^{238}U$-$^{207}Pb/^{235}U$ concordia diagrams (Fig. 5) after Wetherill (1956). For both WIC samples, similar data have been obtained with low uranium (140-185 ppm) and common lead (0.19-1.24 ppm) concentrations and low degrees of discordance. Therefore, it may be assumed that the isotope system has remained almost undisturbed and the resulting ages probably reflect the time of zircon crystallization. In sample GP3 five size fractions are closely grouped with the coarser fractions having lower concentrations of U and a lower degree of discordance, suggesting that Pb loss was primarily a function of uranium content. The best fit chord (MSWD = 0.99) through the 5 points has intercepts of 1764 +21-14 Ma and 420 ± 250 Ma. Sample GP7 displays a similar pattern with a negative correlation between grain size and uranium concentration as well as degree of discordance. Since the fractions are grouped even more closely than in GP3 the lower intercept is poorly defined and has been constrained at 500 Ma, the time of Damaran metamorphism. Four fractions yielded an upper intercept of 1768 +53-24Ma (MSWD = 0.93). Fraction 3 has been excluded from analysis because of the large deviation from the other data points.

Zircons from the smaller intrusives (GP8, GP9) exhibit higher U (350-620 ppm) and common Pb (2.55-36.74 ppm) concentrations, and a higher degree of discordance compared to the WIC. The higher U concentrations coincide with the more evolved magma composition of these samples. The best fit chords have yielded well defined upper intercepts of 1762 +29-27 and 1743 +87-61 Ma, which are again interpreted as the time of zircon crystallization, and lower intercepts of 49 +57-58 and 55 +136-145 Ma, respectively, indicating Tertiary to Cretaceous Pb loss.

Gaub Valley Formation (GVF)

The Gaub Valley Formation is regarded as the stratigraphically highest unit of the Rehoboth Sequence. It is divided into a clastic dominated lower part and a volcaniclastic upper part. The comagmatic evolution of the GVF and WIC has been inferred from field observations. Since no previously collected volcaniclastic samples from the type locality contain any zircons, a gneissic porphyritic boulder (GP15) from the basal GVF was collected and analysed to provide constraints on the age of the provenance and the maximum age for the GVF .

The idiomorphic transparent zircons of this sample are again prismatic to long prismatic with simple crystal faces, and varying in colour from colourless to light red. Cathodoluminescence revealed a zoning and the presence of small euhedral cores. However, the isotopic data differ from those obtained for the previous samples with respect to an increased fraction of common Pb (up to 48.2%), and accordingly a large error in the age calculations. Within the fractions 2 to 5 the grain size correlates negatively with U concentration and degree of discordance but not with common Pb. In the concordia diagram the best fit chord (MSWD = 0.428) has poorly defined upper and lower intercepts of 1929 +125 -141 Ma and 439 +125 -141 Ma, respectively.

Additionally, three volcaniclastic samples of the GVF have been analysed from smaller inliers of the Rostock and Saagberg area (Fig. 2) (Nagel *et al.*, 1996). In the concordia diagram the upper discordia intercepts are 1794 + 146-75 Ma (MSWD = 0.19),1747 +11-8 Ma (MSWD = 2.8) and 1782 +18 -16 Ma (MSWD = 7.69), and have been interpreted as time of crystallization. The

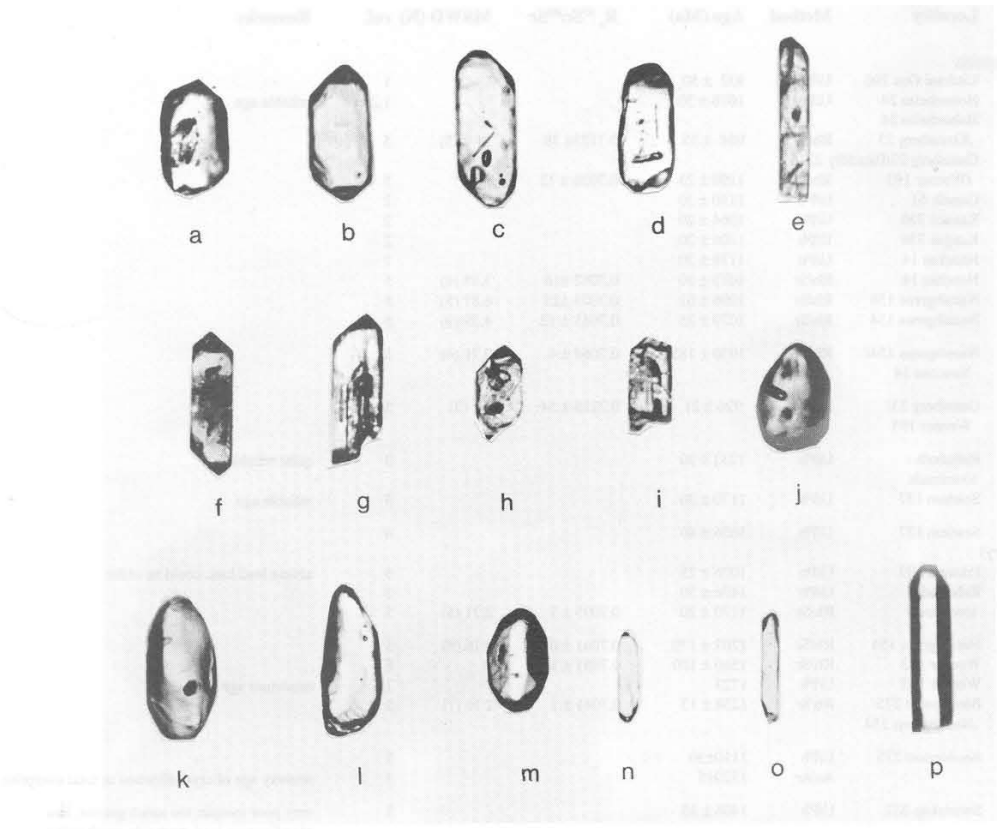

Figure 3: Zircon typologies of samples GP3 and GP7. a-e: clear, idiomorphic; f-i: idiomorphic with small inclusions; j-m: clear, rounded; n-p: clear, long prismatic crystals.

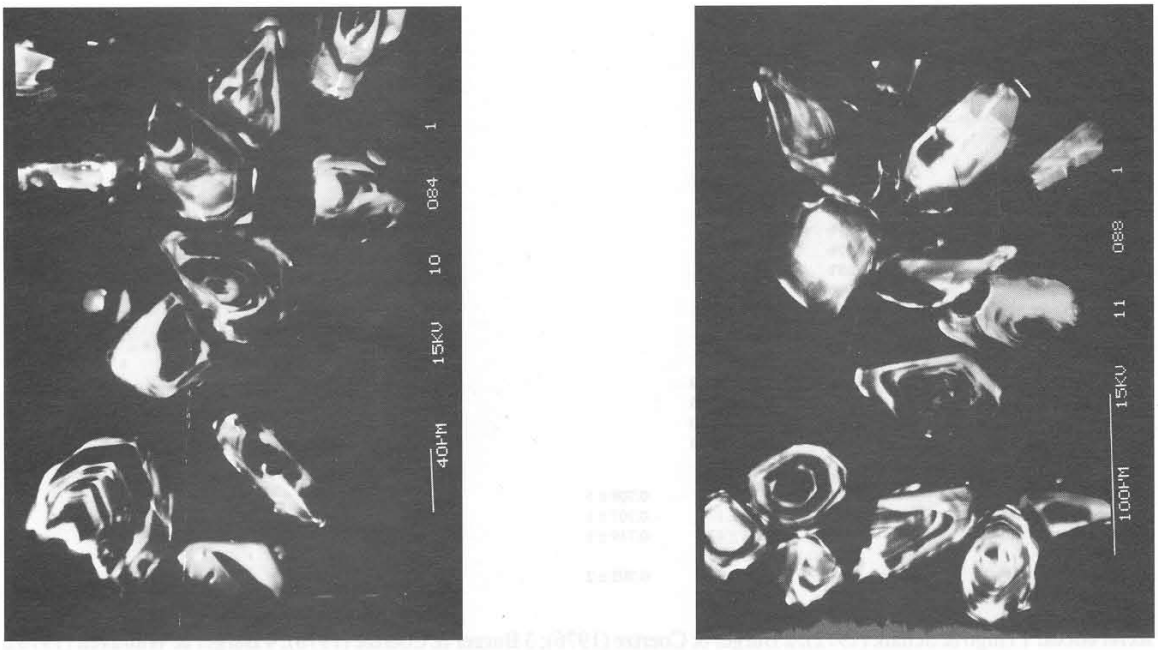

Figure 4: SEM photographs of polished crystals (cathodoluminescence mode), showing small rounded to euhedral cores and zoned rims.

Table 2: Geochronological data for the pre-Damara units of Namibia and neighbouring areas.

Lithological unit	Locality	Method	Age (Ma)	R_o $^{87}Sr/^{86}Sr$	MSWD (N)	ref.	Remarks
Central Namibia							
	Uitdraai Oos 296	U/Pb	932 ± 50			1	
	Hohenheim 24	U/Pb	1078 ± 30			1,2	reliable age
	Hohenheim 24 /Gamsberg 23	Rb/Sr	984 ± 55	0.7123± 39	21.0 (5)	5	
Gamsberg	Gamsberg 23/Picadilly 221 /Weener 193	Rb/Sr	1190 ± 23	0.7026 ± 12		5	
Granite	Ganeib 61	U/Pb	1150 ± 30			2	
	Kanaus 336	U/Pb	1064 ± 20			2	
Suite	Kangas 336	U/Pb	1104 ± 20			2	
	Nauchas 14	U/Pb	1178 ± 20			2	
	Nauchas 14	Rb/Sr	1073 ± 20	0.7082 ±16	3.48 (4)	5	
	Namibgrens 154	Rb/Sr	1096 ± 62	0.7075 ±25	6.87 (5)	5	
	Namibgrens 154	Rb/Sr	1079 ± 25	0.7081 ± 12	4.39 (9)	5	
Post-Gamsberg mafic dykes	Namibgrens 154/ Nauchas 14	Rb/Sr	1030 ± 185	0.7064 ± 4	0.71 (4)	5	
Post-Gamsberg aplites	Gamsberg 23/ Weener 193	Rb/Sr	926 ± 21	0.7215 ± 54	(3)	5	
Marienhof F. (acid lava)	Rehoboth - townlands	U/Pb	1232 ± 30			3	quite reliable
rhyolite	Sesriem 137	U/Pb	1170 ± 30			3	reliable age
Barby F. (quartz porphyry)	Sesriem 137	U/Pb	1656 ± 40			4	
Piksteel Suite	Piksteel 209	U/Pb	1076 ± 25			3	severe lead loss, could be older
	Rehoboth - townlands	U/Pb	1476 ± 30			2	
		Rb/Sr	1170 ± 20	0.7095 ± 7	2.21 (5)	5	
Weener Igneous Complex	Namibgrens 154	Rb/Sr	1207 ± 170	0.7041 ± 6	0.16 (5)	5	
	Weener 193	Rb/Sr	1560 ± 100	0.7051 ± 14		6	
	Weener 193	U/Pb	1723			7,8	minimum age
	Biesiepoort 275/ Namibgrens 154	Rb/Sr	1238 ± 13	0.7041 ± 1	2.16 (7)	5	
Biesiepoort granite	Biesiepoort 275	U/Pb	1110±30			3	
		Ar/Ar	1529±5			3	primary age of crystallization or total overprint
Kam Kam	Swartskap 332	U/Pb	1406 ± 35			3	very poor sample, too much granite, loss of radiogenic lead, probably much older
	Kam Kam 369	U/Pb	986 ± 20			3	minimum age, possibly higher - loss of lead
Kamasis F. (acid lava)	Olivantsvloer 453	U/Pb	1328 ± 25			4	minimum age
Kamasis F.	Neuras 330	U/Pb	1784 ± 45			4	reliable minimum age
Granite	Rehoboth village	U/Pb	1784 ± 45			4	reliable minimum age
Neuhof F.	Hebron 136	U/Pb	1294 ± 25			3	minimum age, could be much older
Abbabis Complex	Central Namibia	U/Pb	1925 ± 300			15	
Kheis Tectonic Province							
Groblershoop Schist F.		U/Pb	1780			9	
Nückopf F. (porphyry)	Auchas 347	U/Pb	1770 ± 35			3	a minimum age at least
Dagbreek F.		U/Pb	1800-2100			10	inherited age
Hartley Andesite F.	Rb/Sr		2026 ± 180	0.7044 ± 3		11	
Outjo district							
Acid lava	Suiderkruis 668	U/Pb	1765 ± 40			2	
Granite	Annabis 677	U/Pb	1815 ± 40			2	
Granodiorite		U/Pb	1850 ± 40			2	
Porphyry Granite		U/Pb	1860 ± 40			2	
Quartz porphyry		U/Pb	1860 ± 40			2	
N. Namibia							
Fransfontein Suite		K/Ar	±2100			12	
Epupa Complex		U/Pb	1795+33/-29			13	
Huab Complex		U/Pb	1811+39/-35			13	
Post-Huab Granitic Gneiss		U/Pb	1749+78/-70			13	
Oas Syenite		U/Pb	2124+68/-54			13	inherited age
Namaqua Metamorphic Complex - S. Namibia							
Tsams/Hom F.		Rb/Sr	1658 ± 280	0.709 ± 5		14	
Khurisberg Subgroup		Rb/Sr	1848 ± 174	0.707 ± 1		14	
Vioolsdrif Suite		Rb/Sr	1676 ± 42	0.719 ± 1		14	
Vioolsdrif Suite		Pb/Pb	1839 ± 58			14	
Gladkop Suite		Rb/Sr	1824 ± 70	0.705 ± 2		14	
Gladkop Suite		Pb/Pb	1770 ± 187			14	

References: 1 Hugo & Schalk (1972); 2 Burger & Coertze (1976); 3 Burger & Coertze (1978); 4 Burger & Walraven (1978); 5 Reid *et al.* (1988); 6 Seifert (1986); 7,8 Ziegler & Stoessel (1991, 1992, 1993); 9 Moen (1976); 10 Barton & Burger (1983); 11 Crampton (1974); 12 De Carvalho (1970); 13 Tegtmeyer & Kröner (1985); 14 Barton (1983); 15 Jacob *et al.* (1978)

Table 3: Results of zircon analyses.

sample	fraction	concentration				measured ratios				calculated ratios		calculated ages (2-stage model, Stacey & Kramers, 1975)		
	[µm]	U [ppm]	Pb^{tot} [ppm]	Pb^{rad} [ppm]	Pb^{com} [ppm]	$^{206}Pb/^{204}Pb$	$^{207}Pb/^{206}Pb$	$^{208}/^{206}Pb$	$^{206}Pb/^{238}U$	$^{207}Pb/^{235}U$	$^{207}Pb/^{206}Pb$	$^{206}Pb/^{238}U$	$^{207}Pb/^{235}U$	$^{207}Pb/^{206}Pb$
GP3/1	>100	174	56.49	55.6	0.87	2828	0.11162	0.17698	0.29254	4.3078	0.11162	1654	1695	1746
GP3/2	80-100	178	56.74	56.4	0.37	5451	0.10909	0.16481	0.29119	4.2794	0.10908	1648	1689	1741
Gp3/3	60-80	178	57.02	56.4	0.58	4146	0.10977	0.16839	0.29087	4.2705	0.10977	1646	1688	1740
Gp3/4	45-60	186	58.50	58.2	0.29	6269	0.10864	0.16551	0.28669	4.2084	0.10864	1624	1675	1739
Gp3/5	<45	186	58.64	58.3	0.39	5925	0.10884	0.17068	0.28624	4.2047	0.10883	1623	1675	1741
Gp7/1	>100	154	50.27	49.4	0.92	2490	0.11207	0.18916	0.28938	4.2535	0.11207	1638	1684	1742
Gp7/2	80-100	162	52.05	51.4	0.66	3426	0.11034	0.18267	0.28809	4.2251	0.11034	1632	1679	1738
Gp7/3	60-80	139	45.27	44	1.24	1361	0.11519	0.19591	0.28865	4.1854	0.11519	1635	1671	1717
Gp7/4	45-60	165	52.60	52.4	0.19	4013	0.10973	0.18872	0.28685	4.2055	0.10973	1626	1675	1737
Gp7/5	<45	160	50.85	50.5	0.33	2868	0.11121	0.19012	0.28544	4.1894	0.11121	1619	1672	1740
Gp8/1	>100	351	106.48	69.7	36.74	109	0.23236	0.45169	0.18389	2.7308	0.10647	1088	1337	1761
Gp8/2	80-100	400	79.36	75.5	3.87	925	0.12133	0.15412	0.17896	2.63016	0.12133	1061	1309	1742
Gp8/3	60-80	424	80.86	77.8	3.05	1164	0.11829	0.14598	0.17422	2.56021	0.11828	1035	1289	1741
Gp8/4	45-60	501	88.36	85.2	3.21	1093	0.1187	0.14693	0.1618	2.33699	0.1187	967	1234	1736
Gp8/5	<45	538	93.22	90.7	2.55	1231	0.11749	0.14514	0.16015	2.34975	0.11749	958	1227	1739
Gp9/1	>100	324	81.12	68.3	12.82	259	0.15642	0.43385	0.17265	2.4657	0.15642	1026	1262	1689
Gp9/2	80-100	471	91.89	82.4	9.48	433	0.13566	0.33987	0.14807	2.1249	0.13566	890	1156	1698
Gp9/3	60-80	553	105.44	98.2	7.21	625	0.12685	0.30772	0.15145	2.1925	0.12685	909	1178	1714
Gp9/4	45-60	606	120.00	113	6.83	764	0.12322	0.29899	0.15914	2.3118	0.12322	952	1216	1721
Gp9/5	<45	620	124.11	117	7.51	706	0.12414	0.30887	0.15957	2.306	0.12414	954	1214	1711
W28.8-11/1	>100	793	164.29	162	2.06	2726	0.10449	0.08512	0.20319	2.7858	0.10449	1192	1352	1614
W28.8-11/2	80-100	754	159.64	158	1.89	3598	0.1038	0.0869	0.20668	2.8492	0.1038	1211	1368	1623
W28.8-11/3	60-80	724	154.93	155	0.06	3215	0.10429	0.09063	0.21095	2.9089	0.10429	1233	1384	1624
W28.8-11/4	45-60	626	143.02	141	1.80	3848	0.10453	0.09611	0.22068	3.07208	0.10453	1285	1426	1642
W28.8-11/5	<45	562	134.12	133	1.43	4089	0.10493	0.10455	0.22934	3.2121	0.10493	1331	1460	1653
W24.8-11/6	>100	763	160	157	2.5	3750	0.10411	0.08606	0.2035	2.81827	0.10044	1194	1360	1632
W24.8-11/7	80-100	718	154.48	152	2.18	3963	0.1043	0.08857	0.20903	2.90624	0.10084	1224	1384	1640
GP15/1	>100	658	175.30	116	59.40	116	0.21734	0.49081	0.15562	2.11602	0.09862	932	1154	1598
GP15/2	80-100	796	218.12	141	77.14	109	0.22444	0.51131	0.15606	2.11931	0.09849	912	1133	1585
GP15/3	60-80	547	159.74	111	48.99	116	0.20648	0.4584	0.17859	2.51845	0.10227	1059	1277	1666
GP15/4	45-60	441	136.37	91.6	44.76	120	0.21853	0.47941	0.18318	2.65327	0.10505	1084	1316	1715
GP15/5	<45	398	188.70	97.7	91.01	70	0.30287	0.68884	0.21241	3.14297	0.10732	1242	1443	1754

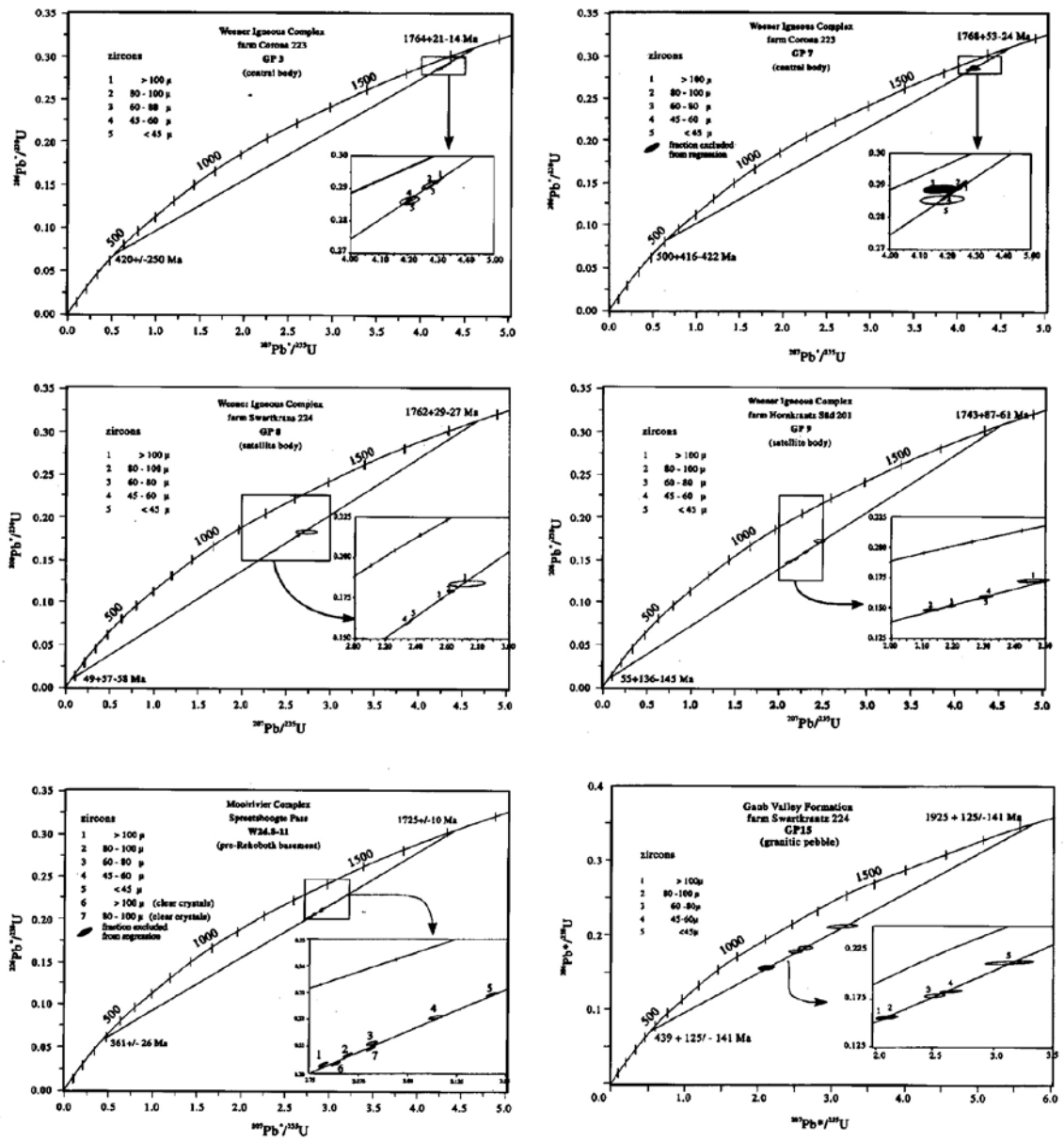

Figure 5: Concordia diagrams for zircons of the analysed samples

poorly defined lower discordia intercepts vary between 386 ± 159 Ma and 325 ± 54 Ma.

Mooirivier Complex

The Mooirivier Complex has been considered to represent the oldest crustal segment in the Southern Margin Zone (SMZ) of the Damara Orogen (Schalk, 1988). The name applies to a whole group of highly metamorphosed rocks mainly preserved as large schollen within younger granitoid intrusives, which have not been previously investigated by means of isotopic or geochemical analyses. Their widespread distribution in numerous small outcrops throughout the whole SMZ attests to the wide area previously underlain by this basement. Intensely folded migmatitic gneiss and amphibolite, together with remnants of quartzite and schist, are the main lithotypes of this unit (SACS, 1980). In its eastern portion the Mooirivier Complex is closely associated with the volcanic Kamasis Formation.

The sample for the zircon study (W.24.8-11) was taken from the largest outcrop at the Spreetshoogte pass (Fig. 2). This gneissic rock with incipient migmatization structures is clearly of igneous origin and intruded the surrounding metabasites parallel to foliation planes. The succession was in turn intruded by younger granitoids, probably of Sinclair age.

Two groups of zircons are distinguished in this sample. The dominant group comprises subhedral prismatic, metamict, yellow to reddish strongly corroded

zircons. Cathodoluminescence reveals the presence of homogeneous rounded to euhedral cores, with overgrowths exhibiting oscillatory zoning. Corrosion of the zircons is indicated by rugged crystal surfaces, and by cracks and tubes within the crystals. The second group displays similar features as described from zircons of the other samples with transparent euhedral prismatic to long prismatic zircons and simple crystal faces (Fig. 6). In contrast to the first group, these specimens are only slightly corroded. Internal structures such as rounded or subhedral cores and overgrowths with oscillatory zoning are recognizable (Fig. 7).

Five fractions from the first and two fractions from the second group have been analysed. In contrast to the other samples, the grain size correlates positively with U concentration (562-793 ppm), degree of discordance, and in general also with common Pb (0.06-2.06 ppm) (Fig. 5). The fractions from the first group define well constrained upper and lower intercepts of 1725 ± 10 Ma and 361 ± 26 Ma (MSWD = 2.99). Both size fractions from the second group are grouped close to the corresponding fraction of the first group and display similar geochemical characteristics (Fig. 5, Table 3). Discordia intercepts are 1721 +36-31 Ma and 303 +89-92 Ma.

Rb-Sr whole-rock ages

Rb-Sr isotopic data have been determined for 5 samples from the WIC and 6 from the GVF. Analytical data are given in Table 4.

Since the variation of the Rb/Sr-ratio is low in the WIC (0.14-0.35), increased errors are inherent a prior to the regression analysis. To improve the significance of the calculated age, previously published analyses from the same locality (Seifert, 1986) have been included. Due to their large deviation from the regression line, two samples have been excluded (KAW 2287, PR18). Even so, the remaining 9 samples poorly define an errorchron (MSWD = 21, Fig. 8) with an age of 1655 ± 123 Ma and an initial $^{87}Sr/^{86}Sr$ ratio of 0.7041 ± 13.

The Rb-Sr whole-rock data for the GVF are plotted in figure 9. Most of $^{87}Rb/^{86}Sr$-ratios are comparable to those in the WIC. The tendency to increased Rb/Sr-ratios (0.16-0.95) coincides with a higher degree of differentiation of the volcanic rocks (Becker *et al.*, in prep.). Five samples define an errorchron (MSWD = 28.2) with an age of 1760± 123 Ma and an initial $^{87}Sr/^{86}Sr$ ratio of 0.7033± 13. However, sample VU11 is distinct from the others in both a higher Rb/Sr ratio and a large negative deviation from the regression line. Supposing an origin from a depleted mantle source for this sample, a maximum model age of 1246 Ma would result. Additional crustal contamination will lead to further rejuvenation. The geochemical analysis of this sample shows an anomalous composition in comparison with the other samples (Becker *et al.*, in prep.). Therefore, a different

Table 4: Results of Rb-Sr whole rock analyses.

lithological unit	sample	concentration		measured ratios		
		Rb [ppm]	Sr [ppm]	Rb^{87}/Sr^{86}	Sr^{87}/Sr^{86}	2MQFM
this study						
	PR04	98.70	298.21	0.95939	0.7267808	0.0000434
	PR10	51.28	359.83	0.412586	0.7140362	0.0000439
WIC	PR13	88.44	317.89	0.80611	0.722662	0.0000939
	PR16	65.79	288.19	0.661329	0.721079	0.0000863
	PR18	50.49	311.60	0.469266	0.717531	0.0003111
	VU08	45.92	281.37	0.47248	0.714873	0.0000701
	VU09	67.39	326.44	0.597894	0.718873	0.0000519
	VU10	97.22	247.44	1.139657	0.734053	0.000138
GVF	VU11	184.43	81.58	6.613083	0.820357	0.0001228
	VU20	125.96	149.59	2.44904	0.761979	0.0000867
	VU22	72.93	243.07	0.869567	0.725065	0.000117
SEIFERT (1986)						
	KAW2282	97.81	273.41	1.019921	0.727762	0.000085
	KAW2287	109.39	319.10	0.976854	0.723074	0.000079
	KAW2288	88.35	245.12	1.027771	0.729274	0.00006
WIC	KAW2289	79.30	337.91	0.668411	0.718556	0.00005
	KAW2290	90.32	243.18	1.058944	0.729032	0.000095
	KAW2291	90.22	321.09	0.80068	0.72311	0.000053
regression error				1%	0.01%	

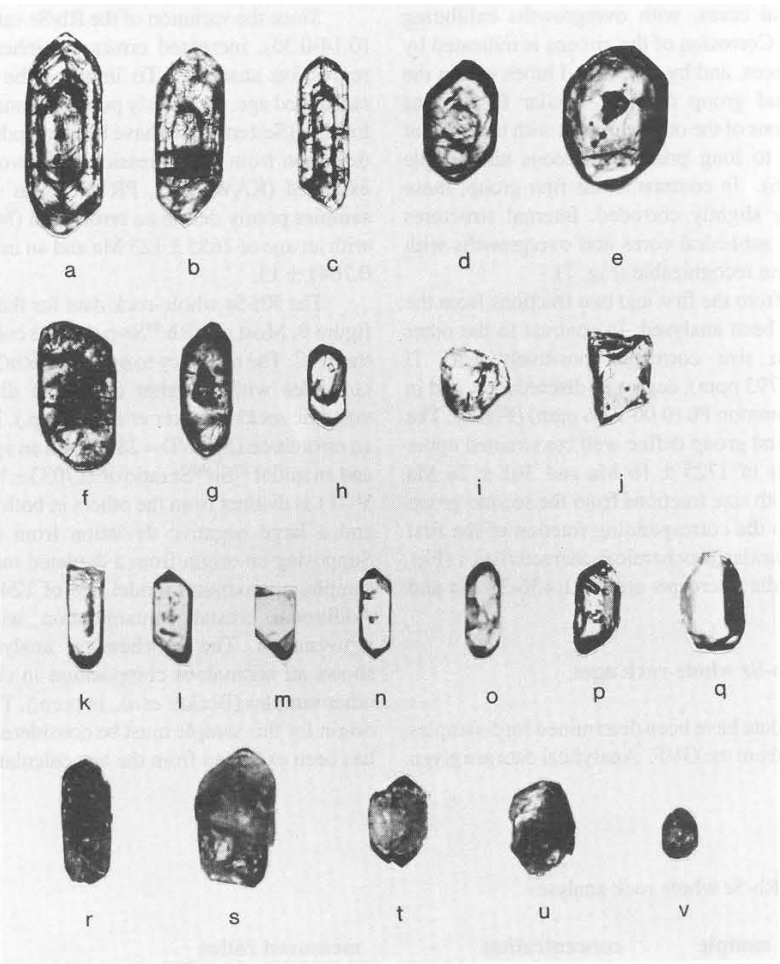

Figure 6: Zircon typologies of sample W24.8-11: a-e: zoned idiomorphic f-j: anhedral to euhedral with cores, k-q clear, unzoned, some with inclusions, r-v: metamict crystals

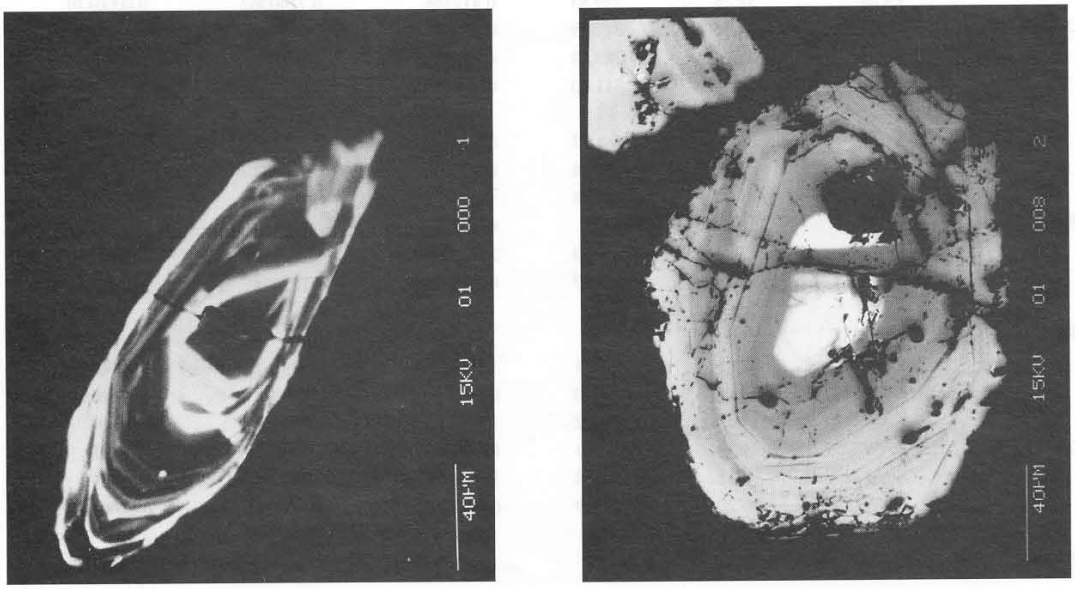

Figure 7: SEM photographs of polished crystals (cathodoluminescence mode), a) zoned zircon of the first group with small euhedral core and holes and microchannels throughout the crystal, b) zoned zircon of the second group.

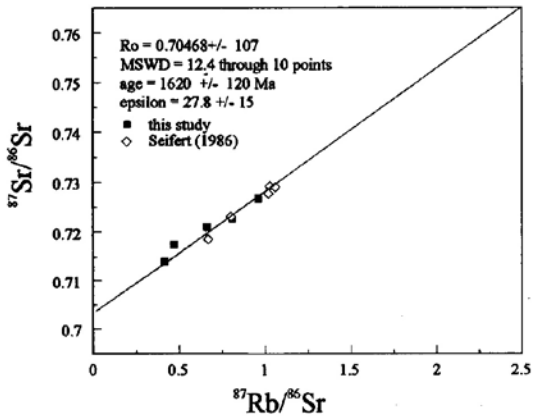

Figure 8: Rb-Sr errorchron diagram of the Weener Igneous Complex.

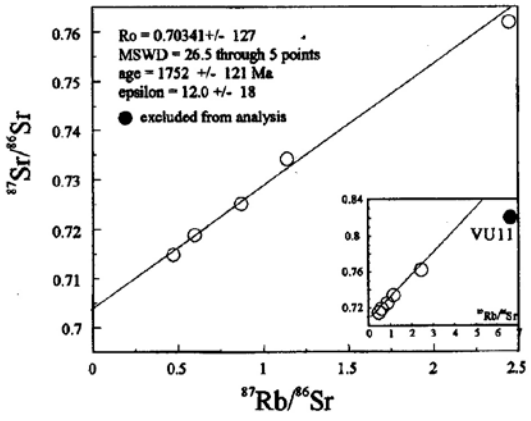

Figure 9: Rb-Sr errorchron diagram of the Gaub Valley Formation.

origin for this sample must be considered and accordingly it has been excluded from the age calculation.

Discussion

U-Pb intercept ages

In the Concordia diagrams after Wetherill (1956) most zircon fractions define discordant chords as a result of radiogenic lead loss. The relationships between the incorporation of common lead, lead loss (expressed in the ratio $^{207}Pb/^{235}U$) and uranium concentration is shown in figures 10 and 11. In most of the samples the uranium concentration and degree of discordance are negatively correlated. Additionally, the sample from the Mooirivier Complex deviates significantly from the regression curve defined by the other samples. This shows, that the loss of radiogenic lead is partly controlled by the uranium concentration. The susceptibility of zircons to lead loss as a function of radiation damage has already been pointed out by Ludwig and Stuckless (1978). However, the mechanism for different degrees of lead loss at different localities remains unknown. Figure 11 shows that in four samples only very low common lead concentrations occur and any correlation will probably be blurred by the analytical error. A negative correlation between uranium and common lead has only been observed in the samples with higher common lead concentrations. Again, the incorporation of common lead into the zircons is only partly controlled by radiation damage and hence an unknown factor must have led to different degrees of exchange at different localities.

For the samples from the WIC and associated smaller intrusive bodies the upper intercept ages range with low 2-sigma errors from 1743 to 1768 Ma. Most of the zircons have remarkably small euhedral cores and broad oscillatory zoned rims. This is taken as evidence for the origin of the crystals in only one magmatic event while the influence of any inherited component is probably negligible. In conclusion, these ages are interpreted as

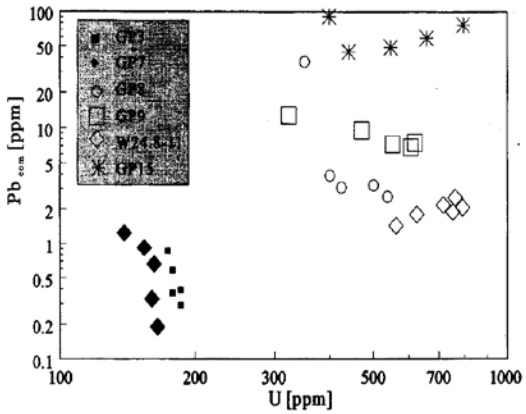

Figure 10: Pb_{com} vs. U diagram of all zircon analyses.

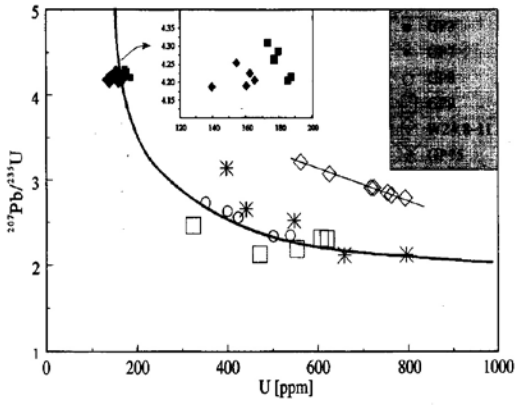

Figure 11: Discordance (expressed as $^{207}Pb/^{235}U$) vs. U diagram of all zircon analyses.

the times of crystallization. A mantle origin of the parental magma is indicated, in application of the classification diagram of Pupin (1980) by simple crystal faces, and additionally supported by the low uranium concentration in the zircons.

In the orthogneissic sample from the Mooirivier Complex, two zircon groups are distinguished. Narrow-spaced broad oscillatory rims attest to the dominant magmatic origin of both groups. In some grains, an inherited sedimentary component is indicated by rounded cores. The coexistence of the two groups may be explained in two ways:

1. the different degrees of metamictization and corrosion are the result of increasing uranium concentrations and may be related to differentiation and mixing of more differentiated magma with early fractionates;
2. the strongly corroded zircons of the first group are evidence for a hybrid magma. These orthogenic xenocrysts were assimilated from the country rock during magma ascent.

The first model is favoured since metamict zircons are much more abundant than clear ones, and because transitions between the two groups have been observed. This model also accounts for the similar upper intercepts of 1725 and 1721 Ma. Altogether this age is rather surprising since the Mooirivier Complex is believed to represent the basement of the Rehoboth Sequence and therefore should yield considerably older ages. Several models could explain this apparent discrepancy:

1. the Mooirivier Complex is coeval with the Rehoboth Sequence and only represents a deeper level of the same crustal segment;
2. the Mooirivier Complex is indeed older than the intrusive rock which had been analysed. The zircon age only provides a minimum age;
3. thermal overprint and isotopic rehomogenisation of the zircons during a high-grade metamorphic event which is indicated by the incipient migmatitic structures.

Since reliable U-Pb zircon ages have not been recorded from the SMZ which attest to basement older than 1860 Ma, the first possibility seems most likely. A similar zircon age of 1784 ± 45 Ma has been obtained from the volcanic Kamasis Formation which is closely associated with the Mooirivier Complex. This age has been interpreted as the time of crystallization (Burger & Walraven, 1979; SACS, 1980; Schalk, 1988).

In conclusion, at present the pre-Rehoboth basement and the Rehoboth Sequence cannot be distinguished on the basis of absolute ages. The different degree of metamorphism and/or additional deformation structures in pre-Rehoboth units as compared to the Rehoboth Sequence do not argue for an earlier origin and may rather result from burial to different crustal levels during later metamorphism. A major thrust system that could have brought units from different crustal positions into juxtaposition is the Areb Shear Zone, which is believed to be of pre-Sinclair age (Schulze-Hulbe, 1979).

The upper intercept of zircons from a magmatic pebble within the clastic GVF is poorly defined, with a large uncertainty in this age caused by the exceptionably high contamination of zircons with common lead. The calculated age of 1929 +125 -141 Ma does not significantly constrain the maximum age of the GVF nor the age of the provenance area. It is the oldest U-Pb zircon age so far obtained in the Southern Margin Zone. However, the $^{207}Pb/^{206}Pb$ ages of the different fractions vary within the same range as the remainder of the analysed samples and do not exceed 1754 Ma (Table 3). A similar poorly defined U-Pb zircon age of 1925 ± 280 Ma has been reported from the Abbabis Inlier which is situated north of the SMZ in the Central Zone of the Damara belt (Jacob *et al.*, 1978). Finally, upper discordia intercepts of 1794 + 146 -75 Ma, 1747 + 11-8 Ma, and of 1782 +18 -16 Ma from pyroclastic samples of the GVF in the Rostock and Saagberg areas, interpreted as time of crystallization, clearly attest to the more or less coeval evolution of the GVF and the WIC (Nagel *et al.*, 1996).

Due to high 2-sigma errors in most of the samples the lower intercepts are difficult to assess. Various geological events are documented by other methods during which episodic lead loss may have occurred. The *ca.* 1200 Ma Sinclair magmatism is regarded as a first regional magmatic event resulting in high-level intrusions with contact metamorphism and basic and acid volcanism. However, no significant disturbance of the U-Pb isotope system is indicated during this time. This is indicated by the data from the WIC which are only slightly discordant despite the proximity of the sample localities to intrusions of Sinclair age (i.e. Gamsberg Granite Suite).

The *ca.* 500 Ma Damara metamorphism probably had a strong effect on the isotope systematics in the SMZ. A compilation of biotite and muscovite isotopic ages (Fig. 12) reveals that K/Ar and Rb/Sr mineral ages of muscovite scatter within a comparatively narrow range between 475 and 525 Ma, whilst the biotite ages were rejuvenated up to 350 Ma. This rejuvenation has been attributed to a hydrothermal event which is recorded by the observed full age spectrum in samples taken only meters apart at Gamsberg Mountain (Seifert, 1986).

A combination of zircon populations from the WIC with low uranium concentrations and low degrees of discordance (i.e. GP3, GP7) fits on a discordia with a lower intercept of 528 ± 163 Ma and may represent the original episodic chord for Damaran metamorphism.

The hydrothermal event possibly is also documented in the sample from the Mooirivier Complex. The lower discordia intercept of 362 ± 27 Ma is in good agreement with K-Ar biotite ages of 347 ± 4 Ma and 357 ± 4 Ma from the same locality (Ziegler & Stoessel, 1993), and with zircon fission track ages of 372 ± 35 and 359 ± 42 Ma from the Gamsberg area (Seifert, 1986). The same holds with higher errors for the samples of the

GVF (386 ± 159 and 325 ± 54 Ma). It is still unknown whether this hydrothermal overprint has to be regarded as a discrete event or rather represents the final stage in evolution of the Damara metamorphism.

The last episodic lead loss can probably be attributed to the break-up of Gondwana accompanied by an increased heat-flow in the crust (Haack, 1983) and/or uplift and erosion in the investigated area. This may have induced the partial resetting of the uranium rich (hence more corroded) zircons due to pressure release, possibly combined with hydrothermal activity (dilatancy model of Goldich & Mudrey, 1972). However, errors in the lower intercepts of samples GP8 and GP9, 49 ± 58 Ma and 55 +136 -145 Ma, are too high to definitely exclude anyone of these mechanisms for lead loss. From the neighbouring Rostock area, lower intercepts varying from 114 ± 9 to 221 ± 18 Ma were reported and interpreted as related to the break up of Gondwana by Pfurr *et al.* (1991).

Rb-Sr isotopic investigations

Due to the high error limits, the results of the Rb-Sr isotopic investigation do not constrain the comagmatic evolution of the WIC and the GVP. The large data scatter may firstly reflect the small variation in Rb/Sr ratios. Secondly, hybrid magmas composed of mantle and crustal materials could have caused variations in the $^{87}Sr/^{86}Sr$-initial ratios as a function of different mixing ratios and would not allow the construction of an isochron at all. Thirdly, the post-emplacement alteration which probably played an important role commonly results in rejuvenation of the isotope system (Hradetzky & Lippolt, 1993).

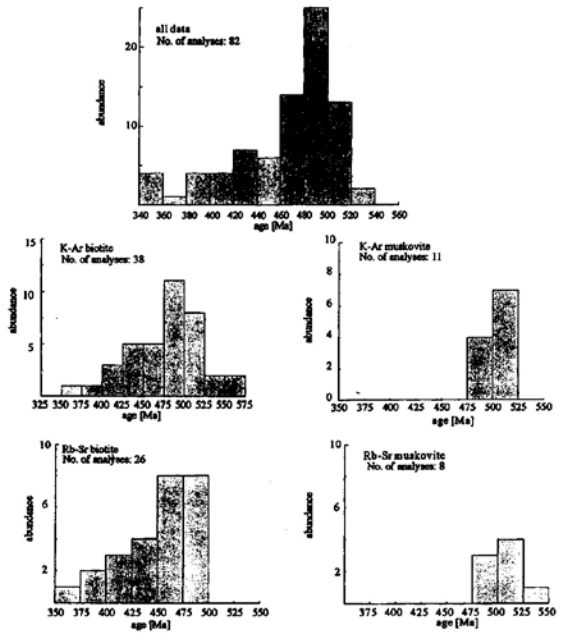

Figure 12: Histograms of Rb-Sr and K-Ar mica ages within the Southern Margin Zone and the Southern Foreland of the Damara Orogen (data compiled from Seifert, 1986, Pfurr, 1990, Ziegler & Stoessel, 1993)

The Rb-Sr errorchron age of 1653 ± 120 Ma for the WIC is considerably younger than the U-Pb zircon ages from this intrusion and therefore points to the third mechanism. Altogether, the data clearly indicate the different ages and origins of the WIC in the type locality and other granodioritic intrusions of Sinclair-age in the SMZ which were attributed to the Werner Intrusive Suite in the past (Reid *et al.*, 1988). In contrast, the Rb-Sr errorchron age of 1760 ± 123 Ma for the GVF coincides well with the zircon data of the WIC. However, the error limits are again too high to attest to a comagmatic evolution of both units.

In contrast to the WIC, no significant radiogenic Sr-loss has occurred in the GVF, provided the age obtained is the time of formation. This may result from dominant incorporation of Rb and Sr into the same mineral (i.e feldspar) whereas in the WIC these elements are concentrated in different minerals (i.e. biotite and feldspar) with variable susceptibility to alteration. If 1750 Ma is the approximate age of these units, the apparent difference in the Sr-initial ratios of the WIC and the GVF would be an artefact. Based on a 1750 Ma age, the recalculation of the $^{87}Sr/^{86}Sr$ isotope ratio of all samples shows there is no difference between the initials of both units (Fig. 13) with weighted mean $\varepsilon^{1750}_{UR}(Sr)$ values of 12.1 ± 17.2 (GVF) and 7.45 ± 10.0 (WIC).

For the WIC, almost all criteria point to classification as calc alkaline I-type magmatic rock: the A/CNK ratios vary from 0.83 to 1.08; K_2O/Na_2O ratio is always below unity; Na_2O concentrations in general exceed 3 wt.%; and the weighted mean $\varepsilon^{1750}_{UR}(Sr)$ of nine samples is low (Becker *et al.*, in prep.). This indicates an upper mantle or lower crustal origin of the magma, in accordance with the zircon typologies.

Conclusions

The results of the isotopic investigations suggest that formation of the pre-Rehoboth units and the Re-

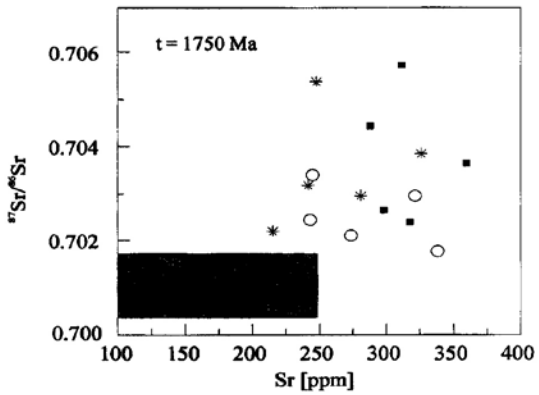

Figure 13: Recalculation of $^{87}Sr/^{86}Sr$ initial ratios at an assumed age of 1750 Ma

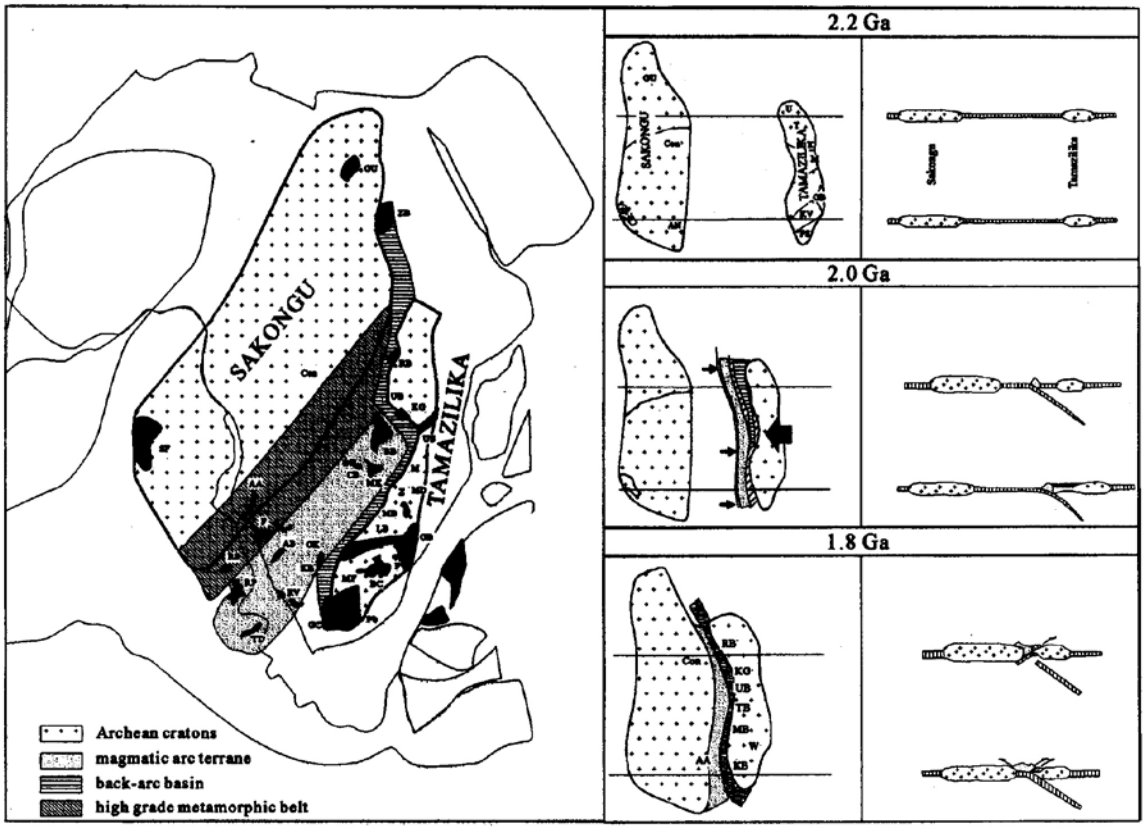

symbol	lithological unit	age	interpretation
AA	Angola Anorthosite	ca. 2.0 Ga	late orogenic intrusion
AB	Abbabis Inlier	ca. 2.0 Ga	magmatic arc
BB	Bangweulu Block	ca. 1.8 Ga	magmatic arc
BC	Bushveld Complex	ca. 2.0 Ga	cratonic layered intrusion (back-arc)
CB	Cooperbelt Basement	ca. 2.0 Ga	magmatic arc
CON	Congo Craton	>2.5 Ga	archaic craton (Sakongu)
F	Franzfontein Inlier	ca. 1.8 Ga	fore-arc basin + post-collisional granitoids
FR	Francevillian	ca. 2.0 Ga	passive continental margin
GB	Grunehogna Block	>2.5 Ga	archaic craton (Tamazilika)
GC	Gascoigne Belt	ca. 1.8 Ga	back-arc basin
GU	Gebel Uweinat	>2.5 Ga	archaic craton (Sakongu)
K	Kasai Craton	>2.5 Ga	archaic craton (Sakongu)
KB	Kheis Belt	ca. 2.0 Ga	back-arc basin
KG	Kapalagulu Complex	ca. 1.8 Ga	cratonic layered intrusion (back-arc)
LB	Limpopo Belt	> 2.5 Ga	archaic mobile belt
M	Malawi	ca. 2.0 Ga	back-arc basin
MB	Magondi Belt	ca. 2.0 Ga	back-arc basin
MD	Mashonaland Dolerites	ca. 1.9 Ga	cratonic dyke swarm (back-arc)
MF	Molopo Farms Complex	ca. 2.0 Ga	cratonic layered intrusion (back-arc)
MK	Mkushi	ca. 2.0 Ga	magmatic arc
MP	Marungu Plateau	ca. 1.8 Ga	magmatic arc (during back-arc closure)
OE	Oendelungu	ca. 2.0 Ga	fore-arc basin + post -collisional migmatites
P	Phalaborwa Complex	ca. 2.0 Ga	cratonic alkali complex (back-arc)
PS	Palala Shear Zone	ca. 1.9 Ga	reactivated structure
QF	Quadrilatero Ferriferro	ca. 2.0 Ga	passive continental margin
RB	Ruwenzori Belt	ca. 2.0 Ga	back-arc basin
RP	Rio de la Plata Craton	ca. 2.0 Ga	magmatic arcn + post-collisional migmatites
RS	Rio Grande do Sul	ca. 2.0 Ga	magmatic arc + post-collisional migmatites
RV	Richtersveld	ca. 2.0 Ga	magmatic arc
SF	Sao Francisco Craton	>2.5 Ga	archaic craton (Sakongu)
TB	Tumbide Belt	ca. 1.8 Ga	back-arc basin
TD	Tandilia	ca. 2.0 Ga	magmatic arc + post-collisional migmatites
UB	Ubendian Belt	ca. 1.8 Ga	back-arc basin
US	Usagaran Belt	ca. 1.8 Ga	aulakogen
W	Waterberg Basins	ca. 1.8 Ga	strike-slip basin (collisional stage)
Z	Zimbabwe Craton	>2.5 Ga	archaic craton (Tamazilika)
ZB	Zalingi Belt	ca. 2.0 Ga	back-arc basin ?

Figure 14: Plate tectonic model for the Eburnian orogeny (from Master, 1993).

hoboth Sequence occurred in a single major magmatic event approximately 1750 Ma ago. Similar ages have been obtained in crustal segments which extend from southern Brazil through southern Africa to equatorial Africa and constitute a major crust-forming event during Paleoproterozoic times (Eburnian-Ubendian cycle). A plate tectonic model for the evolution of this belt was first proposed by Master (1993). According to this model (Fig. 14), convergence of two late Archaean continents and southeastward subduction of oceanic crust occurred between 2.2 - 2.0 Ga, resulting in the formation of a magmatic arc and back arc on the leading plate in the south. At *ca.* 1.8 Ga ocean closure and collision ended in major orogenic deformation, high-grade metamorphis~ and collision related magmatism. A separate evolution is assumed for the northern part of this magmatic belt with a second stage of back arc opening and the formation of a magmatic arc which overprints the earlier *ca.* 2.0 Ga magmatic arc.

The isotopic ages obtained from granitoids of the Rehoboth Basement Inlier mostly spread between 1700-1860 Ma. Similar age data from other inliers in Namibia indicate widespread magmatism during this period and would point to formation of most of the magmatic rocks during the proposed collisional or post-collisional event (Table 2). However, geochemical data for the WIC and the GVF rather support an origin in a primitive magmatic arc or back arc setting (Becker, 1995). This is indicative of evolution of the RBI similar to the north of the proposed belt, with prolonged or renewed ocean opening and subduction related magmatism. The different metamorphic grade of units which are classified as pre-Rehoboth basement as compared to units of the Rehoboth Sequence may be explained by submersion to different crustal levels during subsequent thrust or extension tectonics.

Acknowledgements

This study was funded by the research grant AZ 1166/5.1 of the Deutsche Forschungsgemeinschaft (DFG). It was carried out as part of a University Research Project in cooperation with the Geological Survey of Namibia which supported the field work. A first draft was kindly corrected by H. Porada.

References

Barton, E.S. and Burger, A.J. 1983. Reconnaissance isotopic investigations in the Namaqua Mobile Belt and implications for Proterozoic crustal evolution-Upington geotraverse. *Spec. Publ. geol. Soc. S. Afr.*, **10**, 173-191.

Becker, T. 1995. Die Geologie, Geochemie und Altersstellung des Weener Igneous Komplex und der Gaub Valley Formation am Südrand des Damara Orogens, Namibia und ihre Bedeutung für die Genese der frühproterozoischen Rehoboth Sequenz. *Cuvillier Verlag, Göttingen*, 250 pp.

Becker, T., Ahrendt, H. and Weber, K. 1994. Report: the geological history of the Pre-Damaran Gaub Valley Formation and Weener Igneous Complex in the vicinity of Gamsberg. *Comm. Geol. Surv. Namibia*, **9**, 79-91.

Burger, A.J. and Coertze, F.J. 1976. Age determinations - April 1972 to March 1974. *Ann. geol. Surv. S. Afr.*, **10**, 135-142.

Burger, A.J. and Coertze, F.J. 1978. Summary of age determinations carried out during the period April 1974 to March 1975. *Ann. geol. Surv. S. Afr.*, **11**, 317-322.

Burger, A.J. and Walraven, F. 1978. Summary of age determinations carried out during the period April 197 5 to March 1976. *Ann. geol. Surv. S. Afr.*, **11**, 323-329.

Burger, A.J. and Walraven, F. 1979. Summary of age determinations carried out during the period April 1976 to March 1977. *Ann. geol. Surv. S. Afr.*, **12**, 415-431.

Crampton, D. 1974. A note on the age of the Matsap Formation of the northern Cape Province. *Trans. geol. Soc. S. Afr.*, **77**, 71-72.

De Carvalho, H. 1970. Contribution à la géo-chronologie du sudouest de l' Angola. *Bolm Servs. Geol. Min. Angola*, **19**, 23-35.

De Waal, S.A. 1966. *The Alberta Complex, a metamorphosed layered intrusion north of Nauchas, SWA: the surrounding granites and repeated folding in the younger Damara system*. D.Sc. Thesis, Univ. Pretoria (unpubl.), 203 pp.

Goldich, S.S. and Mudrich, M.G. 1972. Dilatancy model for discordant U-Pb zircon ages, 415-418. *In*: A.J. Tugarinov (ed.) *Contributions to Recent Geochemistry and Analytical Chemistry*. Moscow, Nauka Publ. Office, 654 pp.

Haack, U. 1983. Reconstruction of the cooling history of the Damara Orogen by correlation of radiometric ages with geography and altitude. *In*: H. Martin and F.W. Eder (eds.) *Intracontinental fold belts - Case studies in the Variscan Belt in Europe and the Damara Belt in Namibia*. Springer, Berlin, 945 pp.

Hill, R.S. 1975. Geological map 2315 BD-Rostock, scale 1:50000. *Geol. Surv. SWA/Namibia* (unpubl.).

Hradetzky, H. and Lippolt, H.J. 1993. Generation and distortion of Rb/Sr whole-rock isochrons - effects of metamorphism and alteration. *Eur. J. Mineral.*, **5**, 1175-1193.

Hugo, P.J. and Schalk, K.E.L. 1972. The isotopic ages of certain granites and acid lavas in the Rehoboth and Maltahohe Districts, SWA. *Ann. geol. Surv. S. Afr.*, **9**, 103-105.

Jacob, R.E., Kröner, A and Burger, A.J. 1978. Areal extent and first U-Pb age of the pre-Damaran Abbabis Complex in the central Damara belt of South West Africa/Namibia. *Geol. Rundsch.*, **67**, 706-718.

Krogh, T.E. 1973. A low contamination method for hy-

drothermal decomposition of zircon and extraction of U and Pb for isotopic age determinations. *Geochim. Cosmochim. Acta*, **37**, 485-494.

Ludwig, K.R. 1980. Calculation of uncertainties of U-Pb isotope data. *Earth Plan. Sci. Let.*, **46**, 212-220.

Ludwig, K.R. and Stuckless, J.S. 1978. Uranium-lead isotope systematics and apparent ages of zircons and other minerals in Precambrian granitic rocks, Granite mountains, Wyoming. *Contr. Mineral. Petrol.*, **65**, 243-254.

Master, S. 1990. The "Ubendian" cycle in equatorial and southern Africa: accretionary tectonics and continental growth. *In*: Rocci, G. and Deschamps, M. (eds.) *New data in African earth sciences.* 15th Coll. Afr. Geol., Orleans, CIFEG Occ. Publ., **22**, 41-44.

Master, S. 1993. Early Proterozoic assembly of "Ubendia" (Equatorial and Southern Africa and adjacent parts of South America): tectonic and metallogenic implications. Symposium Early Proterozoic, Geochemical and Structural constraints - metallogeny, *CIFEG Occ. Publ.* **23***, Dakar*, 103-107.

Nagel, R., Warkus, F., Becker, T. and Hansen, B.T. 1996. U/Pb-Zirkondatierungen der Gaub Valley Formation am Südrand des Damara Orogens, Namibia, und ihre Bedeutung für die Entwicklung des Rehoboth Inlier. *Z. Geol. Wiss.*, **24** (5), 611-618

Pfurr, N. 1990. *Die Altersstellung von Rotgneisen im Rostock Deckenkomplex am Südrand des Damara Orogens, Namibia, abgeleitet aus U/Pb- und Rb/Sr-Isotopenuntersuchungen, und ihre Bedeutung für die Basement-Cover-Beziehungen in der Damara Südrandzone*. Dr. rer. nat. thesis (unpubl.) Univ. Göttingen, 179 pp.

Pfurr, N., Ahrendt, H., Hansen, B.T. and Weber, K. 1991. U-Pb and Rb-Sr isotopic study of granitic gneisses and associated metavolcanic rocks from the Rostock massif, southern margin of the Damara Orogen: implications for lithostratigraphy of this crustal segment. *Comm. geol. Surv. Namibia*, **7**, 35-48.

Pupin, J.P. 1980. Zircon and Granite Petrology. *Contr. Mineral. Petrol.*, **73**, 207-220.

Reid, D.L., MaIling, S. and Allsopp, H.L. 1988. Rb-Sr ages of granitoids in the Rehoboth-Nauchas area SWA Namibia. *Comm. geol. Surv. SWA/Namibia*, **4**, 19-28.

Schalk, K.E.L. 1988. Pre-Damaran basement rocks in the Rehoboth and southern Windhoek districts (areas 2217D, 2316, 2317A-C) - a regional description. *Unpubl. Rep. geol. Surv. SWA, Windhoek*.

Schulze-Hulbe, A. 1979. Pre-Damaran Formations on Marienhof 577, Aroams 315, Doornboom 316 and Gollschau 20, Areas 2316BC and BD, Rehoboth district. *Unpubl. Rep. geol. Surv. SWA, Windhoek*.

Seifert, N. 1986. Geochronologie am Sudrand des Damara Orogen, SWA/Namibia: hydrothermale beeinflussung von Isotopensystemen und Abkuhlalter in prakambrischen basementgesteinen. *Schweiz. miner. petro gr. Mitt.*, **66**, 413-451.

South African Committee For Stratigraphy (SACS) 1980. Stratigraphy of South Africa, South West Africa/Namibia and the Republics of Bophuthatswana, Transkei and Venda. *Hand. geol. Surv. S. Afr.*, **8**, 690 pp.

Stacey, J.S. and Kramers, J.D. 1975. Approximation of terrestrial lead isotope evolution by a two stage model. *Earth Plan. Sci. Let.,* **26**, 207-221.

Steiger, R.H. and Jäger, E. 1977. Subcommission on geochronology: Convention on the use of decay constants in geo- and cosmochronology. *Earth Plan. Sci. Let.*, **36**, 359-362.

Tegtmaier A. and Kröner, A. 1985. U-Pb zircon ages for the granitoid gneisses in Northern Namibia and their significance for Proterozoic crustal evolution of Southwestern Africa. *Precamb. Res.*, **28**, 311-328.

Teufel, S. 1988. Vergleichende U/Pb- und Rb-Sr-altersbestimmungen an gesteinen des übergangsbereiches Saxothuringikum/Moldanubikum, NE Bayern. *Göttinger Arb. Geol. Pal.*, **35**, 87 pp.

Watters B.R 1976. Possible late Precambrian subduction zone in South West Africa. *Nature,* London. **259**, 471-473.

Wetherill, G.S. 1956. Discordant uranium-lead ages. *J. Trans. Am. Geophys. Union*, **37**, 320-326.

York, D. 1969. Least-squares fitting of a straight line with correlated errors. *Earth Plan. Sci. Let.*, **5**, 320-324.

Ziegler, D.RF. and Stoessel, G.F.U. 1991. Isotope geology and geochemistry of the Rehoboth Basement Inlier, Namibia/SWA; a multimethod case history. *Bull. Swiss. Assoc. of Petroleum Geol. & Eng.*, **56**, 13-33.

Ziegler, U.R.F. and Stoessel, G.F.U. 1992. Note: New constraints on the age of the Weener Intrusive Suite, the Gamsberg Granite and the crustal evolution of the Rehoboth Basement Inlier, Namibia. *Comm. geol. Surv. SWA/Namibia*, **7**, 75-78.

Ziegler, D.R.F and Stoessel, G.F.D. 1993. Age determinations in the Rehoboth Basement Inlier, Namibia. *Mem. Geol. Surv. Namibia*, **14**, 106 pp.

Communs geol. Surv. Namibia, ***11*** *(1996), 49-53*

Precise U-Pb zircon ages for early Damaran magmatism in the Summas Mountains and Welwitschia Inlier, northern Damara belt, Namibia

P.P. Hoffman[1], D.P. Hawkins[2], C.E. Isachsen[2] and S.A. Bowring[2]

[1]*Department of Earth and Planetary Sciences, Harvard University, Cambridge, MA 02138, USA*

[2]*Department of Earth, Atmospheric and Planetary Sciences, Massachusetts Institute of Technology, Cambridge, MA 02139, USA*

Three new U-Pb zircon ages are reported for early Damaran, rift-related, igneous rocks in northern Namibia. An age of 756 ± 2 Ma for the Oas quartz syenite intrusion, western Welwitschia Inlier, provides a minimum age for lower Nosib Group terrigenous sedimentation in that area. An ash-flow tuff near the top of the Lower Naauwpoort Formation (upper Nosib Group) in the Summas Mountains and a rhyolite lava flow in the Upper Naauwpoort Formation (lower U gab Group) directly north of the Summas Mountains have statistically identical ages of 746 ± 2 and 747 ± 2 Ma, respectively. The age equivalence indicates that the contact between the sampled Upper and Lower Naauwpoort Formations represents either a brief hiatus or a tectonic repetition. Rift-related magmatism in northern Namibia is similar in age to that in northwest India, the Trans-Antarctic Mountains, and the northern Cordillera and southern Appalachians of North America.

Introduction

Igneous rocks related to Neoproterozoic continental rifting occur sporadically for 400 km along the northern margin of the Damara belt in northern Namibia (Fig. 1) (Miller, 1983). Alkaline and peralkaline rhyolite ash-flow tuffs predominate, but other felsic extrusive rocks, epizonal intrusions and subordinate mafic rocks also occur (Smit, 1962; Frets, 1969; Miller, 1974, 1980, 1983; Hedberg, 1979). Their great thickness (up to 6.6 km) and highly localized distribution suggest that emplacement was associated with tectonic extension and/or cauldron-subsidence structures. Volcanism is principally associated with the upper part of the Nosib Group, regionally comprised of non-marine feldspathic sandstones and conglomerates deposited in an extensional tectonic regime (Hedberg, 1979; Miller, 1983). Locally, igneous activity continued during deposition of the lower Ugab Subgroup (Miller, 1980), a mixed association of syn- to post-extensional carbonates and terrigenous sediments. Conceivably, the igneous activity coincided with continental breakup at the southern promontory of the Congo craton (Hoffmann, 1994).

Previous attempts to date the igneous activity have yielded imprecise and partly conflicting results. Whole-rock Rb-Sr systematics of devitrified volcanic rocks of the upper Nosib Group (Naauwpoort Formation) have isochron ages of 557 ± 10 Ma (De Villiers, 1968) and 521 ± 45 Ma (Hawkesworth *et al.*, 1983), interpreted as metamorphic ages. Zircons from two quartz porphyry rhyolite lavas in the lowest exposed part of the Naauwpoort Formation in the Summas Mountains (Fig. 1) yielded discordant U-Pb upper intercept ages of 750 ± 60 and 728 ± 40 Ma (Miller and Burger, 1983). The zircon ages are statistically indistinguishable from a whole-rock Rb-Sr isochron age of 764 ± 60 Ma for the Lofdal nepheline syenite in Welwitschia Inlier (Fig. 1), which is included in the rift-related igneous suite on petrogenetic grounds but is not physically in contact with the Nosib Group (Hawkesworth *et al.*, 1983). However, the nearby Oas quartz syenite, which intrudes lower Nosib Group sediments in Welwitschia Inlier (Frets, 1969), yields Rb-Sr whole-rock isochron ages of 840 ± 13 and 652 ± 11 Ma, interpreted as intrusive and metamorphic ages respectively (Kröner, 1982). If the older isochron is accepted as a minimum age for the intrusion, then a major hiatus must exist between the lower Nosib Group sediments and the upper Nosib Naauwpoort volcanics. On the other hand, Tegtmeyer and Kröner (1985) analysed three size-fractions of zircons from a marginal phase of the Oas quartz syenite and regressed the U-Pb ratios obtained to a chord (MSWD=1) having upper and lower intercept ages of 2124 +68/-54 and 736 +133/-141 Ma, respectively. The latter is presumed to reflect the intrusive age and is statistically consistent with a concordia intercept age, based on three zircon fractions from the central part of the intrusion, of 783 ± 18 Ma (Burger and Kröner, unpublished data cited in Tegtmeyer and Kröner, 1985).

To help resolve these uncertainties, samples of upper Nosib Group rhyolite lava and Oas quartz syenite from Welwitschia Inlier were collected for U-Pb zircon geochronology, as were samples of upper Nosib Group ash-flow tuff and lower Ugab Subgroup rhyolite lava from the Summas Mountains (Fig. 1). Results from all but the first of these samples are reported and discussed below. Single- and multi-grain fractions were hand-picked for analysis from the clearest, least cracked, inclusion-free zircons. The selected grains were air-abraded until all facets had been removed, and then analysed by conventional isotope dilution thermal ionization mass spectrometry according to the methods described by Bowring *et al.* (1993).

Oas quartz syenite, Welwitschia Inlier (sample PH.10.93)

The Welwitschia Inlier is a satellitic basement massif south of the larger Kamanjab Inlier, located near the junction of the Damara and Kaoko belts (Fig. 1). The

two inliers are flanked by Damaran strata, comprising three groups (Nosib, Swakop/Otavi, Mulden) separated by angular unconformities. The Oas hornblende-quartz syenite is a medium-grained, epizonal, intrusive body, about 50 km^2 in area, situated near the southwestern end of the Welwitschia Inlier (Fig. 2). Its northern margin is intrusive into pre-Damaran Huab gneiss and its western margin intrudes pebbly feldspathic quartzite of the lower Nosib Group (Frets, 1969). Its southern contact is faulted and/or overlain non-conformably by carbonates and fine clastics of the Swakop Group. West of the Gas intrusion, the upper Nosib Group includes rhyolitic lava and ash-flow tuff (Naauwpoort Formation) and porphyritic bostonite (Blaukrans porphyry), none of which is in contact with the Gas intrusion. Frets (1969) presents clear cut evidence that the Gas intrusion post-dates the lower Nosib Group and pre-dates the lower Swakop Group. He concludes that the intrusion is broadly coeval with upper Nosib Group volcanism and with an extensive swarm of east- to east-northeast-striking fel-

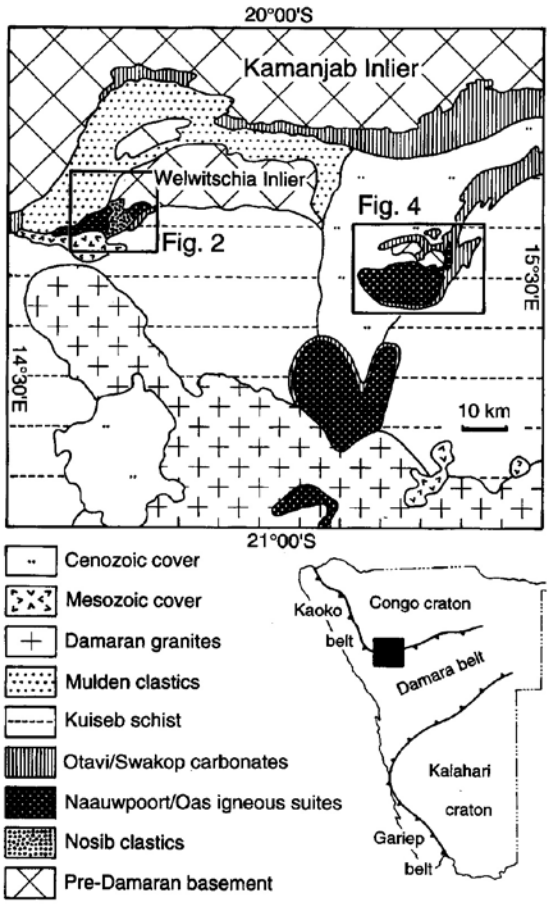

Figure 1: Distribution of early Damaran igneous rocks (Naauwpoort volcanics and Oas intrusion) south of Kamanjab Inlier near the junction of the Damara and Kaoko belts (modified from Miller, 1974). The areas detailed in figures 2 and 3 are shown.

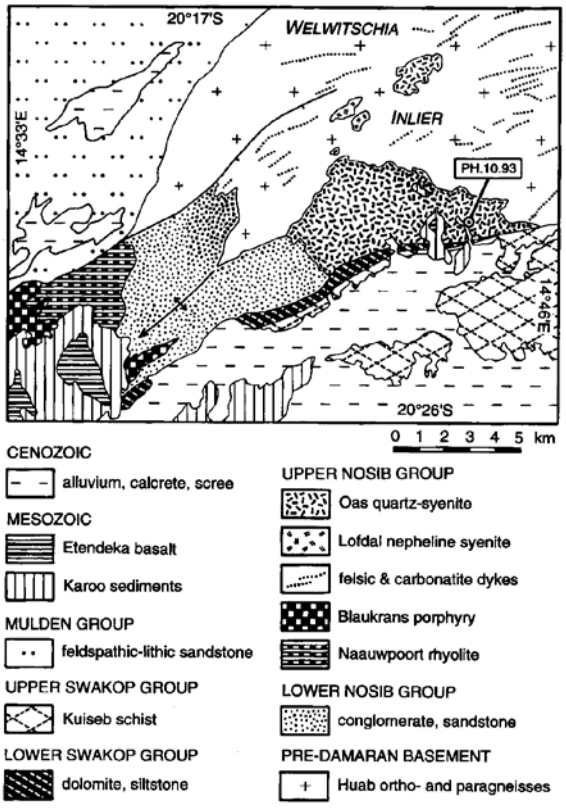

Figure 2: Geological sketch map of the western Welwitschia Inlier area (modified from Frets, 1969), showing the Oas quartz syenite sample site (PH.10.95).

sic and carbonatite dykes cutting basement rocks north and east of the Gas intrusion.

Sample PH.10.93 was collected at 20°21'45"S, 14°43'30"E, 1.5 km east of the Cretaceous Honerub outlier near the center of farm Oas 486. The location is in the east-central part of the Oas intrusion. Heavy mineral separates from the 35 kg sample were divided into five magnetic fractions and eight zircon grains were hand-picked for analysis from the least magnetic fraction. Two 300 μm grains and one 200 μm grain were analysed individually (fractions nm1.Z1-3); five smaller grains (50-100 μm) were analysed collectively (fraction nm1.Z4). The analysed grains were clear, euhedral prisms. Although free of visible inclusions, the two largest grains (.Z2 and .Z3) did contain fine cracks. The analytical data are given in Table 1 and plotted on a concordia diagram (Fig. 3). All four fractions are concordant and yield a weighted mean (^{207}Pb/^{206}Pb) age of 756 ± 2 Ma, which is taken as the time of intrusion.

Upper Nosib ash-flow tuff, Summas Mountains (sample PH.12.93)

The Summas Mountains Inlier is a 150 km^2 exposure of Naauwpoort volcanic rocks (Miller, 1974, 1980)

situated on the boundary between the Otavi fold belt to the north and the allochthonous Outjo fold belt to the south (Hoffmann, 1987), 60 km east-southeast of the Oas quartz syenite (Fig. 1). The main mass of the mountains is a structural dome (Fig. 4), exposing alkaline to per-alkaline rhyolite ash-flow tuff and subordinate quartz-feldspar porphyry having a composite stratigraphic thickness in excess of 6.6 km (base not exposed) (Miller, 1980). These rocks have been correlated with the upper Nosib Naauwpoort Formation west of the Welwitschia Inlier and are called "Lower Naauwpoort Formation" in the Summas Mountains (Miller, 1980) to distinguish them from volcanic rocks in the overlying Ugab Subgroup.

Sample PH.12.93 was collected at 20°29'30"S, 15°17'30"E high on the northeast flank of the Summas Mountains dome near the eastern boundary of farm Renosterkop 389. According to Miller (1980), the sampled unit should lie about 1000 m stratigraphically below the Nosib/Ugab unconformity. Lithologically, the sample is a purplish-grey, feldspar-phyric, vitric, ash-flow tuff. A moderately strong tectonic foliation (dipping 70° to N20°E) is superimposed on a primary(?) eutaxitic foliation (dipping 88° to S10°W).

Zircons separated from the sample are largely clear to pale yellow, elongate, euhedral prisms, mostly 100-200 μm in length. Five weakly magnetic (m0) and six magnetic (m6) fractions were hand-picked for analysis. They range from clear and flawless to slightly cracked and containing fine, dark inclusions. Four of the magnetic grains were analysed individually (m6.Z1-4); the other analysed fractions ranged from three to ten grains each. Both single and multi-grain fractions define a discordant array indicating the presence of inherited components (Fig. 3). Three concordant analyses and one discordant analysis define an upper intercept age of 746 ± 2 Ma (lower intercept = -17 ± 113, MSWD = 0.19), which is taken as the age of upper Nosib Group volcanism at the sample site.

Lower Ugab rhyolite lava, Summas Mountains (sample PH.11.93)

The north side of the Summas Mountains dome is a fault zone across which the thick ash-flow tuffs and porphyries of the Lower Naauwpoort Formation are truncated. Rocks of the overlying Ugab Subgroup directly onlap pre-Damaran Huab gneisses and schists north of the fault zone (Fig. 4) (Miller, 1980). Regionally, the Ugab Subgroup is a mixed assemblage of dolomites, quartzites and schists correlative with the Abenab Subgroup of the Otavi fold belt to the north (SACS, 1980). It is overlain disconformably by a unit of diamictite and iron formation. This is correlated with the Chuos Formation which forms the base of the Khomas Subgroup. The latter is equivalent to the Tsumeb Sub-group of the Otavi fold belt. On the east flank of the Summas Mountains dome, Lower Naauwpoort ash-flow tuffs are di-

Table 1: U-Pb analytical data

		Composition			Atomic Ratios								Ages (Ma)		
Sample fraction	wt. (μg)	U (ppm)	Pb (ppm)	(Pb)c (pg)	$^{206}Pb/^{204}Pb$	$^{208}Pb/^{206}Pb$	$^{206}Pb/^{238}U$	%err	$^{207}Pb/^{235}U$	%err	$^{207}Pb/^{206}Pb$	%err	$^{206}Pb/^{238}U$	$^{207}Pb/^{235}U$	$^{207}Pb/^{206}Pb$
Note: (1)	(2)	(3)	(3)	(4)	(5)	(6)	(7)	(8)	(7)	(8)					
Oas Quartz syenite: PH10-93															
nm1 Z1	3.7	536	69	2.3	7026	0.136	0.12440	(.15)	1.10510	(.16)	0.06443	(.06)	755.6	755.8	755.8
nm1 Z2	27.6	405	52	4.8	18243	0.129	0.12423	(.21)	1.10350	(.23)	0.06442	(.09)	754.9	755.0	755.5
nm1 Z3	21.6	472	63	38.4	2064	0.151	0.12452	(.12)	1.10658	(.15)	0.06445	(.09)	756.5	756.5	756.5
nm1 Z4	1.4	550	70	1.3	4469	0.125	0.12449	(.23)	1.10681	(.25)	0.06448	(.10)	756.4	756.6	757.5
Lower Naauwpoort ash-flow tuff: PH12-93															
m0 Z1	11.0	92	13	2.4	3441	0.219	0.12402	(.29)	1.10646	(.31)	0.06470	(.09)	753.7	756.5	764.7
m0 Z2	9.1	79	11	2.1	2765	0.224	0.12233	(.36)	1.08149	(.40)	0.06412	(.16)	744.0	744.4	745.5
m0 Z3	6.1	70	9	1.8	1867	0.214	0.12314	(.51)	1.09681	(.55)	0.06460	(.18)	748.6	751.8	761.3
m0 Z4	12.0	134	18	7.3	1715	0.225	0.12243	(.27)	1.08301	(.31)	0.06416	(.14)	744.5	745.1	746.8
m0 Z5	13.5	73	12	32.0	251	0.216	0.12288	(.42)	1.09005	(.65)	0.06434	(.45)	747.1	748.5	752.8
m6 Z1	12.2	78	11	13.3	531	0.243	0.11484	(.48)	1.01590	(.56)	0.06416	(.26)	700.8	711.8	746.8
m6 Z2	13.8	50	7	6.3	878	0.228	0.12463	(.61)	1.11471	(.63)	0.06487	(.15)	757.1	760.4	770.1
m6 Z3	1.5	328	45	3.4	1166	0.235	0.12283	(.82)	1.08621	(.84)	0.06414	(.18)	746.8	746.7	746.1
Upper Naauwpoort rhyolite: PH11-93															
nm5 Z1	2.5	258	34	5.7	1657	0.214	0.12180	(.37)	1.07839	(.39)	0.06421	(.13)	740.9	742.8	748.6
nm5 Z2	2.5	308	41	6.6	902	0.180	0.12041	(.58)	1.06496	(.63)	0.06415	(.23)	732.9	736.3	746.5
nm5 Z3	2.9	241	32	1.9	2873	0.188	0.12216	(.39)	1.08072	(.42)	0.06416	(.13)	743.0	744.0	746.9
m6 Z1	1.8	258	34	2.3	1595	0.184	0.12290	(.61)	1.08722	(.65)	0.06416	(.21)	747.2	747.2	747.0
m6 Z4	2.5	574	84	34.5	310	0.220	0.11365	(.37)	1.00616	(.59)	0.06421	(.41)	693.9	706.9	748.5

Notes: (1) all fractions are air abraded zircons. m. nm = magnetic, non-magnetic at indicated degree of tilt on a Frantz isodynamic separator operated at 1.4 to 1.6 amps. (2) sample weights estimated using a video monitor with a gridded screen are known to within 40%. (3) expressed as ppm U and ppm radiogenic Pb. (4) picograms common Pb. (5) measured ratio corrected for fractionation - Pb fractionation correction is 0.12%±0.04% per atomic mass unit (amu) for multicollector analyses and 0.15%±0.04% per amu for single collector analyses. (6) radiogenic Pb. (7) corrected for fractionation, spike, blank and initial common Pb: U blank =1pg±50%, Pb blank = 3.5pg±50% (for fractions containing less than 3.5pg common Pb, the total comon Pb was assumed to be blank); initial comon Pb composition calculated from Stacey and Kramers (1975) using the interpreted age of the sample. (8) errors given in percentage at the two-sigma confidence interval.

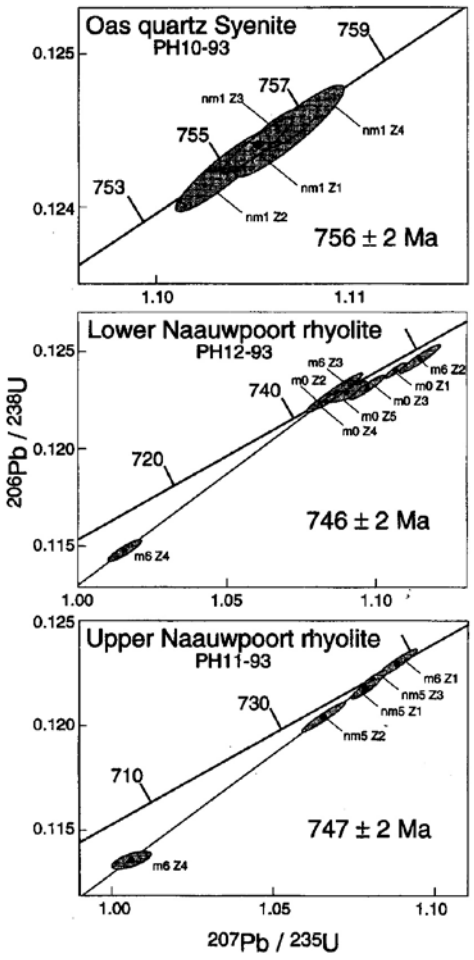

Figure 3: Concordia diagrams for zircons from the Oas quartz-syenite, Lower Naauwpoort ash-flow tuff and Upper Naauwpoort rhyolite lava. Ages (Ma) are marked on the concordia curves and individual analyses are depicted as 2 error ellipses identified by fraction number (see text and table).

rectly overlain by well-bedded rhyolite lapilli tuffs and intercalated tuffaceous siltstone and dolomite, all of which are assigned to the lower Ugab Subgroup (Miller, 1980). The lower Ugab volcanic rocks were termed "Upper Naauwpoort Formation" by Miller (1980) to distinguish them from the ash-flow tuffs and porphyries in the core of the Summas Mountains.

Directly north of the Summas Mountains, the top of the Lower Naauwpoort Formation is not exposed and the base of the Ugab Subgroup is composed of poorly sorted boulder conglomerate and paraconglomerate derived from the Huab basement (Fig. 4). Above the conglomerate are rhyolite lavas and tuffs, intermediate porphyries, greenstones, and conglomerates composed of volcanic and subordinate gneiss and quartzite clasts. If the fault zone bounding the Lower Naauwpoort ash-flow tuffs and porphyries is a cauldron subsidence structure, the Upper Naauwpoort volcanics may be related to "resurgent doming" (Smith and Bailey, 1968) of the cauldron. Alternatively, the Lower Naauwpoort Formation and lower Ugab rocks to the east and northeast may have been thrust northward over the Huab gneiss and lower Ugab strata exposed directly north of the Summas Mountains (K.H. Hoffmann, *pers. comm.*, June 1994).

Sample PH.11.95 was collected at 20°28'40"S, 15°17'25"E on the north side of the Löwenfontein River near the east boundary of farm Renosterkop 389. The sample site lies directly north of the Summas Mountains and the fault zone bounding the Lower Naauwpoort Formation (Fig. 4) (Miller, 1980). The 35 kg sample was collected from a reddish, spherulitic, feldspar-phyric, massive to flow-banded, rhyolite lava dome that overlies lower Ugab paraconglomerate and dolomitic sandstone. The base of the Ugab Subgroup is not exposed directly beneath the sampled rhyolite but, according to Miller (1980), the paraconglomerate should represent the basal unit. The paraconglomerate is a dark greenish grey phyllite containing matrix-supported boulders of Huab gneiss up to 1.5 m in diameter.

Zircons separated from the rhyolite are mostly clear, stubby, euhedral prisms, 100-200 μm in length. Five single grains, three magnetic (m6) and two non-magnetic (nm5.Z1-2), and one multi-grain fraction (nm.Z3) were analysed (Fig. 3). The data define an upper intercept age anchored by one concordant analysis of 7471: 2 Ma (lower intercept = -15 ± 147; MSWD = 0.34), which we take to be the eruptive age of the rhyolite lava dome.

Conclusions

Our results imply that igneous activity associated with early Damaran extensional tectonism at the southern promontory of the Congo craton lasted for at least 10 m.y. Lower Nosib Group rift-related sedimentation began before intrusion of the Oas quartz-syenite at 756 ± 2 Ma and volcanism in the Summas Mountains lasted at least until 746 ± 2 Ma.

Rift-related magmatism at about 750 Ma is globally widespread, presumably associated with the fragmentation of a Neoproterozoic supercontinent. It occurs in the basal Windermere Supergroup of western North America (Roots and Parrish, 1988; Devlin *et al.*, 1988) and the basal Beardmore Group of the Trans-Antarctic Mountains (Borg *et al.*, 1990; Storey *et al.*, 1992). These sequences developed on conjugate margins of the Pacific basin (Moores, 1981; Ross, 1991; Powell *et al.*, 1993; Li *et al.*, 1995). Contemporaneous intraplate magmatism occurred in northwestern India (Crawford and Compston, 1970; Kochhar, 1994) and southeastern North America (Aleinikoff *et al.*, 1995; Fetter and Goldberg, 1995). These areas evolved into continental margins bordering the Mozambique (Dalziel, 1981; Stern, 1994) and Iapetus oceans, respectively, although the latter did not finally open until the Vendian (Williams and Hiscott, 1987; Kumarapeli *et al.*, 1989; Kamo

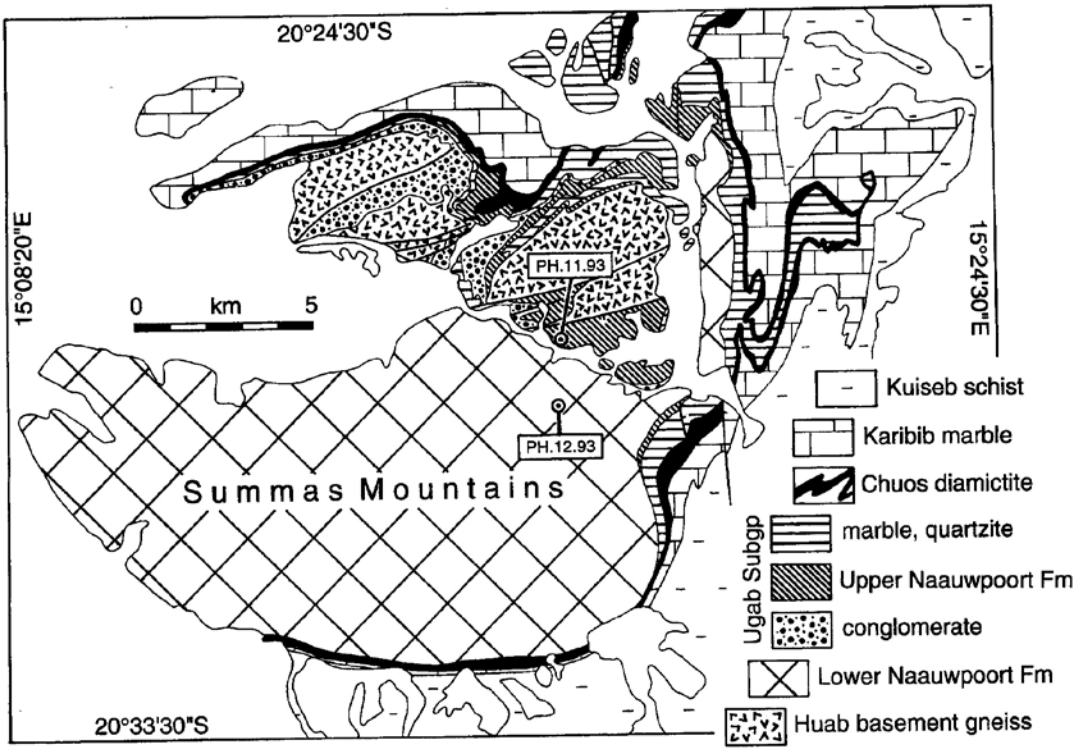

Figure 4: Geological sketch map of the Summas Mountains area (modified after Miller, 1980), showing the Lower (PH.12.93) and Upper (PH.11.93) Naauwpoort rhyolite sample sites.

et al., 1989, 1995).

Young (1995) proposed that Neoproterozoic glacial deposits fall into two age groupings, the older (Sturtian-Rapitan: ca 750 Ma) associated with the opening of the Pacific basin and the younger (Miranoan-Varanger: *ca* 600 Ma) associated with opening of the Iapetus basin. The age of 746 ± 2 Ma for the Lower Naauwpoort Formation establishes a maximum age for the glaciogenic Chuos Formation east of the Summas Mountains and, assuming stratigraphic equivalence of the Ugab and Abenab Subgroups (SACS, 1980), the age of 747 ± 2 Ma should be a minimum age for the glaciogenic(?) Varianto Formation, which occurs discontinuously at the top of the Nosib Group in the Otavi fold belt. The Varianto and Chuos Formations appear to belong to Young's (1995) older glacial suite (Hoffmann, 1994), but tectonic links between the opening of the Adamastor basin (Hartnady *et al.*, 1985; Stanistreet *et al.*, 1991) in southwest Gondwanaland and the contemporaneous opening of the Pacific basin remain unresolved.

Acknowledgements

This study was undertaken as an adjunct to a continuing programme of geological mapping and related topical studies of the Otavi fold belt in the Kunene District, supported jointly by the Geological Survey of Namibia, the National Science and Engineering Research Council and the University of Victoria (Canada), and the National Science Foundation and Harvard University (U.S.A). Andrew Bekker and Hu Guowei assisted with sample collecting and Kathy Davidek prepared the samples for zircon picking. We are grateful to N.J. Beukes, K.H. Hoffmann and R.McG. Miller for relevant discussions. Richard Armstrong and Roy Miller made valuable comments on the manuscript.

References

Aleinikoff, J.N., Zartman, R.E., Walter, M., Rankin, D.W., Lyttle, PT. and Burton, W.C. 1995. U-Pb ages of metarhyolites of the Catoctin and Mount Rogers Formations, central and southern Appalachians: evidence for two pulses ofIapetan rifting. *Am. J. Sci.*, **295**, 428-454.

Borg, S.G., DePaolo, D.J. and Smith, B.M. 1990. Isotopic structure and tectonics of the central Trans-Antarctic Mountains. *J. geophys. Res.*, **95**, 6647-6667.

Bowring, S.A, Grotzinger, J.P., Isachsen, C.E., Knoll, A.H., Pelechaty, S.M., and Kolosov, P. 1993. Calibrating rates of Early Cambrian evolution. *Science,* **261**, 1293-1298.

Crawford, A.R. and Compston, W. 1970. The age of the Vindhyan System of Peninsular India. *J. Geol. Soc.*, **125**, 351-371.

Dalziel, I.W.D. 1991. Pacific margins of Laurentia and East Antarctica-Australia as a conjugate rift pair: evidence and implications for an Eocambrian supercontinent. *Geology,* **19**, 598-601.

De Villiers, J. 1968. Geochronology. *6th ann. Rep. Precamb. Res. Unit, Univ. Cape Town*, 34-36.

Devlin, W.J., Brueckner, H.K., and Bond, G.C. 1988. New isotopic data and a preliminary age for volcanics near the base of the Windermere Supergroup, northeastern Washington, U.S.A. *Can. J. Earth Sci.*, **25**, 1906-1911.

Fetter, A.H. and Goldberg, S.A. 1995. Age and geochemical characteristics of bimodal magmatism in the Neoproterozoic Grandfather Mountain rift basin. *J. Geol.*, **103**, 313-326.

Frets, D.C. 1969. Geology and structure of the Huab-Welwitschia area, South West Africa. *Bull. Precamb. Res. Unit, Univ. Cape Town*, **5**, 235 pp.

Hartnady, C., Joubert, P. and Stowe, C. 1985. Proterozoic crustal evolution in southwestern Africa. *Episodes,* **8**, 236-244.

Hawkesworth, C.J., Gledhill, A.R., Roddick, J.C., Miller, R. McG. and Kröner, A. 1983. Rb-Sr and ^{40}Ar/39Ar studies bearing on models for the thermal evolution of the Damara belt. *In*: Miller, R.McG., (ed.) *Evolution of the Damara Orogen*. Spec. Publ. geol. Soc. S. Afr., **11**, 323-338.

Hedberg, R.M. 1979. Stratigraphy of the Ovamboland Basin, South West Africa. *Bull. Precambr. Res. Unit, Univ. Cape Town*, **24**, 325 pp.

Hoffmann, K.H. 1987. Application of tectono-stratigraphic terrane analysis in the Damara Province of central and northern Namibia. *In*: Abstract Volume. A.L. du Toit Golden Jubilee Conference on Tectonostratigraphic Terrane Analysis. *Roy. Soc. and Geol. Soc. S. Afr., Cape Town*, 25-27.

Hoffmann, K.H. 1994. New constraints on the timing of continental breakup and collision in the Damara belt. *Abstracts - Proterozoic Crustal and Metallogenic Evolution*. Geol. Soc. and geol. Surv., Namibia, **30**.

Kamo, S.L., Gower, C.F., and Krogh, T.E. 1989. Birthdate for the Iapetus Ocean? A precise U-Pb zircon and badddeleyite age for the Long Range dikes, southeast Labrador. *Geology,* **17**, 602-605.

Kamo, S.L., Krogh, T.E., and Kumarapeli, P.S. 1995. Age of the Grenville dyke swarm, Ontario-Quebec: implications for the timing of lapetan rifting. *Can. J. Earth Sci.*, **32**, 273-280.

Kochhar, N. 1994. Role ofMalani anorogenic magmatism in the crustal evolution of the northwest Indian shield. *Abstracts - Proterozoic Crustal and Metallogenic Evolution*. Geol. Soc. & geol. Surv. Namibia, Windhoek, **43**.

Kröner, A. 1982. Rb-Sr geochronology and tectonic evolution of the Pan-African Damara belt of Namibia, southwestern Africa. *Am. J. Sci.*, **282**, 1471-1507.

Kumarapeli, P.S., Dunning, G.R., Pintson, H. and Shaver, J. 1989. Geochemistry and U-Pb zircon age of comenditic metafelsites of the Tibbit Hill Formation, Quebec Appalachians. *Can. J. Earth Sci.*, **26**, 1374-1383.

Li, Z.X., Zhang, L. and Powell, C.McA. 1995. South China in Rodinia: part of the missing link between Australia-East Antarctica and Laurentia? *Geology,* **23**, 407-410.

Miller, R.McG. 1974. The stratigraphic significance of the Naauwpoort Formation of east central Damaraland, South West Africa. *Trans. geol. Soc. S.Afr.*, **77**, 363-368.

Miller, R.McG. 1980. Geology of a portion of central Damaraland, South West Africa/Narnibia. *Mem. geol. Surv. S. Afr., S.W.Afr. Ser.*, **6**, 78 pp.

Miller, R.McG. 1983. The Pan-African Damara orogen of South West Africa! Namibia. *In*: Miller, R.McG., (ed.) *Evolution of the Damara Orogen*. Spec. Publ. geol. Soc. S. Afr., **11**, 431-515.

Miller, R.McG. and Burger, A.J. 1983. U-Pb zircon age of the Early Damaran Naauwpoort Formation. *In*: Miller, R.McG., (ed.) *Evolution of the Damara Orogen*. Spec. Publ. geol. Soc. S. Afr., **11**, 267-272.

Miller, R.McG. and Schalk, KE.L. 1980. Geological map of South West Africa/Namibia (1: 1 000 000). *Geol. Surv. Namibia*, Windhoek, 4 sheets.

Moores, E.M. 1991. Southwest U.S.-East Antarctica (SWEAT) connection: a hypothesis. *Geology,* **19**, 425-428.

Powell, C.McA., Li, Z.X., McElhinny, M.W., Meert, J.G. and Park, J.K 1993. Paleomagnetic constraints on timing of the Neoproterozoic breakup of Rodinia and Cambrian formation of Gonwana. *Geology,* **21**, 889-892.

Roots, C.P. and Parrish, R.R. 1988. Age of the Mount Harper volcanic complex, southern Ogilvie Mountains, Yukon. *In*: *Radiogenic Age and Isotopic Studies: Report 2*. Geol. Surv. Can. Pap., **88-2**, 29-35.

Ross, G.M. 1991. Tectonic setting of the Windermere Supergroup revisited. *Geology,* **19**, 1125-1128.

SACS (South African Committee for Stratigraphy) 1980. Damara Sequence. *In*: Kent, L.E. (compiler), *Stratigraphy of South Africa, Part 1*. Handbook Geol. Surv. S. Afr., **8**, 415-438.

Smit, J.M. van der Merwe. 1962. Stratigraphy and metamorphism of the Otavi Series south-east of Otavi, South West Africa. *Trans. geol. Soc. S. Afr.*, **65**, 63-78.

Stanistreet, I.G., Kukla, P.A. and Henry, G. 1991. Sedimentary basinal response to a Late Precambrian Wilson cycle: the Damara orogen and Nama foreland, Namibia. *J. Afr. Earth Sci.*, **13**, 141-156.

Stern, R.J. 1994. Arc assembly and continental collision in the Neoproterozoic East African orogen: implications for the consolidation of Gondwanaland. *Ann. Rev. Earth Planet. Sci.*, **22**, 319-351.

Storey, B.C., Alabaster, T., Macdonald, D.I.M., Millar, I.L., Pankhurst, R.I. and Dalziel, I.W.D. 1992. Up-

per Proterozoic rift-related rocks in the Pensacola Mountains, Antarctica: precursors to supercontinent breakup? *Tectonics,* **11**, 1392-1405.

Smith, R.L. and Bailey, R.A. 1968. Resurgent caldrons. *In*: Coats, R.R. and others, (eds.) *Studies in Volcanology*. Geol. Soc. Am. Mem., **116**, 613-662.

Tegtmeyer, A. and Kröner, A. 1985. U-Pb zircon ages for granitoid gneisses in northern Namibia and their significance for Proterozoic crustal evolution of southwestern Africa. *Precamb. Res.*, **28**, 311-326.

Williams, H. and Hiscott, R.N. 1987. Definition of the Iapetus rift-drift transition in western Newfoundland. *Geology,* **15**, 1044-1047.

Young, G.M. 1995. Are Neoproterozoic glacial deposits preserved on the margins of Laurentia related to the fragmentation of two supercontinents? *Geology,* **23**, 153-156.

Communs geol. Surv. Namibia, ***11*** *(1996), 57-69*

The Rössing-SJ Dome, Central Zone, Damara Belt, Namibia: an example of mid-crustal extensional ramping

G.J.H.Oliver and J.A. Kinnaird

Department of Geology, University of St. Anarews, St Andrews, Fife, Scotland, KY169ST.
e-mail: gjho@st-and.ac.ukandkinnaird@iol.ie

The core of the Rössing-SJ Dome has been variously assigned to either the 1-2 billion year old Abbabis Metamorphic Complex or the Etusis Formation of the Damara cover sequence. In this work, rocks within the Dome have been remapped and a new stratigraphy and structural history is presented. When this is compared to the Abbabis Metamorphic Complex it is concluded that the core of the Rössing-SJ Dome is not Abbabis Metamorphic Complex but Damaran Etusis Formation. An intraformational upper amphibolite facies (and therefore mid-crustal) extensional ductile shear zone (the Rössing-SJ Shear Zone) has been recognised: it stretches out the stratigraphy within the dome and ramps down the sequence towards the SW where it presumably links with the Khan River Detachment along the basement-cover contact.

Introduction

The Central Zone of the Damara Orogen in Namibia (Fig. 1) is characterised by domes, often with cores of 1.1-2 billion year old Abbabis Metamorphic Complex basement (Kröner *et al.*, 1991; Jacob *et al.*, 1978), surrounded by metasedimentary units of the Damara Sequence (Miller, 1983). The Rössing-SJ Dome, (so named informally by Rössing Mine geologists), is a spectacularly exposed example and has added interest in that the Rössing Uranium Mine is situated along its southern margin.

Smith (1965) mapped the core of the Rössing-SJ Dome as remobilised and granitised red gneisses and granites with metasedimentary relicts of the Abbabis Basement. He thought that the remobilisation was.a consequence of the Damara orogenesis. Jacob *et al.* (1983), on their regional map of central Namibia, included the Rössing-SJ Dome core as Nosib Group meta-arkoses and metaquartzites. In contrast, Brandt (1987) mapped the core as Abbabis Basement whilst Miller & Grote (1988) mapped it as migmatised Etusis Formation. The core of the Dome is allocated to the "Abbabis Metamorphic Complex" on the Geological Survey of Namibia Sheet 2215A (Ebony) (Lehtonen *et al.*, 1993). Oliver (1994) briefly discussed the Rössing-SJ Dome problem and assigned the core to the Abbabis Metamorphic Complex. The controversy between whether the rocks within the core of the Dome are Abbabis basement or Damara cover is understandable in that in the field red migmatised Nosib meta-arkoses look similar to red gneissose basement.

Oliver (1994) also recognised a major SJ-Shear zone within the Rössing-SJ Dome and debated whether it was either equivalent to the Khan River Detachment or an extensional shear zone in the Damara cover linked to the Khan River Detachment in the subsurface. If the latter hypothesis were applicable, then it would be expected that the shear zone would ramp down the stratigraphy from NE towards the SW to meet the Khan River Detachment, possibly under the Rössing Mine.

In this paper, on the basis of new field work and structural studies, we conclude that the core of the Rössing-SJ Dome is made up of Nosib Group meta-sediments and that an extensional ductile shear zone, re-named the Rössing-SJ Shear Zone, ramps down the stratigraphy from NE to SW. This is the first report of mid-crustal extensional ramping in the Central Zone of the Damara Belt.

Lithostratigraphy

The stratigraphy of this part of the Central Zone is composed of the Damara Nosib Group which is subdivided into the Etusis and Khan Formations (Berning, 1986). The basal Damara (Nosib Group) lies unconformably on the Abbabis Metamorphic Complex basement (Gevers, 1934; Smith, 1965; Berning, 1986). Carbonates and pelites of the lower and upper Swakop Groups lie on top of the Nosib Group. Several generations of Damaran granite intrude both the basement and cover. Uraniferous pegmatitic leucogranite (alaskite) is mined at Rössing Mine.

Abbabis Metamorphic Complex

The Abbabis Metamorphic Complex at the type locality (Abbabis Farm, see Fig. 1) has been examined by one of us (GJHO). It is composed of granodioritic qua rtz+feldspar+biotite+muscovite L-S augen gneisses cut by dykes of foliated quartz+feldspar+biotite+muscovite leucogranite. Both these lithologies are cut by unfoliated quartz +feldspar+garnet leuco-granite dykes, which are themselves crossed by unfoliated pink quartz+feldspar pegmatite. The augen are interpreted to be the tectonised relicts of feldspar phenocrysts that crystallised in the original granodiorite magma. The Abbabis Metaorphic Complex in its type section is therefore largely made up of orthogneisses. On the neighbouring farm, Narubis 67,5 km west of Abbabis farmhouse, Brandt

(1987) called these the Narubis Granitoid Complex. Here, Steven (1993) mapped pelitic and psammitic meta-sediments as well as quartzofeldspathic orthogneisses, all crossed by an ENE-WSW trending metadolerite dyke swarm. Pegmatites cut the metadolerites. Marlow (1981) divided the Abbabis rocks into an older sequence of meta-sedimentary, metavolcanic and pyroclastic rocks, and a younger series of orthogneisses. The Abbabis Metamorphic Complex is therefore a rather heterogeneous assemblage of rocks. Steven (1993) identified one Damaran and two Abbabis deformational episodes.

The bulk zircon (unabraided) U-Pb upper intercept age of ~1925 ± 300 Ma given by Jacob *et al.* (1978) for the Abbabis gneisses from Abbabis Farm is difficult to interpret since the zircons analysed included indeterminate amounts of inherited material which suffered unknown amounts of Pb loss. New zircon dating is required. Kröner *et al.* (1991) reported ~1100 Ma concordant U-Pb zircon ages for the basement granitic gneiss in the Khan River area.

In the prominent gullies, 1500 m south of Abbabis farmhouse, there is a profound tectonic contact with 3 m of ultramylonites separating basement rocks from

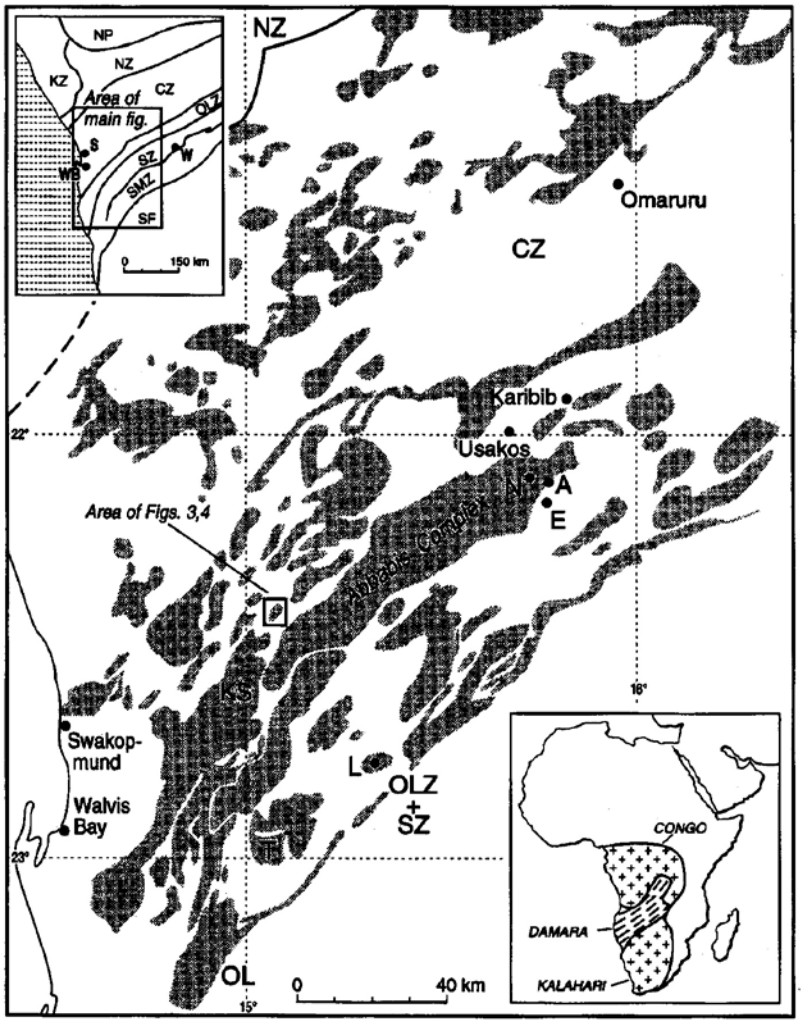

Figure 1: Location of the Rössing-SJ Dome. Lower inset shows the location of the Damara Belt between the Congo and Kalahari Cratons. Upper inset shows the major tectonostratigraphic divisions of the Damara Belt modified after Miller & Hoffmann (1981): NP = Northern Platform (Congo Craton), KZ = Kaoko Zone, SMZ = Southern Margin Zone, SF = Southern Foreland and Platform (Kalahari Craton); S = Swakopmund, WB = Walvis Bay, other abbreviations as in main figure. Main figure shows elongate dome structures (shading) of the Central Zone (CZ) as defined by Miller (1983, Fig. 19, p. 460). Northern Zone =NZ, Okahandja Lineament = OZ, Okahandja Lineament Zone = OLZ, Southern Zone = SZ of the Damara Belt. The boundary line taken to separate domes from basins is the top of either the Karibib Formation, the Nosib Group (Khan Formation) or the basement. A = farm Abbabis 70; E = farm Etusis 75; KS = Khan-Swakop confluence; L = Langer Heinrich Mountain; N = farm Narubis 67; T = Tumas Dome. The area indicated between Swakopmund and Usakos is covered in figures 3 and 4.

the overlying Damaran Etusis Formation. Basal Etusis conglomerates (containing pebbles of quartz, quartzite, granite, biotite schist and gneiss, but lacking local basement L-S tectonite pebbles) are highly strained for 20 m above the ultramylonite zone, whilst basement gneisses are highly strained, forming augen gneisses for at least 500 m below the ultramylonite. This high strain ductile shear zone dips steeply to the SE, subparallel to the Etusis strata. Oliver (1996) correlated this shear zone with the Khan River Detachment which separates basement from cover in the region of the Khan-Swakop River confluence (see Fig. 1). Therefore, at Abbabis River, the basement-cover contact is now tectonic.

Nosib Group

The Nosib Group comprises the Etusis Formation (mainly coarse- to fine-grained quartzites, arkoses and conglomerates) and Khan Formation (mainly medium-grained biotite, hornblende, clinopyroxene schists and gneisses).

Etusis Formation

The Etusis Formation is defined from the type section on Etusis 75 farm (Fig. 1; Smith, 1965), although the most complete section of the Etusis Formation occurs in the Langer Heinrich area, 45 km SE of the Rössing-SJ Dome (Fig. 1; Downing, 1983). It is the basal unit of the Damara Sequence and shows large thickness variations from 100 m to 3000 m. The main rock type is pinkish, coarse- to medium-grained, massive to thinly bedded, poorly to moderately sorted, feldspathic quartzite (Miller, 1983). At Langer Heinrich, although the base is not seen, there are 3000 m of arenite, quartzitic conglomerate and minor pelite exposed (Downing, 1983). Sedimentary logs of this relatively undeformed area show planar and cross-stratification, some of which have log deposits in the foresets. Both fining-up and coarsening-up cycles are common. Lensoid bar units of conglomerate and sand occur. Pebble horizons are prevalent in the middle of the succession.

The arenaceous rock types vary between feldspathic quartzites and arkoses with a feldspar content of between 20 and 40 vol. % and up to 10% pelitic material. Magnetite is ubiquitous and the cement is usually quartz. Interbedded pelitic units are confined essentially to the uppermost 500 m of the Langer Heinrich succession, where the overall grain size of the psammites is also finer. Sillimanite schists occur at the top of fining -upward cycles and as sharply bounded extensive bands never more than 100 mm in thickness (Downing, 1983).

Sedimentological features in the Langer Heinrich area indicate that the Etusis sequence represents an alluvial fan deposit, laid down by low-sinuosity, high- discharge braided streams in an arid to semi-arid environment. Downing (1983) suggested that the more pelitic units may indicate more stable meandering stream channels with well-developed flood basins which, in the upper parts of the unit, replaced the braided stream channels.

Nash (1971) was the first to define units within the formations around Rössing Mine. Berning *et al.* (1976) presented a table showing the Khan Formation with three units and the Etusis with five; whereas in their text they attribute four units to the Khan Formation, as in Nash (1971). Berning (1986) perpetuated this confusion by showing only two Khan subunits in his table, yet still four in the text.

For the Rössing-SJ Dome area we propose subdivision of the Kahn Formation into four new members (Fig. 2). In Table 1, an attempt is made to relate this subdivision with that of Berning *et al.* (1976).

Lower botite schist member

The lowest exposed lithology in the Rössing-SJ Dome is the lower biotite schist member which crops out in an elliptical pattern in the core of the dome (Fig. 3). It grades upwards at Locality 1 into coarse, cross- bedded flaggy arkosic quartzite beds that are from 10 to 30 cm thick at the base. The exposed schist has a minimum thickness of 15 m. Composed principally of feldspar + biotite, the schist is dark grey and locally black in colour, depending on the proportion of biotite.

In the central valley at Locality 2 (Fig. 3), the schist takes on the appearance of a streaky banded gneiss because of the abundance of anastomosing granite veins. Spots of hercynite with elongate feldspar halos are aligned along the foliation. Unfoliated pegmatitic leucogranite sheets, locally referred to as alaskite sheets (Berning, 1986), follow the foliation of the schists within the core of the Dome.

Lower metaquartzite member

The base of the lower meta-quartzite member is defined at Locality 3 (Fig. 3). In a gradation over a few metres the more arkosic schist of the lower biotite schist member transforms through flaggy micaceous quartzite, into metre-thick, bedded arkosic quartzites showing both graded bedding and cross-bedding. Both indicate

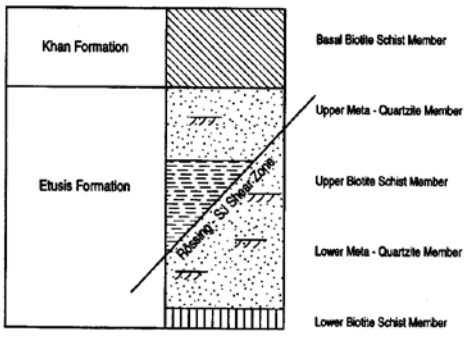

Figure 2: Tectonostratigraphic column for the Rossing-SJ Dome, Central Zone, Namibia.

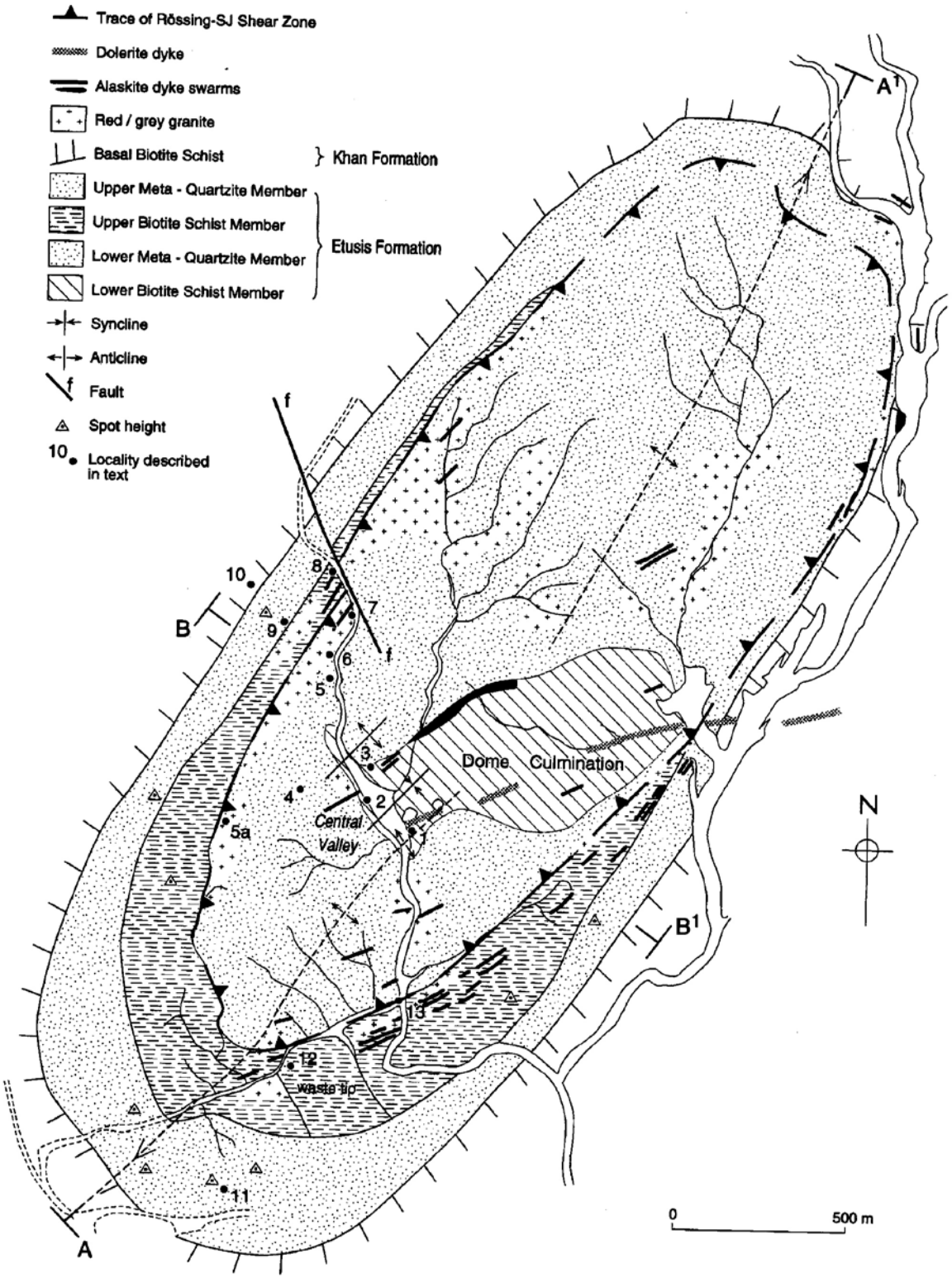

Figure 3: Geological map of the Rössing-SJ Dome. Structural orientation data is given in figure 4 and plotted on stereograms in figure 6.

that the beds are the right way up. In this part of the Dome there is little migmatite development and few alaskites.

At Locality 4 (Fig. 3), massive quartzite, striking at 010° and dipping 30° W, has clear right-way up cross-bedding younging WNW. Individual foresets are in the order of 30 cm thickness, indicating strong hydraulic regimes. The overall thickness of the lower metaquartzite member is estimated to be at least 70 m.

Both to the west and east of the central valley, the quartzite loses recognisable cross-bedding due to the development of higher strain zones. On the western flank of the Dome, at Locality 5, the original quartzitic nature is still apparent and asymptotic trough cross-bedding now indicates an inverted younging direction to the south-east. Here the rock is intimately banded with centimetre-scale, coarse-grained quartz-feldspar stromatolithic leucosomes separating similar scale melanosomes of biotite gneiss. Our interpretation is that these leucosomes represent *in situ* melting of the arkosic protolith. Non-foliated white and pink pegmatitic leucogranite sheets, commonly on the scale of 30 cm in thickness, lie sub-parallel to and parallel to the migmatite banding. These field relationships within migmatised arkoses make it difficult to distinguish individual outcrops from the basement "granitised gneiss" which has a very similar appearance. However, the protolith to these rocks in the dome is obviously meta-arkose, whereas basement protolith at Abbabis is undoubtedly granodioritic. At Locality 5a (Fig. 3), the migmatite has a different aspect in that the leucosomes form an anastomosing patchwork within metaquartzites. We would classify these rocks as agmatites formed by *in situ* partial melting of an arkosic rocktype.

At Locality 6 (Fig. 3), banded and foliated meta-arkose is interlayered with a mafic (>70% diopside + hornblende + biotite) sill-like body, 10 m thick, with centimetric thick epidote bands and ptygmatic folded alaskite veins. The banding and foliation within the mafic rock is parallel to that within the metaquartzite. Cut-offs and asymptotic cross-bedding clearly indicate that the quartzite youngs eastward. This has implications for interpretation of the structure since Locality 6 is on the NW flank of the dome where all the other indications are that the sequence youngs to the north-west.

Upper biotite schist member

The base of this member is defined at Locality 7 (Fig. 3) by a transition from the micaceous lower metaquartzite member into a grey biotite (+amphibole) schist. In the central valley this upper biotite schist member is about 100 m in thickness, but in the southern marginal portions of the Dome it thickens to a maximum of 200 m. In contrast, across the fault that runs along the central valley, it appears to thin out towards the north of the Dome and ceases to be a mappable unit.

At Locality 8 (Fig. 3), where Smith (1965) placed the basement-cover contact, there is a 100 m long continuous outcrop which shows from SE to NW the transition from quartzo-feldspathic biotite schist and subsidiary metaquartzites through grey quartzofeldspathic granitic schist, then red migmatised metaquartzites and arkoses into flaggy metaquartzite, all cut by pink and white pegmatitic leucogranites (apparently identical to the alaskites of Rössing Mine) which are sub-parallel to the foliation (004°/66°W). No evidence was found here for an angular unconformity or basal conglomerate. The grey granitic schist is strongly foliated and flattened in comparison with neighbouring schists. In thin section, the fabric has undergone grain-size reduction followed by significant annealing. We therefore interpret this rock as a mylonite and conclude that the

Table 1: Comparative stratigraphic columns for the Rössing-SJ Dome, Central Zone of the Damara Belt, Namibia.

Berning *et al.* (1976)		**This study**	
Formation	*Lithostratigraphic Units*	*Formation*	*Members*
Khan	Biotite-amphibole schist Upper pyroxene-hornblende gneiss Pyroxene-garnet gneiss/ amphibolite Lower pyroxene-hornblende gneiss	**Khan**	
	Upper biotite gneiss		Basal Biotite Schist
Etusis	Marker quartzite Lower biotite gneiss Feldspathic quartzite	**Etusis**	Upper Metaquartzites Upper Biotite Schist *Rössing-SJ Shear Zone* Lower Metaquartzite
	Unconformity	Lower Biotite Schist	
Abbabis Metamorphic Complex			not exposed

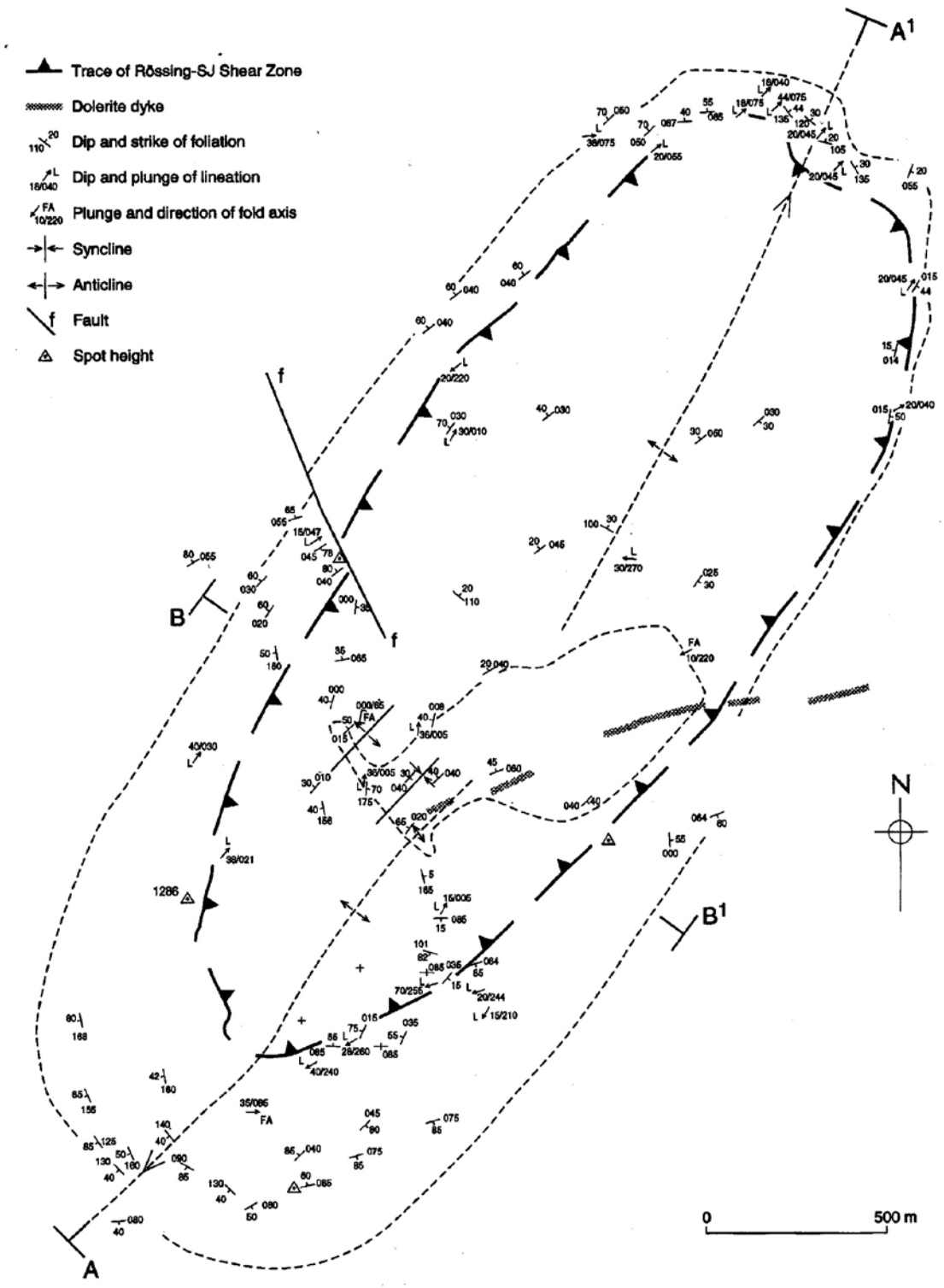

Figure 4: Structural map of the Rössing-SJ Dome. Cross sections AA[1] and BB[1] are given in figure 5.

transition between the migmatised meta-arkoses and -quartzites and the biotite schists is a ductile shear zone. This was named the SJ-Shear Zone by Oliver (1994): it is proposed to rename this the Rössing-SJ Shear Zone to indicate that it is associated with the Rössing Mine area. Details of mylonite petrography are given in a subsequent section.

Upper metaquartzite member

The base of this unit is clearly seen at Locality 9 (Fig. 3), where there is a sharp transition from biotite schists into cross-bedded and flaggy meta-quartzites. This is the base of the upper metaquartzite member. Uniformly bedded (cross-bedding plus graded bedding) quartzites with right-way up younging to the west directions are approximately 100m thick. Cross-bedding is defined by prominent heavy mineral laminae. Metre- bedded quartzites in the lower part of the member gradually become thinner-bedded upwards until they produce flaggy centimetre-bedded quartzites in the upper part. This upper metaquartzite member is the last significant quartzite in the Nosib Group.

Khan Formation

In contrast with the quartzofeldspathic Etusis Formation, the Khan Formation is dominated by gneisses and schists containing plagioclase, biotite, hornblende and clinopyroxene. We therefore place the Etusis-Khan boundary at the top of our Etusis upper metaquartzite member, equivalent to Berning's Marker Quartzite unit (see Table 1). The overlying Khan basal biotite schist member is the lowest unit of the Khan Formation.

Basal biotite schist member

This is equivalent to the upper biotite gneiss unit of the Etusis Formation as designated informally by Berning *et al.* (1976) (see Table 1). The base of the newly defined Khan Formation is best seen at Locality 10, where grey micaceous flaggy schist is transitional over 20 m downwards into flaggy, micaceous, yellowish Etusis quartzite. The contact can be followed around the margins of the Dome, close to the break in slope that defines the topographic dome feature.

The finer grain size relative to the Etusis Formation suggests more distal environments than the sandy braided fluvial systems. Smith (1965) and Jacob (1974) have suggested quiet shallow-water environments for the calcareous semipelites of the Khan Formation. De Kock and Botha (1989) suggest a coastal and tidal flat setting. Henry (1992) suggested that distal fluvial and flood - plain environments of rivers accumulated calcareous and fine-grained sediment which produced the calc-silicate rocks of the Khan Formation.

Metamorphism

These rocks await study by electron probe but some preliminary observations can be made. Etusis rocks are dominantly metamorphosed quartzites and arkoses but include also marble, calc-silicate rock, amphibolite and pelitic and semi-pelitic schists. The following mineral assemblages have been seen in individual thin section:

calc-silicate rock:
quartz+plagioclase+biotite+hornblende+diopside+opaques

amphibolites:
plagioclase+biotite+hornblende+diopside+opaques
plagioclase+k-feldspar+diopside+sphene+opaques

pelite:
quartz+plagioclase+k-feldspar+cordierite+garnet+biotite+opaques
k-feldspar+plagioclase+quartz+biotite+opaque+sillimanite

semipelites:
quartz+plagioclase+k-feldspar+biotite+opaques

The plagioclase is oligoclase, occasionally antiperthitic; K-feldspar is microcline, commonly perthitic. The lack of primary muscovite is notable, more schistose pelitic lithologies simply have more biotite. These are interpreted to be equilibrium assemblages (based on granoblastic textures) and diagnostic of the upper amphibolite facies. Secondary minerals (due to alteration) include fibrolite, chlorite, muscovite, sericite and epidote. An example of extreme alteration from Locality 7, (Fig. 3), within the Rössing-SJ Shear Zone, is a lenticular mass off ibrolite (5 mmx 0.5 mm) surrounded by a 0.5 mm wide corona of very fine grained disorientated muscovite, all in a matrix of quartz, K-feldspar, plagioclase, biotite and opaques.

Rocks below the upper biotite schist member are characterised by centimetre scale stromatolithic migmatite and diatextitic agmatite patches, composed of poorly foliated pink and white granite segregations (containing quartz+plagioclase+microcline+biotite+opaques). The geological map (Fig. 3) shows areas of more extensive red and grey biotite granite. It is possible that the migmatite melt migrated into these larger bodies. These observations suggest that the rocks were hot enough to have begun melting during metamorphism. Inspection of the P-T diagram for quartz-saturated partial melting of metapelites and metagreywackes in the presence of fluids, given by Vielzeuf & Holloway (1988), and comparison with the mineral assemblages noted above, allows peak PT conditions to be estimated. The lack of muscovite and presence of biotite+quartz+K-feldspar in pelites and migmatite partial melts (without garnet) requires temperatures of more than 730°C. The presence of hydrous fluid, biotite and cordierite and the lack of orthopyroxene restricts maximum temperature to 780°C. Because of the relatively low proportion of melting seen in outcrop, the lower temperature estimate is more probable. The presence of cordierite+garnet rather than garnet+sillimanite and the lack of orthopyroxene restricts the pressure to between 3 and 6 kbar.

Structure

Rössing - SJ Dome

Around central and northern parts of the Dome, the contact between the Khan and Etusis Formations is well exposed. Bedding and foliation dips are generally outwards (Fig. 4), but in places on the SW and SE sides of the Dome, the bedding is overturned and dips 80°NE and NW respectively. The cross-section AA' (see Fig. 5a) along the long axis of the Dome shows that it is asymmetric and overturned in the SW. The sense of vergence is towards the SW. The cross-section BB' across the dome culmination is nearly symmetrical (Fig. 5b). These cross-sections are used to suggest that Abbabis Metamorphic Complex (and therefore the Khan River Detachment) is not too far below the surface since the Etusis Formation is estimated to be 800 m thick in the Khan River Gorge.

Where bedding planes can be distinguished from compositional banding and heavy mineral layering, it is clear that tabular metamorphic minerals are lying in the same plane. Thus S_0 and S_1 are parallel. S-surfaces are picked out by the parallel orientation of biotite. Figure 6a is a stereographic projection of S_0 and S_1 measured from all around the Dome. Generally there is a scatter of plots over the whole of the stereogram as might be expected from a dome structure. Contouring shows a prominent girdle through the centre of the stereogram, reflecting the dominance of measurements from the long flanks of the Dome, the bias towards moderate dips in the NE and the near vertical dips in the SW terminations. On the map scale (Figs. 3 and 4) the form of the Etusis-Khan contact is elliptical. The simple form of the Etusis-Khan contact around the Rössing-SJ Dome means that repetitions of strata by large isoclinal folds can be excluded. However, the occurrence of inverted bedding on the NW flank of the dome at Locality 6 requires that there is a certain amount of parasitic folding associated with the dome formation. Outcrops of folds are rare; however, a minor ESE verging fold in thin-bedded quartzites, 50 m west of Locality 8, has its near vertical axis orientated parallel to the main NE-SW trending axis of the dome. A set of SW verging horizontal plunging minor folds in calc silicate bands in aim thick marble at Locality 11, trend 090° with axial planes striking at 090° and dipping 80°S. This vergence direction does not fit the concept of F_1 being re-folded by F_2 as proposed by Smith (1965). No outcrop-sized examples of interfering type F_1 and F_2 folds of Smith (1965) were observed during this mapping.

L_1-lineations are defined by the elongation of quartz, plagioclase and K-feldspar aggregates and lepidoblastic biotite. The stereogram of lineations in the Rössing-SJ Dome (Fig. 6b) shows that they are mostly orientated parallel to the long axis direction of the dome (Fig. 3).

Rössing-SJ Shear Zone

Granoblastic foam-like microtextures of high strain rocks within the SJ-Shear Zone show that the rocks have recovered and annealed during the metamorphic peak conditions. In thin section, grains lack undulose extinction, lack kinking, have straight or curving contacts, with few jigsaw piece-shaped sutured contacts and commonly exhibit 120° triple junctions. Thin sec-

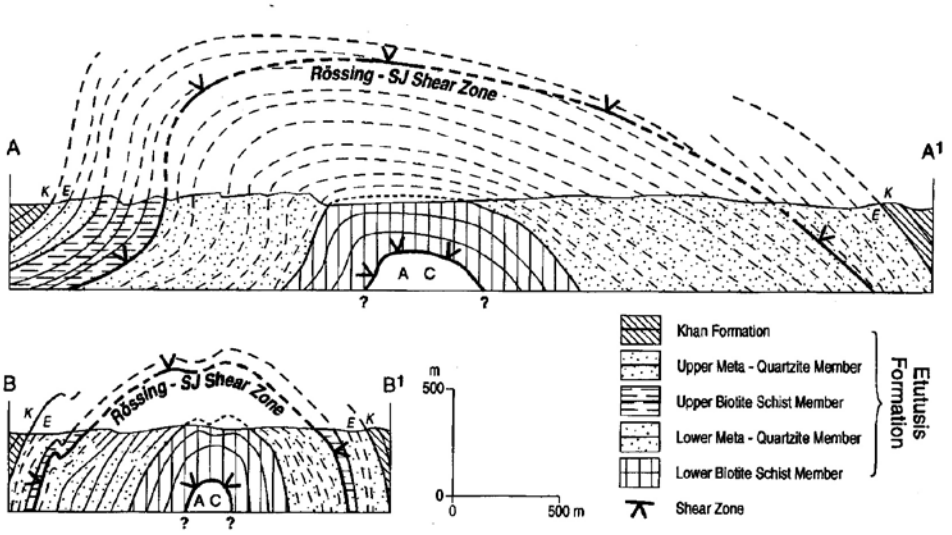

Figure 5: Cross-sections of the Rössing-SJ Dome: a) NE-SW cross section AA¹, and b) WNW-ESE cross section BB¹ (located on Fig. 4). Note that the Rössing-SJ Shear Zone is located adjacent to the Khan-Etusis boundary (=EK) in the NE and SE sides of the Dome, whereas it is lower in the sequence towards the SW: i.e. the Rössing-SJ Shear Zone ramps down the stratigraphy towards the SW. AC = Abbabis Complex; ?? indicates possible position of the Khan River Detachment.

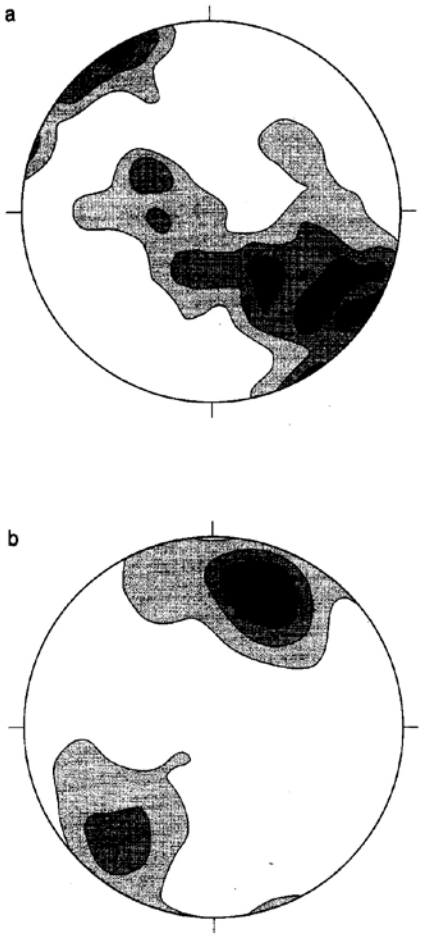

Figure 6: Structural stereograms - a) Equal area stereographic plot of 124 S_o+S_1 readings (which are parallel), contoured at 2, 4, 6 and 8 times uniform; b) Equal area stereographic plot of 30 l_1 readings, contoured at 1, 2, 3 and 4 times uniform.

tions are alternately layered into quartz and feldspar-rich ~2 mm thick stripes or ribbons. The average grain size for quartz and plagioclase varies between layers i.e. ~0.5 mm in some layers and ~0.2 mm in others. Microcline varies in size with largest grains of ~2.0 mm and the more common at ~1 mm. Grain size of the matrix in these mylonites is therefore fine to medium, a rare phenomenon in mylonites. According to White and Mawer (1986), the occurrence of rodded aggregates of plastically deformed K-feldspar in mylonites indicates syn-shearing temperatures greater than ~750°C. Below this temperature, K-feldspar has brittle properties and would be expected to form porhpyroclasts; these have not been recorded. Since the mineralogy within the shear zone is identical to the peak metamorphic mineralogy outside the zone, it is assumed that the shear zone operated at peak upper amphibolite facies metamorphic conditions. Within the shear zone at Locality 13, L/S- tectonites have X:Y:Z ratios of quartz and feldspar ribbons of 5:2:1 indicating deformation in the field of constriction (Flinn, 1958).

Occasionally biotites have chlorite replacement along their cleavages and sericitisation of feldspars is patchy; only a limited amount of hydrous fluid infiltrated parts of the shear zone after the deformation. The sillimanite + muscovite corona association (muscovite randomly orientated) reacting within a K-feldspar+quartz matrix in the SJ Shear Zone suggests that thermobaric relaxation took place in a slightly hydrous but non-tectonic environment. This is not taken as evidence for more than one regional metamorphic episode: rather, the later growth of sillimanite may be attributed to thermal relaxation and decompression after the metamorphic peak.

Most thin sections show fabrics that are so well annealed that shear sense indicators are absent. Despite this, orientated thin sections from Locality 8 show mica-fish textures indicating that the hanging wall to the shear zone moved towards the SW. The sense of shear in higher strain shear bands was also identified by the deflection of mica foliation (Simpson and Schmid, 1983; Simpson and Depaor, 1993).

In the core of the Dome, between Localities 1 and 2, structurally about 500 m below the Rössing-SJ Shear Zone where bedding and foliation are parallel and flat lying, packets of quartzite beds have suffered boudinage and rotation, and the asymmetry of the boudins indicates that the top side has moved towards the SW. This, plus the fact that the Dome envelope is asymmetric along its NE-SW long axis and verges SW, together with the SW vergence evidence from small folds at Locality 11, builds a consistent picture that the hanging wall to the Rössing-SJ Shear Zone moved down towards the SW.

Discussion

Oliver (1994) discussed the concept of the Central Zone domes being the result of combined crustal NW -SE compression and SW-NE extension when the cover was detached from the basement along the Khan River Detachment, flowed plastically and escaped towards the SW during collision of the Kalahari and Congo Cratons. Under these conditions the principle ductile strains would become constructional with $\lambda 1 > 1 > \lambda 3$ (see Ramsay, 1967, Fig. 3.54, field 2) and this would explain why the dominant extension lineation is orientated parallel to the elongation direction of the domes. Interfering fold phases of different ages are not required in this model. The fact that the extension lineation neither follows around the margins of the Rössing-SJ Dome nor radiates down dip away from its core argues against diapiric rise (see Ramberg, 1972) and/or ballooning (see Kröner, 1984) as a cause of doming.

It can be seen from figure 4 that the Rössing-SJ Shear Zone is located adjacent to the Khan-Etusis boundary on the NE side of the Dome whereas it is much lower in the sequence towards the SW. The NE-SW cross

section shown in figure 5a illustrates this and shows how the upper biotite schist member thins out to the NE as a consequence of tectonic stretching. In figure 5a the Rössing-SJ Shear Zone is seen ramping down the stratigraphy towards the SW (or alternatively, ramping up towards the NE). A low-angle detachment fault, that has the hanging wall moving down stratigraphy without repetition of strata, must be extensional by definition. This fits the model of crustal extension proposed by Oliver (1994) for the Damara Central Zone in which it was suggested that shear zones in the middle crust should eventually ramp up the sequence towards the NE into half graben sedimentary basins. Oliver (1994) also suggested that they should ramp down the sequence towards the SW to meet the Khan River Detachment (see Fig. 10 in Oliver, 1994). Current mapping has not located this branch line; it might lie under Rössing Mine. Figure 7 is a block diagram illustrating how this might occur. Figure 8 is a series of cartoons that reconstruct the sequence of events that formed the Rössing-SJ Dome and Shear Zone. Firstly, due to crustal extension the middle crust has failed along the basement-cover unconformity, forming a flat basal or sole detachment; this detachment would have reached the surface as a series of half-grabens. Secondly, with more extension (perhaps involving ~20% stretching and 20% flattening) the middle and upper crust failed on a subsidiary extensional shear zone: this shear zone can be followed along flats and down ramps until it joins and extends the sole detachment surface. It is possible that a series of linked extensional shear zones are present in the Damara - it remains to be seen if they can be located. Thirdly, the shear zones were folded to produce the dome structure (although this might occur syn-shearing).

Locally in the Dome there has been a high degree of partial melting so that the rocks are not unlike Abbabis Metamorphic Complex gneisses in appearance. It would be possible to believe that, in a SE traverse along the central valley through the W side of the Dome, there was a transition from the Etusis Formation through a high strain zone into basement-like meta-quartzites and arkoses. However, the whole of the north and central part of the Dome consists of meta-quartzites and meta- arkoses with varying degrees of melt locally becoming streaky and migmatitic but usually retaining recognisable patches of cross-bedded quartzite. These meta-quartzites and meta-arkoses look nothing like the typical Abbabis Metamorphic Complex in its type section on Abbabis farm where granitic augen gneisses and various cross-cutting granite dykes occur. Nor do Rössing-SJ Dome metasediments look like typical Abbabis metasediments found on Narubis: the latter do not include any meta-arkose. Significantly, the Rössing-SJ Dome lacks the cross-cutting metadolerite dyke swarm which is so conspicuous on Narubis farm.

Lastly, the two episodes of deformation described by

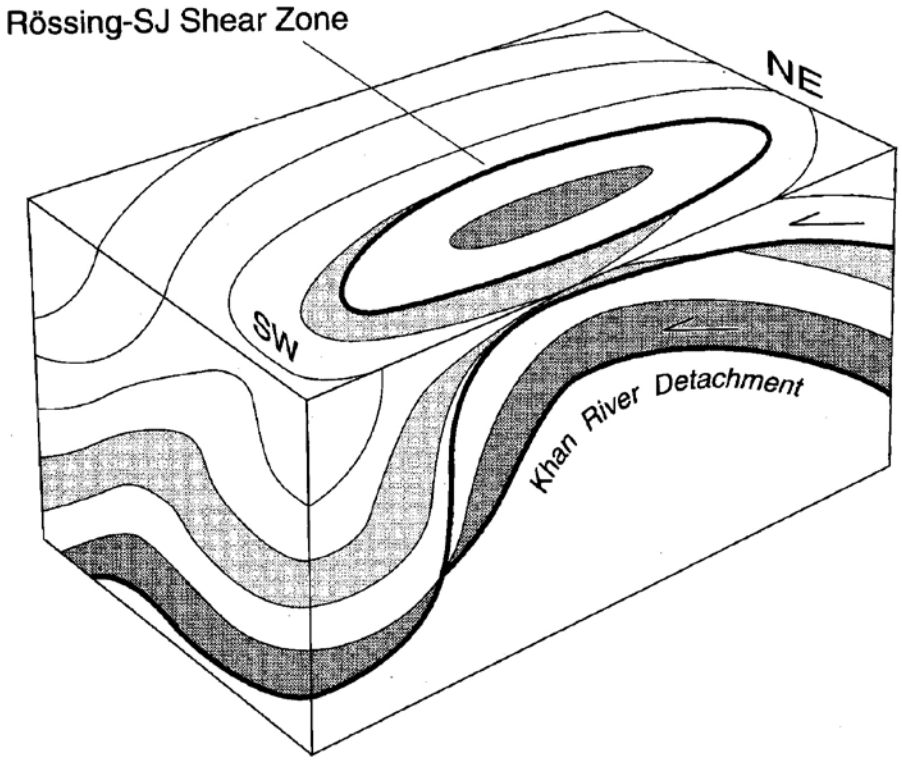

Figure 7: Block diagram of the Rössing-SJ Dome area showing how the Rössing-SJ Shear Zone ramps down the stratigraphy towards the southwest to join the Khan River Detachment.

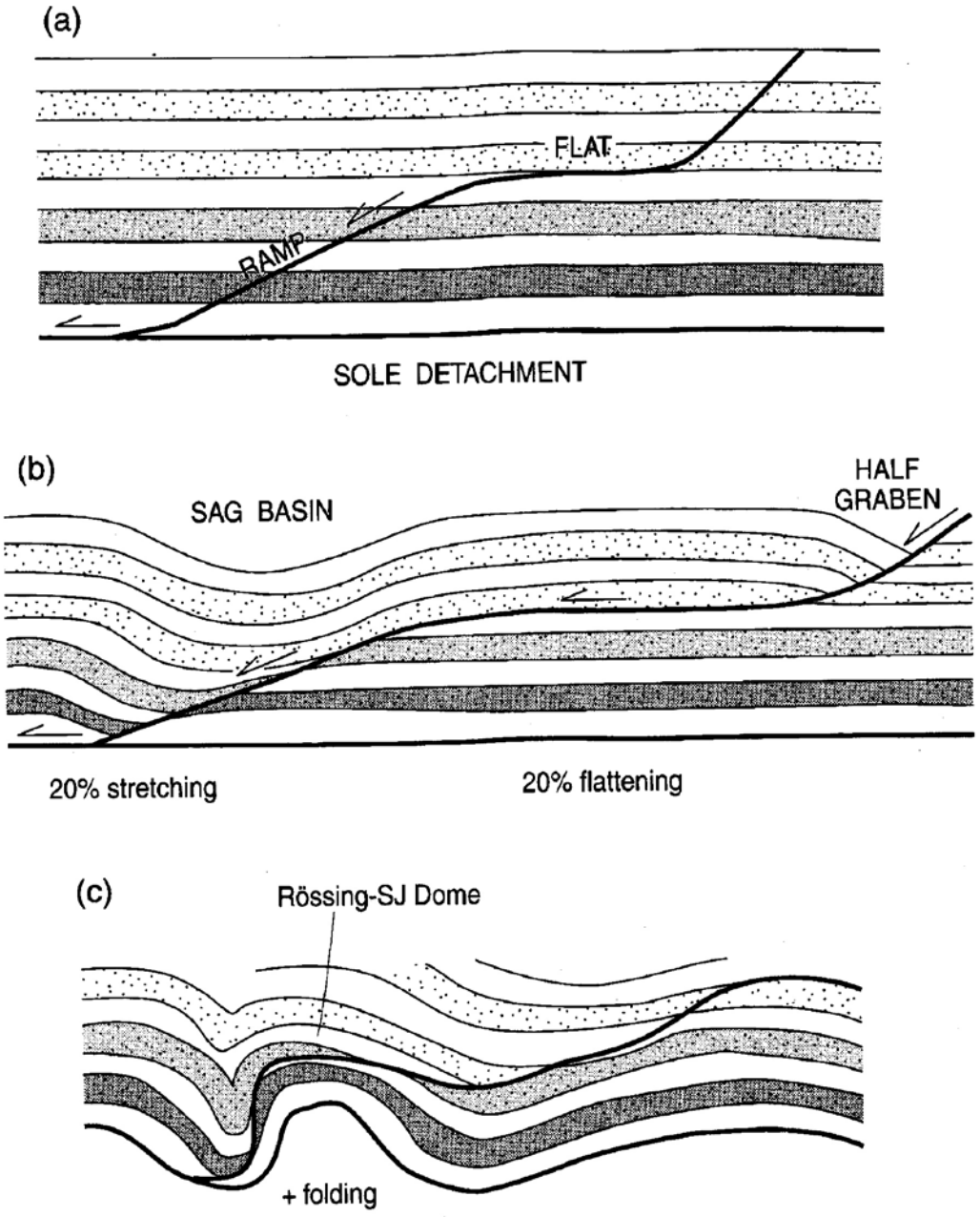

Figure 8: Cartoons of structural development of the Rössing-SJ Dome area: a. Flat lying strata showing the trace of a future extensional shear zone ramping down stratigraphy: the middle crust has already failed along the basement-cover unconformity forming a flat sole detachment; b. The middle and upper crust has failed along the extensional shear zone - this shear zone can be followed along flats and down ramps until it joins and extends the sole detachment surface. Note how half-grabens and sag basins might form at the surface; c. Shear zones were folded during regional constriction to produce the dome structure; field and petrographic evidence suggests synchronous folding and shearing.

Steven (1993) for the Abbabis Metamorphic Complex are not recognised in the core of the Rössing-SJ Dome.

Conclusions

1. The core of the Rössing-SJ Dome consists of Etusis Formation quartzite and biotite schist members that have undergone varying degrees of partial melting. This is in agreement with Jacob *et al.* (1983) and Miller & Grote (1988).
2. The Rössing-SJ Shear Zone was active during the regional peak metamorphism as an extensional ductile shear zone that ramped down the stratigraphy from NE to SW to connect with the Khan River Detachment.

Acknowledgements

We thank F. Solesbury of Geotec Namibia, members of the Geology Department at Rössing Mine and the Geological Survey of Namibia for all their help. Paul Nex was a valuable field assistant. G. Sandeman prepared the figures. Reviews by K.H. Hoffmann and an anonymous referee greatly improved the paper. GJHO was funded by NERC grant GR9/1152.

References

Berning, J., Cooke, R., Hiemstra, S.A. and Hoffman, U. 1976. The Rössing Uranium Deposit, South West Africa. *Econ. Geol.*, **7**, 351-368.

Berning, J. 1986. The Rössing Uranium deposit, South West Africa/Namibia. *In*: Annhaeusser, C.R. and Maske, S. (eds.) *Mineral deposits of southern Africa*. Geological Society of South Africa, Johannesburg, 1819-1832.

Brandt, R. 1987. A revised stratigraphy of the Abbabis Complex in the Abbabis inlier, Namibia. *S. Afr. J. Geol.*, **90**, 314-323.

De Kock, G.S. and Botha, B.J.V. 1989. Depositional environment and basin analysis of the Etusis Formation in the central Damara orogen. *S. Afr. J. Geol.*, **92**, 183-196.

Downing, K.N. 1983. The stratigraphy and palaeo-environment of the Damara Sequence in the Okahandja Lineament zone. *In*: Miller, RMcG. (ed.) *Evolution of the Damara Orogen of South West Africa*. Spec. Publ. geol. Soc. S. Afr., **11**, 37-41.

Flinn, D. 1958. On the nappe structure of North-east Shetland. *Q. J. geol. Soc. Lond.*, **114**, 107-136.

Gevers, M.A. 1934. Geology of the Windhoek District in South- West Africa. *Trans. geol. Soc. S. Afr.*, **36**, 221-251.

Henry, G. 1992. *The sedimentary evolution of the Damara Sequence in the Lower Khan River Valley, Namibia*. Ph.D. thesis (unpubl.), University of Witwatersrand, 217 pp.

Jacob, R.E., Kröner, A. and Burger, A.J. 1978. Areal extent and first U-Pb age of pre-Damara Abbabis Complex in the central Damara belt of S W Africa (Namibia). *Geol. Rndsch.*, **67**, 706-717.

Jacob, R.E. 1974. Geology and metamorphic petrology of part of the Damara Orogen along the lower Swakop River, South West Africa. *Bull. Precambr. Res. Unit, Univ. Cape Town*, **17**, 185 pp.

Jacob, R.E., Snowden, P.A. and Bunting, F.J.L. 1983. Geology and structural development of the Tumas basement dome and its cover rocks. *In*: Miller, R.McG., (ed.) *Evolution of the Damara Orogen of South West Africa*. Spec. Publ. geol. Soc. S. Afr., **11**, 157-172.

Kröner, A. 1984. Dome structures and basement reactivation in the Pan-African Damara belt of Namibia. *In*: Kröner, A. and Greiling, R.O., (eds). *Precambrian Tectonics Illustrated*, Nagele u. Obermiller, Stuttgart, 191-206

Kröner, A., Retief, E.A., Compston,W., Jacob, RE. and Burger, A.J. 1991. Single-grain and conventional zircon dating of remobilised basement gneisses in the central Damara belt of Namibia. *S. Afr. J. Geol.*, **94**, 379-387.

Lehtonen, M., Manninen, T. and Schreiber, U. 1993. Geological Map 1:100 000 Sheet 2215A Ebony. Open file geological map, Geological Survey of Namibia, Windhoek.

Marlow, A.G. 1981. *Remobilisation and primary uranium generation in the Damaran Orogenic Belt*. Ph.D. Thesis, (unpubl.) University of Leeds, 277p.

Miller, R.McG. 1983. The Pan-African Damara orogen of South West Africa/Namibia. *In*: Miller, RMcG., (ed.) *Evolution of the Damara Orogen of South West Africa*. Spec. Publ. geol. Soc. S. Afr., **11**, 431-515.

Miller, RMcG. and Grote, W. 1988. Geological Map of the Damara Orogen, 1:500,000. Map accompanying Miller, R.McG. (ed.) *Evolution of the Damara Orogen of South West Africa*. Spec. Publ. geol. Soc. S. Afr., **11**, 515 pp

Miller, R.McG. and Hoffmann, K.H. 1981. *Guide to the excursion through the Damara Orogen*. Geocongress 81, Geol. Soc. S. Afr., 103 pp.

Nash, C.R. 1971. Metamorphic petrology of the SJ area Swakopmund District South West Africa. *Bull. Precambr. Res. Unit, Univ. Cape Town*, **9**, 77 pp.

Oliver, G.J.H. 1994. Mid-crustal detachment and domes in the Central Zone of the Damara Orogen, Namibia. *J. Afr. Earth Sci.*, **19**, 331-344.

Oliver, G.J.H. 1996. The Central Zone of the Damara Orogen, Namibia, as a deep metamorphic core complex. *Commun. geol. Surv. Namibia*, **10**, 33-41.

Ramberg, H. 1972. Theoretical model of density stratification and diapirism in the earth. *J. geophys. Res.*, **77**, 877-889.

Ramsay, J.G. 1967. *Folding and Fracturing of Rocks*. McGraw-Hill, New York, 568 pp.

Simpson, C. and Schmid, S.M. 1983. An evaluation of criteria to deduce the sense of movement in sheared

rocks. *Bull. geol. Soc. Am*, **94**, 1281-1288.

Simpson, C. and Depaor, D.G. 1993. Strain and kinematic analysis in general shear zones. *J. struct. Geol.*, **15**, 1-20.

Smith, D.A.M. 1965. The geology of the area around the Khan and Swakop Rivers in South West Africa. *Mem. geol. Surv. S. Afr., SWA Series*, **3**, 113 pp.

Steven, N.M. 1993. A study of epigenetic mineralisation in the Central Zone of the Damara Orogen, Namibia with special reference to gold, tungsten, tin and rare earth elements. *Mem. geol. Surv. Nam.*, **16**, 166 pp.

Vielzeuf, D. and Holloway, J.R. 1988. Experimental determination of the fluid-absent melting relations in the pelitic system. *Contrib. Mineral. Petrol.*, **98**, 257-276.

White, J.C. and Mawer, C.K 1986. Extreme ductility of feldspars from a mylonite, Parry Sound, Canada. *J. struct. Geol.*, **8**, 133-143.

Communs geol. Surv. Namibia, ***11*** *(1996), 71-82*

Report: lithostratigraphy of the area between the Swakop, Khan and lower Omaruru Rivers, Namib Desert

M.I. Lehtonen[1], T.E.T. Manninen[2] and U.M. Schreiber[3]

[1]Geological Survey of Finland, Betonimiehenkuja 4, 02150 Espoo, Finland;
[2]Geological Survey of Finland, P.B. 77, 96101 Rovaniemi, Finland;
[3]Geological Survey of Namibia, P.O. Box 2168, Windhoek, Namibia

The study area, situated between the Khan, Swakop and lower Omaruru Rivers, comprises rocks of the Abbabis Metamorphic Complex overlain by the Damara Sequence, as well as a variety of Cambrian and Mesozoic intrusives. Field studies assisted by LANDSAT image interpretation have led to a revision of the stratigraphy of the Central Zone of the Damara Orogen, which has been subject to controversy. A schist - calc silicate rock - marble sequence present between the Chuos and Karibib Formations is introduced into the stratigraphic nomenclature as the Arandis Formation, and correlated with the Oberwasser, Okawayo and Spes Bona Formations of the Karibib area. However, distinct lithostratigraphic successions are recognised in the northern and southern parts of the Central Zone, separated by the Omaruru Lineament.

Introduction

The study area is situated along the central coast of Namibia between the towns of Swakopmund and Henties Bay, and extends inland to the Khan River (Fig. 1, inset). Tectonically it lies within the western Central Zone of the Damara orogenic belt. The oldest rocks present comprise highly metamorphosed and deformed gneisses of the Mokolian Abbabis Metamorphic Complex, which outcrop in domal and anticlinal cores along the Khan River (Fig. 1). They are unconformably overlain by folded and metamorphosed sediments of the Neoproterozoic coarse to fine clastic Nosib Group and the carbonates and fine-grained clastics of the Swakop Group (Damara Sequence). The Nosib and Swakop Groups are separated by a paraconformable contact (Henry, 1992). On the plains northwest of the Omaruru Lineament extensive sand and calcrete cover prevails and outcrops are scarce.

Both the Abbabis Metamorphic Complex and the overlying Damara Sequence exhibit complex small and large scale fabrics, while on a regional scale northeast striking folds are the predominant deformational features in the mapped area (Brandt, 1985). The northeast striking Omaruru Lineament transects the area (Fig. 1) and separates the southern and northern Central Zone of the Damara Orogen. Facies changes across it and the preservation of higher stratigraphic levels in the northern Central Zone are ascribed to vertical movement along this lineament (Klein, 1980). The style of folding appears to be tighter in the southern Central Zone.

Widespread granitic to granodioritic melts intruded the sedimentary sequence during the Neoproterozoic (late Namibian) and Cambrian in association with the various deformational events of the Damara Orogeny. In the study area porphyritic biotite "Salem" granites and red granites are common, while leucocratic granites are relatively scarce. Pegmatites are associated with all of these suites. Younger intrusions comprise the Cretaceous Henties Bay Syenite (Fig. 1), as well as numerous northeast trending dolerites and subordinate acidic dykes of Jurassic and Cretaceous age.

Parts of the area were previously mapped and studied by Smith (1965), Jacob (1974), Marlow (1981) and Brandt (1985). The present mapping was undertaken within the framework of the Finnish-Namibian Geological Mapping and Maps Project with the aim of providing a more detailed lithostratigraphic description of a previously poorly known area, and thus contribute towards clarifying the ambiguous stratigraphy of the Central Zone of the Damara Orogen (Table 1). In accordance with the recognition of a schist and marble unit below the Karibib Formation in the study area, the subdivision of the middle Swakop Group, established by Botha (1978) along the lower Omaruru River and by Badenhorst (1987, 1992) in the Karibib area, has been revised. The newly introduced Arandis Formation (Table 1) conformably overlies the Chuos Formation mixtites and comprises the Oberwasser, Okawayo, Spes Bona and Karub Members, of which the first three are correlatives of the Oberwasser, Okawayo and Spes Bona Formations of the Karibib District (Badenhorst, 1992). The basal marble layer (Karub Member) appears to be restricted to the area between the Khan River and the Omaruru Lineament. The Arandis Formation is exposed south of Rössing Mountain and in narrow belts surrounding the domes and anticlines along the Khan River. Isolated outcrops are also found among the largely sand covered areas north of the lower Swakop River and east of Henties Bay.

Lithostratigraphy of the area mapped

Abbabis Metamorphic Complex

The highly metamorphosed rocks of the pre-Damara Abbabis Complex outcrop in the cores of domes and anticlines adjacent to the Khan River (Fig. 1). This heterogeneous sequence, in which primary features have been almost entirely obliterated, comprises augen, migmatit-

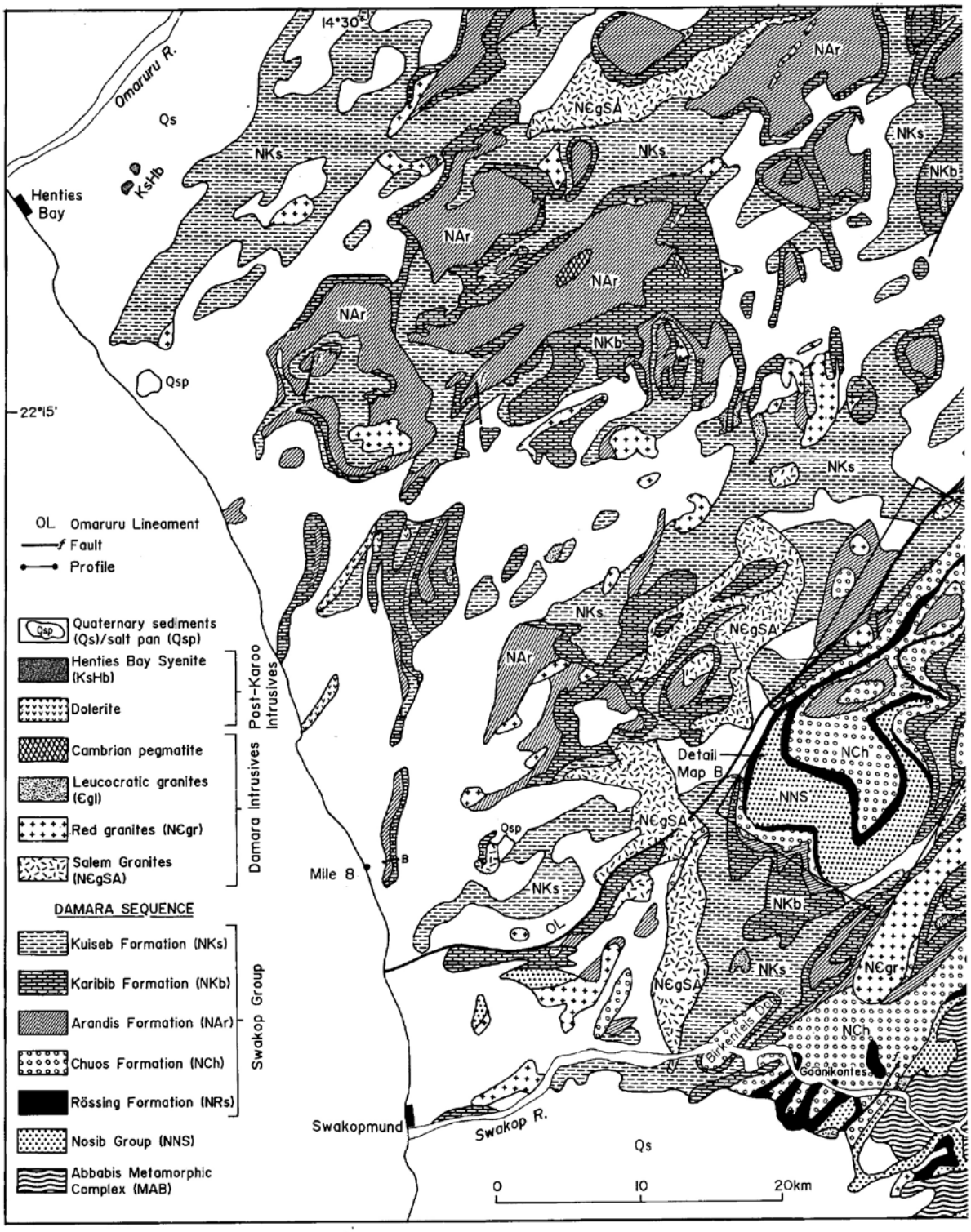

Figure 1: Generalised geological map and location of the study area (inset). The areas covered by detailed maps in figures 2, 4 and 6 are shown and labelled as Maps A, B and C, respectively.

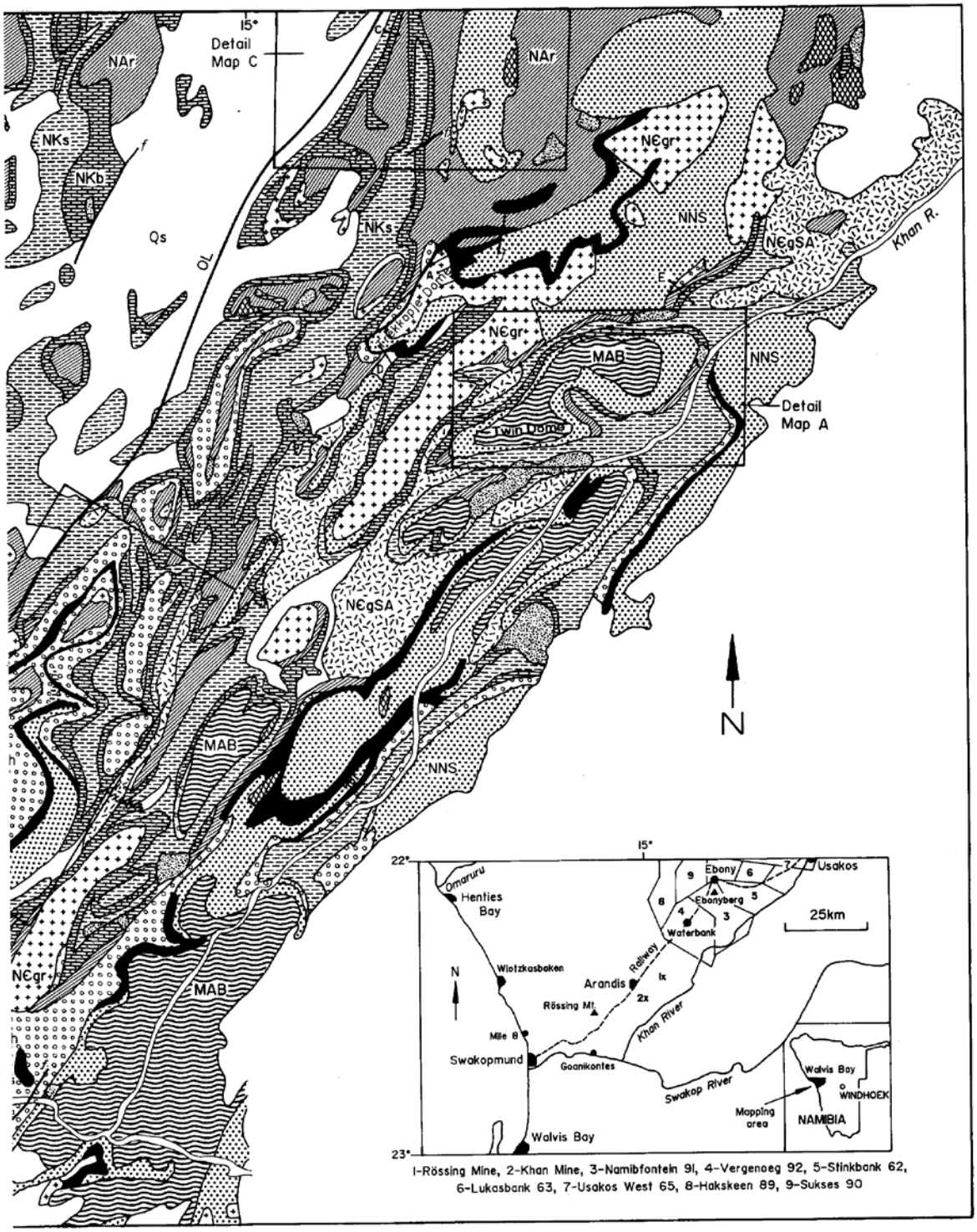

1-Rössing Mine, 2-Khan Mine, 3-Namibfontein 91, 4-Vergenoeg 92, 5-Stinkbank 62, 6-Lukasbank 63, 7-Usakos West 65, 8-Hakskeen 89, 9-Sukses 90

ic, biotite sillimanite and granitic gneisses, biotite schist and amphibolite. The predominant augen gneiss consists of large (5 to 20 mm) microcline porphyroblasts in a foliated quartz-biotite-feldspar matrix. Local granitic bodies and pegmatite dykes probably were generated at various stages in the Damara Orogeny. Amphibolite inclusions in granitic gneisses in the Khan River area are up to tens of metres in thickness. They represent either boudinaged pre-Damara basic dykes or volcanic flows similar to metabasalts of the Naob Formation in the Abbabis Inlier (Marlow, 1981; Brandt, 1987). Dark magnetite and sillimanite bearing quartzofeldspathic gneisses around the western part of the "Twin Dome" (Kröner, 1984) possibly can be correlated with the biotite sillimanite gneisses and dark biotite schists of the lower Naob Formation (Smith, 1965; Brandt, 1987).

Damara Sequence

Nosib Group

Etusis Formation The up to 3500 m thick Etusis Formation commonly grades down into the increasingly metamorphosed rocks of the Abbabis Complex. Recognition of the contact between the units is further complicated by the general conformity of the foliation. The arkosic and micaceous gneisses and feldspathic quartzites of the Etusis Formation outcrop in narrow zones around the granitic or gneissic cores of domes and anticlines (Fig. 2). Red syntectonic granites present in some dome cores (Fig. 1) were possibly derived from these rocks and the underlying gneisses during orogenic events. Commonly characterised by low relief and poor exposure in the mapping area, the Etusis Formation forms hills and ranges east of the Khan River. Contrary to previous mapping, the Rössing Dome (Fig. 1) is now thought to consist entirely of Etusis gneisses and quartzites exhibiting various stages of metamorphism and deformation (Oliver and Kinnaird, 1996).

The predominant, light-brown to pink, fine-to medium-grained quartzites and meta-arkoses vary in appearance according to metamorphic grade. Parallel bedding and low angle crossbedding are well preserved in the Khan River area (e.g. on the farm Namibfontein 91), where the grade is comparatively low. Within the more intensely deformed and metamorphosed domes parallel bedding and cross-laminae are defined by thin heavy mineral layers. The microscopic texture of the feldspathic quartzites is predominantly blastoclastic (recognisable relict lithic clasts) to granoblastic. The rare rocks in which primary clastic grains remain recognisable consist of rounded to subangular quartz and feldspar, the latter commonly exhibiting perthitic and microperthitic intergrowths. Garnet is usually present as an accessory.

A 10 to 15 m thick intraformational conglomerate, consisting of 5 to 15 cm deformed quartz and quartzite pebbles in an arkosic matrix, is present on the farm Stinkbank 62 (Fig. 1, inset). On the farm Sukses 90, one to 3 m thick graded beds of quartz pebble conglomerate, fining upward into medium grained meta-arkose, occur in the upper third of the Etusis Formation. Elsewhere, the uppermost part of the formation often consists of a some tens of metres thick red arkosic gneiss with oriented white quartz sillimanite nodules. Mica schist and calc silicate quartzite are encountered within the unit at various stratigraphic levels.

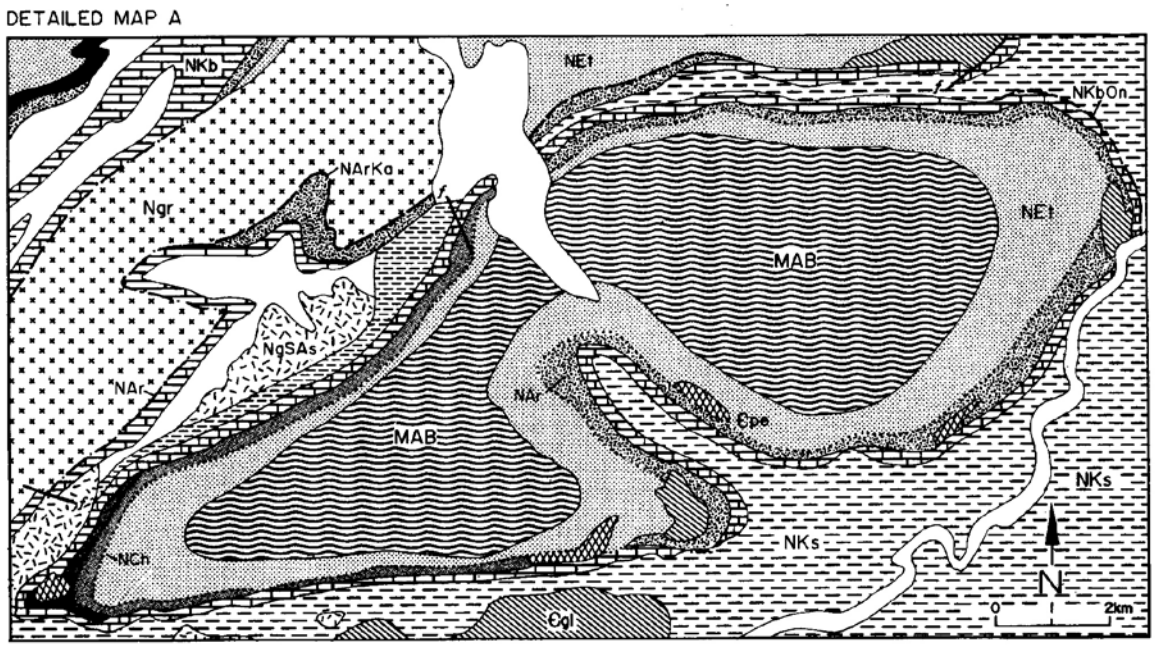

Figure 2: Detailed geological map (marked A in Fig. 1) of the"Twin Dome" area, Farms Vergenoeg 92 and Namibfontein 91 *(legend on facing page).*

Khan Formation Generally the pyroxene-, amphibole- and feldspar-bearing quartzites and gneisses of the Khan Formation form a sharp contact with the underlying Etusis Formation. In places, however (e.g. on the farms Namibfontein 91 and Vergenoeg 92), the Khan Formation is represented by a calc silicate-rich interlayer of variable thickness within the upper part of the Etusis quartzites, indicating an interfingering relationship. The prominent inselberg of Rössing Mountain consists of greenish-grey scapolite-bearing calc-silicate quartzites of the Khan Formation, which in the west of the area reach up to 1000 m in thickness (Fig. 4). At Rössing Mountain they are thickly bedded, whereas thin bedding, emphasised by alternating light-coloured arkosic and greenish pyroxene-amphibole-bearing layers, is predominant in the Khan River area. Intraformational conglomerates, consisting of rounded quartzite pebbles (< 10 cm) in a coarse-clastic matrix, are exposed southeast of Ebonyberg, at Rössing Mountain,

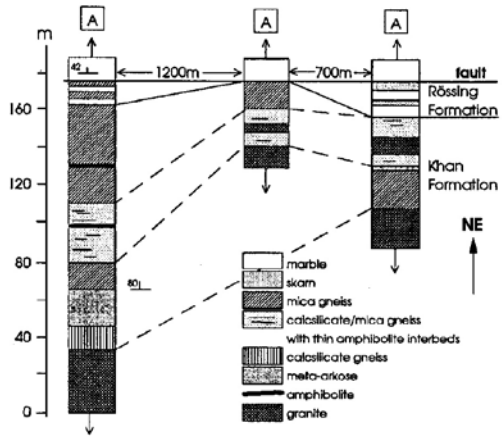

Figure 3: Lithostratigraphic profiles for the upper part of the Khan and lower part of the Rössing Formation, Farm Vergenoeg 92 (profiles A in Fig. 1).

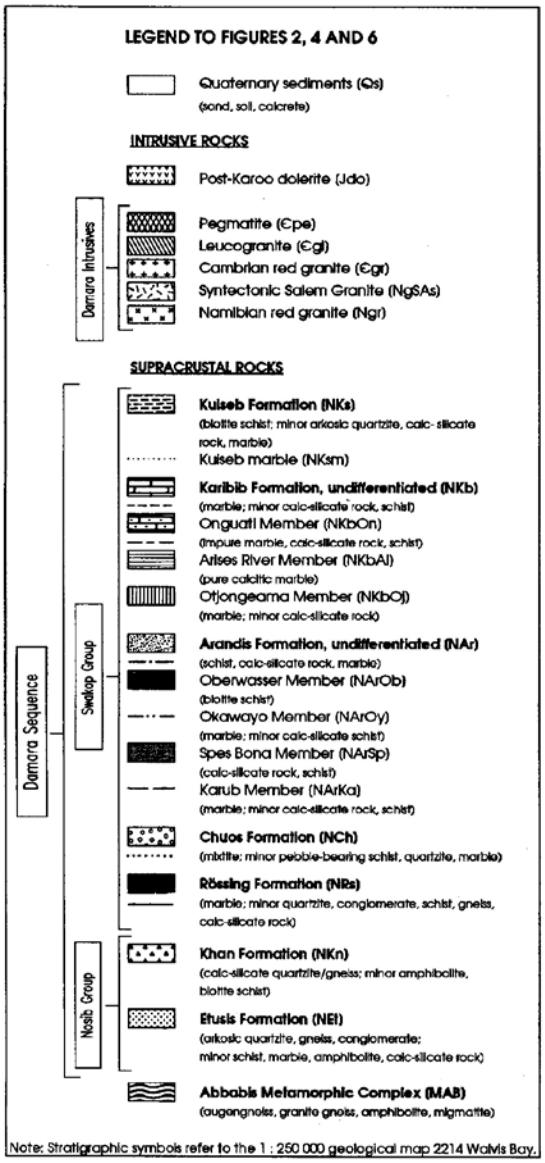

on the farm Namibfontein 91 (Fig. 1, inset), and in the lower Swakop gorge, near Goanikontes, where they resemble the mixtites of the overlying Chuos Formation. An up to 20 m thick dark biotite - amphibole schist or amphibolite layer forms the uppermost part of the Khan Formation near the Rössing Uranium Mine, in the Trekkopje Dome (Fig. 3) and in the Goanikontes area (P. Nex, *pers. comm.*).

Swakop Group

Rössing Formation The Rössing Formation is lithologically heterogeneous and paraconformably (Henry, 1992) overlies the Nosib Group (Fig. 3). At the mouth of the Khan Mine gorge and around Rössing Dome it reaches ca. 200 m in thickness (Jacob, 1974) and consists of impure dolomitic marble, calc-silicate gneiss, quartzite, conglomerate and biotite-cordierite schist. From the Rössing Dome it thins rapidly to the northeast, where it is represented by a thin schist or marble layer. Towards the coast it is characterised by light-grey to buff marble forming prominent, continuous ridges. At Mile 8, the Rössing Formation is represented by a clastic meta-arkose displaying graded bedding, whilst in one locality, northeast of Swakopmund, a 10 to 30 m thick massive serpentine-bearing (up to 35 modal per cent) marble surrounds a dome of red granite and Khan Formation gneisses. Northeast of Rössing Mountain the same marble horizon locally forms sharp-crested anticlines. On the Swakop River, near Goanikontes, the formation comprises predominant arkosic quartzite, with interbedded conglomerate and biotite schist.

West of the Omaruru Lineament the Rössing Formation is exposed only in the core of a northeast plunging anticline situated some 15 km north of Swakopmund. Here, it is characterised by light-grey marble and laminated quartzite. The latter contains sulphide and sillimanite and is locally stained dark grey by disseminated graphite.

Figure 4: Detailed geological map (marked B in Fig. 1) of the area around Rössing Mountain, northeast of Swakopmund.

Chuos Formation The Chuos Formation rests unconformably on the Rössing Formation and outcrops extensively between the Khan River and the Omaruru Lineament (Fig. 1). The up to 700 m thick massive mixtite typically consists of deformed clasts in a dark grey to greenish-grey gritty, foliated quartz-biotite-feldspar matrix. The clast-size decreases from angular to subrounded boulders and cobbles in the Khan River gorge to rounded pebbles and minor cobbles further to the west. Concomitant with size, the predominantly metasedimentary and granitic clasts which are derived from underlying units decrease in abundance. Epidotised marble clasts are found northeast of Rössing Mountain.

A thin layer of pebbly schist is present in the "Twin Dome" (Fig. 2). Subordinate rock types within the Chuos Formation are thin marble beds in the Goanikontes area, and iron formation at Mile 8 (Fig. 5, profile B) and in the Khan River area (Henry *et al.*, 1986). Along the northwestern limb of the Trekkopje Dome (Fig. 1) a lateral lithological change from grey massive fragment-bearing rock in the southwest to atypical greyish light-brown gritty meta-arkose in the northeast is observed. The meta-arkose, which underlies the Karub Member of the Arandis Formation, shows a blastoclastic texture with angular to subrounded quartz grains. It contains sericitised andesine, as well as accessory biotite, sphene and apatite.

Arandis Formation Since the first published reference to the schist layer between the Chuos mixtite and the Karibib marble (Gevers, 1931), the nature and stratigraphic status of this unit has been subject to controversy. It has been correlated with either the underlying Chuos or the overlying Karibib Formation (e.g. Jacob, 1974; Bunting, 1977; Marlow, 1981; Miller, 1983; Henry, 1992). Table 1 gives an overview of the stratigraphic nomenclature and correlations used by previous authors. Botha (1978) named the schist unit below the Karibib marble Oberwasser Formation (after the farm Oberwasser 118 in the lower Omaruru River area), while Brandt (1983, 1985) assigned this name to a calc-silicate rock in the same stratigraphic position between Henties Bay and the farm Sukses 90 (Fig. 1, inset). However, the exact stratigraphic position of the Oberwasser Formation remained unresolved due to the absence of the Chuos mixtites in these areas. Watson (1982) and Miller (1983) correlated the marble and mixed calc silicate/schist units underlying the Oberwasser schist with the Rössing and Khan Formations, respectively (Table 1). In the Karibib area, Badenhorst (1987,1992) subdivided the up to 3500 m thick sequence below the Karibib marble into three formations. Reserving the name Oberwasser for the upper schist, he named the underlying impure marble Okawayo Formation and the lower schist Spes Bona Formation. The Spes Bona schist which rests directly upon Chuos mixtites defines the stratigraphic position of the sequence in this area.

No lithostratigraphic unit corresponding to the Ober-

Table 1 Stratigraphic nomenclature and correlations of the Central Zone of the Damara Orogen

Botha 1978 (lower Omaruru River)	Klein 1980 (upper Omaruru River)	Watson 1982 (Karibib area)	Brandt 1985 (Henties Bay and Karibib areas)	Miller 1983 (summary)		Badenhorst 1992 (Karibib area)	This study		Lithology
Rietkuil Formation	Kuiseb Formation	Kuiseb Formation	Kuiseb Formation	Kuiseb Formation		Kuiseb Formation	Kuiseb Formation		schist; calc-silicate rock, marble, quartzite
Junmon and Hoopverloor Formations	Onguati Member	not developed	Karibib Formation	Onguati Member		Onguati Formation	Karibib Formation	Onguati Member	marble, calc-silicate rock, schist
	Arises River Member	Karibib Formation: Arises River Member		Arises River Member		Karibib Formation: Arises River Member		Arises River Member	calcitic marble
	Otjongeama Member	Karibib Formation: Otjongeama Member		Otjongeama Member		Karibib Formation: Otjongeama Member		Otjongeama Member	marble, calc-silicate rock
	Harmonie Member	Karibib Formation: Harmonie Member		Harmonie Member		Karibib Formation: Harmonie Member		not developed	marble, calc-silicate rock, schist
Oberwasser Formation	Chuos Formation*	Oberwasser Formation	Oberwasser Formation	Oberwasser Formation	(a)	Oberwasser Formation	Arandis Formation	Oberwasser Member	schist
Geluk Formation	Rössing Formation	Rössing Formation		Rössing Formation		Okawayo Formation		Okawayo Member	marble, schist, calc-silicate rock
Tsaun Formation	Khan Formation	Khan Formation		Khan Formation		Spes Bona Formation		Spes Bona Member	schist, calc-silicate rock
		Etusis Formation		Etusis Formation		not developed		Karub Member	marble, calc-silicate rock, schist
						Chuos Formation	Chuos Formation		mixtite, pebbly schist
					(b)	Rössing Formation	Rössing Formation		marble, quartzite, schist, calc-silicate rock
						Khan Formation	Khan Formation		calc-silicate rock, biotite schist, amphibolite
						Etusis Formation	Etusis Formation		arkosic quartzite, gneiss, biotite schist

(a) — — — Correlation after Botha, Klein, Watson, Brandt and Miller

(b)——— Correlation after Badenhorst and this study

* no correlates of the Oberwasser Formation recognized

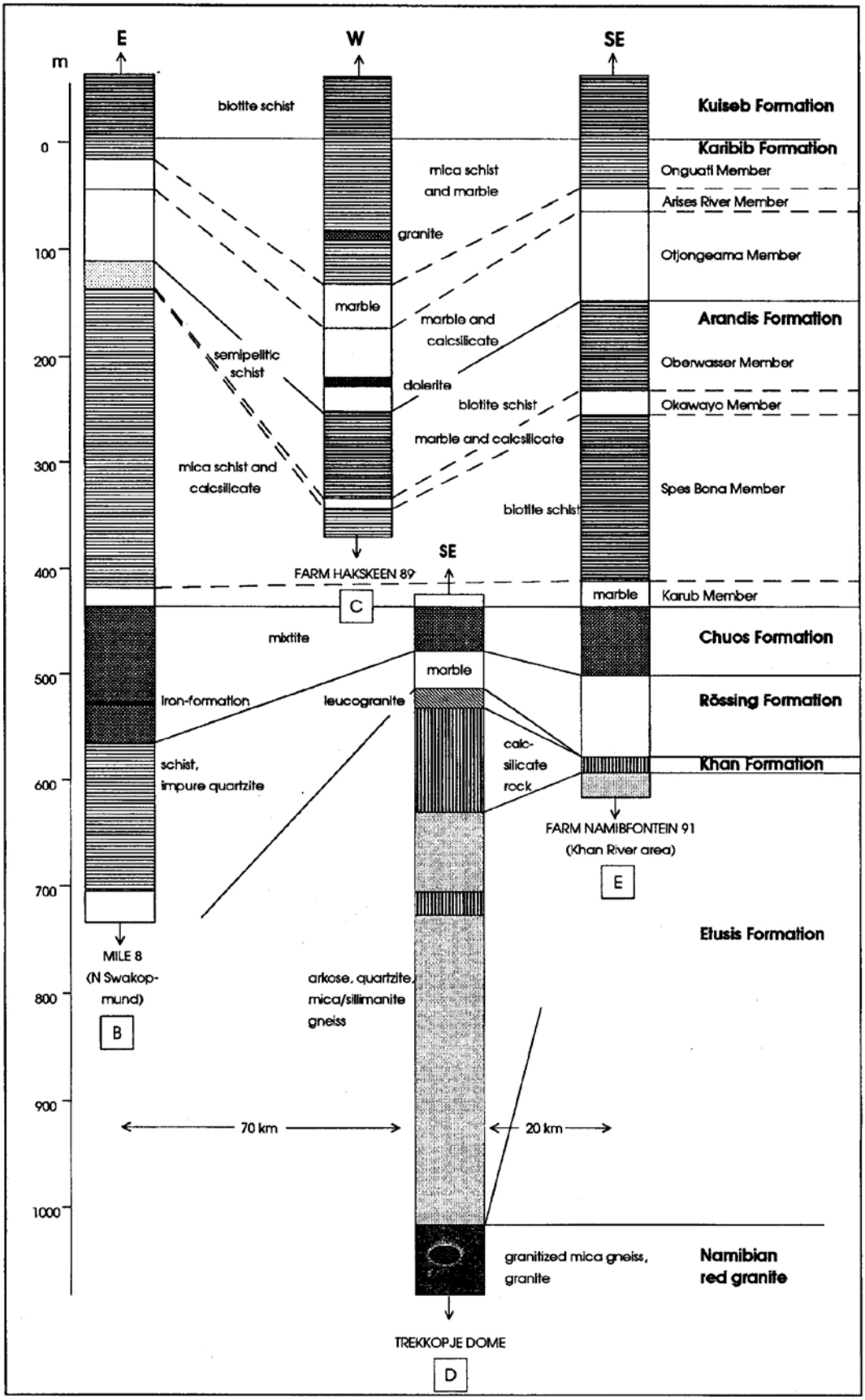

Figure 5: Lithostratigraphic profiles through the Damara Sequence between the coast and the Khan River area (profiles B, C, D and E in Fig. 1).

wasser, Okawayo and Spes Bona Formations was previously recognised in the Khan - Swakop area. In the course of the present mapping an up to 650 m thick schist, calc silicate rock and marble sequence was encountered between the lower Khan River and the coast. This horizon, which forms a conformable unit between the Chuos and the Karibib Formations, is continuous throughout the study area. It is extensively exposed south of Rössing Mountain and east of Henties Bay (Fig. 1). Due to the similarity of the rocks, identification of the lower and upper schist units, however, may be difficult in areas of intense deformation and metamorphism or poor exposure. Therefore, and because of the greatly reduced thickness of the schists and the interlayered marble in the mapping area, they are reassigned lithostratigraphic member status by the current authors, and the name Arandis Formation is introduced for the undifferentiated schist/calc-silicate rock

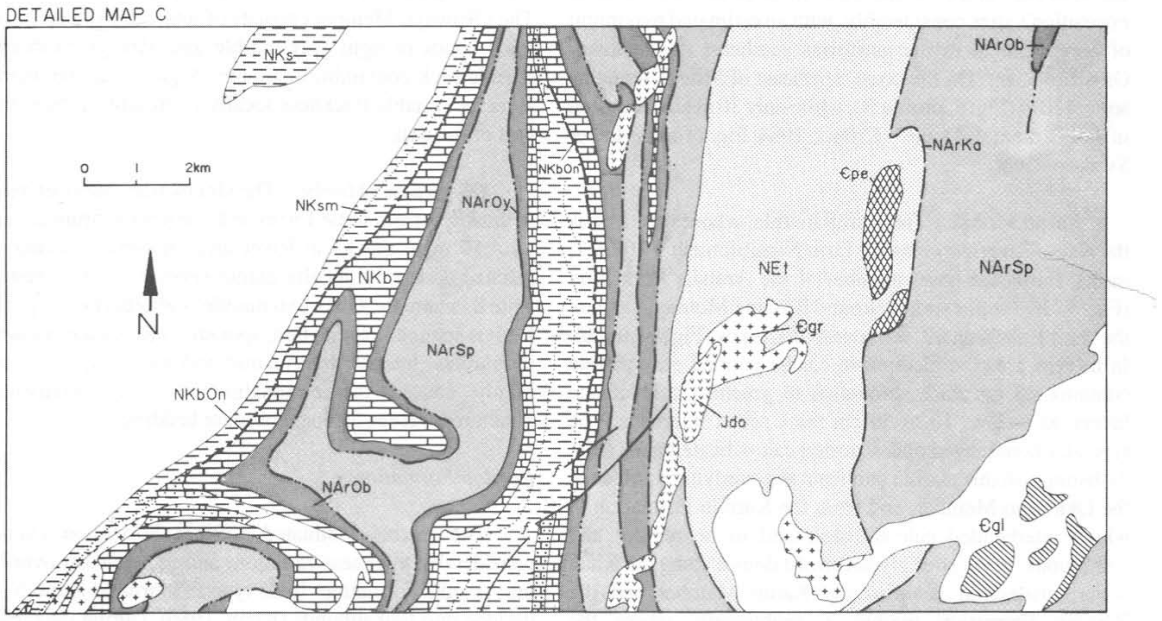

Figure 6: Detailed geological map (marked C in Fig. 1) of Farms Hakskeen 89 and Sukses 90, southwest of Usakos.

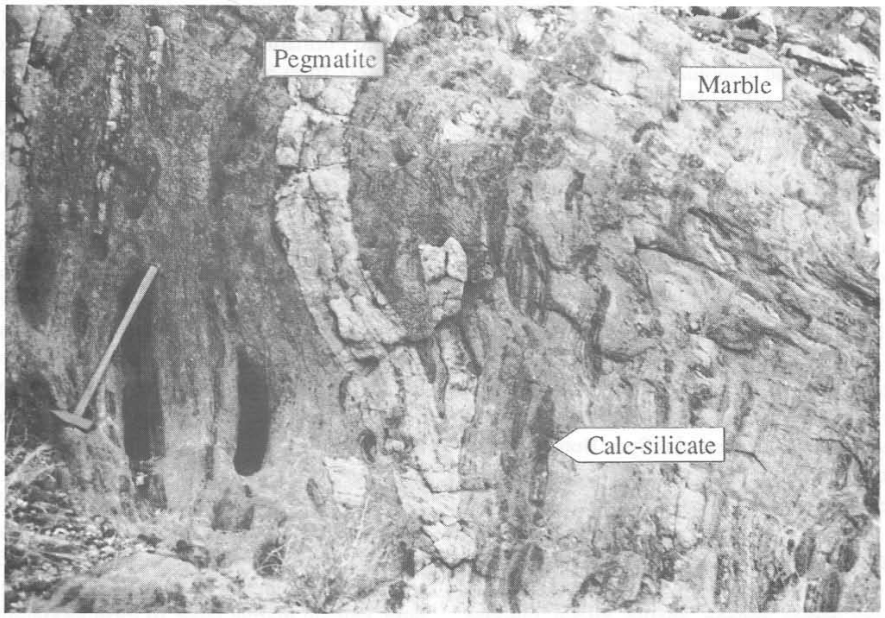

Figure 7: The Karub Member in a tributary of the Khan River: greyish marble with boudinaged calc silicate interlayers (pegmatite dyke in the centre).

sequence present between the Chuos mixtite and the Karibib marble within the tight anticlines of the Khan River area and on the sand covered plains southeast of the lower Omaruru River (Fig. 1).

The newly recognised formation is best exposed in the region centering on the town of Arandis (Fig. 1, inset). Where it is completely developed, it can be subdivided into the Oberwasser, Okawayo, Spes Bona and Karub Members. The latter underlies the Spes Bona schists between the Khan River and the Omaruru Lineament, but has not been encountered further to the east. In thickness the Arandis Formation varies considerably, with an estimated maximum of about 650 m in the antiforms southeast of the lower Omaruru River. On the coast, northeast of Mile 8, it attains some 420 m (Fig. 5, profile B), while only 30 m are measured in the "Birkenfels Dome" (Kröner, 1984; Fig. 1) on the lower Swakop River.

Karub Member The Karub marble, whose type area is the Karub River gorge on the farm Namibfontein 91 (Fig. 1, inset), forms the basal member of the Arandis Formation (Fig. 5). It is well exposed around Rössing Mountain and on the farm Hakskeen 89, southwest of Usakos (Figs. 4 and 6). In its type area the medium- to coarse-grained grey marble contains <5 cm thick, brownish to greenish calc-silicate layers, as well as 10 to 50 cm thick schist interbeds. The typically boudinaged and distorted calc-silicate bands (Fig. 7) distinguish this marble unit from the overlying marbles of the Okawayo Member, and from the Karibib Formation in which interbedded calc-silicates tend to be regular and continuous. In the strongly deformed domes along the Khan River, distinction between the Karub Member and the Rössing Formation marble is problematic where the intervening Chuos Formation is not exposed.

The Karub Member thins from 40 to 60 m near the Khan River to less than 40 m in the tight domal structures west of the Khan River. West of the railway (Fig. 1, inset) it is represented by a 2 to 5 m thick bluish, dense, skarnlike rock, which forms a narrow ridge. This calc-silicate rock contains major pyroxene, biotite and scapolite, as well as subordinate plagioclase. The upper contact of the Karub Member is gradational, with the number of schist interbeds increasing upwards.

Spes Bona Member The calc-silicate bearing schists of the Spes Bona Member dominate the Arandis Formation. They decrease in thickness from 280 m north of Swakopmund to between 30 and 120 m in the Khan River area. At Mile 8 the well preserved, dark greenish, bedded schists consist of 1 to 50 mm thick alternating biotite- and calc silicate-bearing layers, showing graded lamination only in thin section. In contrast, in the highly deformed and metamorphosed Khan River area, the Spes Bona Member comprises dark grey, foliated biotite schist (Fig. 5, profile E), resembling the overlying Oberwasser Member and Kuiseb Formation.

The biotite and calc-silicate schists of the Spes Bona Member have a granoblastic to porphyroblastic texture and contain accessory garnet, sphene, apatite, zircon, chlorite, tourmaline and carbonate. Atypical, fine- to medium-grained dark grey quartzite, present on the farms Lukasbank 63 and Usakos West 65 (Fig. 1, inset), contains scapolite and is blastoclastic to granoblastic.

Okawayo Member Separating the Oberwasser and Spes Bona Members, which are commonly lithologically indistinguishable schists due to strong deformation and metamorphism, this 2 to 25 m thick marble is an important marker horizon (Fig. 5). It forms characteristic low ridges and hogbacks, which are readily discernible on aerial photographs and satellite images. The contacts of the Okawayo Member with the underlying and overlying schist units are gradational, with 1 to 2 m thick transition zones. The Okawayo Member consists of intercalated 5 to 20 mm thick bands of light grey marble and dark greenish calc-silicate rock containing scapolite. A grey, massive marble layer of variable thickness locally is present in the central part of the unit.

Oberwasser Member The Oberwasser Member varies in thickness from some 150 m on the lower Omaruru River to 10 - 50 m in the Khan River area. It consists mainly of foliated dark grey, locally garnet-bearing biotite schist. At Mile 8, where the Okawayo marble is absent (Fig. 5, profile B), it is semipelitic with thin, sporadic calc silicate or marble interlayers. Intense deformation and metamorphism commonly caused the elimination of most sedimentary structures, except for local obscure bedding.

Karibib Formation

The marble-dominated Karibib Formation exhibits considerable thickness variations and conformably over-lies the Arandis Formation. In its type area around Karibib it is divided into four subunits (Klein, 1980). During the present mapping the Otjongeama, Arises River and Onguati Members were also recognised in the Khan - Swakop area, while the basal Harmonie Member appears to be absent.

Otjongeama Member The lower most member of the Karibib Formation present in the mapped area increases in thickness from about 40 m along the Omaruru and Khan Rivers towards the centre of the study area. In the Swakop River gorge it exceeds 200 m in thickness, whereas at Mile 8 (Fig. 5) it measures only 50 m. Within the domes and anticlines of the Khan River area this unit is represented by marble bands less than 10m thick.

The light-grey to yellowish-brown Otjongeama marble is characterised by 1 to 5 cm thick, green to dark brown calc silicate interlayers. They are commonly

continuous, but polyphase folding locally caused distortion and boudinage. The contact with the pure marble of the overlying Arises River Member tends to be sharp, except where the distinguishing calc silicate bands decrease in abundance or are absent.

Arises River Member The Arises River Member averages some tens of metres in thickness (Fig. 5), but between the Omaruru Lineament and the Omaruru River reaches 200 m locally. Due to its weathering resistance the pure, calcitic marble tends to form topographic highs. It is predominantly white to light or bluish grey, with a subordinate dark grey, sulphide-bearing variety. One to 2 mm graphite flakes locally make up as much as 5 modal percent of the light-coloured rock, imparting a speckled appearance. The marble is commonly very coarse-grained with fist-sized calcite crystals and massive, but in some outcrops a distinct regular lamination or colour-banding can be observed.

Onguati Member The Onguati Member forms the transition zone between the calcitic Karibib and the pelitic

Kuiseb Formations (Badenhorst, 1992). It consists of thinly interlayered calc-silicate and marble beds with minor schist. Commonly less than 10 m thick, it attains 100 to 150 m in the Swakop River gorge west of Goanikontes, and on the farm Hakskeen 89 (Fig. 6). A well-developed sequence of alternating calc-silicate, marble and schist is exposed in a tributary gorge of the Khan River east of the "Twin Dome" (Fig. 2).

Kuiseb Formation The youngest lithostratigraphic unit of the Damara Sequence is exposed in most synclines between the domes and anticlines of the Swakop -Khan area (Figs. 2 and 4), and underlies the sand-covered plains west of the Omaruru Lineament (Fig. 1). However, due to the poor weathering resistance of the highly deformed and metamorphosed schists good outcrops are scarce. Along the Khan River, cross-bedding and graded bedding are locally preserved, but to the west most sedimentary structures have been obliterated by deformation and metamorphism. Boudinaged calc silicate interlayers and concretions are frequent within the Kuiseb schists, and several metres thick marble interbeds occur on the farm Hakskeen 89 (Fig. 6).

The predominant dark grey quartz-biotite schists commonly contain garnet and cordierite, while local greenish-grey calc-silicate rocks carry pyroxene, scapolite, epidote, carbonate and sphene. Near the Omaruru River, the Kuiseb Formation is more feldspathic, and alternating quartz-feldspar-rich and biotite-rich layers are discernible inspite of the intense metamorphism. The feldspathic composition of the Kuiseb Formation in this area led Botha (1978) to associate it erroneously with the Nosib Group (Tsaun Formation).

Summary

During the course of the present mapping, a lithostratigraphic succession corresponding to the Oberwasser, Okawayo and Spes Bona Formations of the Karibib region has been recognised in the Khan - Swakop - lower Omaruru River area. Due to the reduced combined and individual thickness of these units (total 650 m as opposed to 3500 m around Karibib), as well as to the difficulty of distinguishing the schists of the Oberwasser and Spes Bona Formations in highly tectonised and metamorphosed or poorly exposed country, they are relegated to member status in the study area, and the name Arandis Formation is introduced for undifferentiated schists and calc-silicate rocks between the Chuos mixtite and the Karibib marbles. The name Karub Member is proposed for the marble horizon underlying the Spes Bona schist between the Khan River and the Omaruru Lineament.

Acknowledgements

The Finnish-Namibian Geological Mapping and Maps Project, within whose framework the present study was carried out, was financed by the Finnish International Development Agency (FINNIDA) and the Ministry of Mines and Energy (Namibia). Messrs. K.-H. Hoffmann and F.P. Badenhorst are thanked for introducing the authors to the field area, and P. Nex (University College Cork/Ireland) for supplying his field data from the Goanikontes area.

References

Badenhorst, F.P. 1987. Lithostratigraphy of the Damara Sequence in the Omaruru area of the Northern Central Zone of the Damara Orogen and proposed correlation across the Omaruru Lineament. *Communs. geol. Surv. N. W. Africa/Namibia*, **3**, 3-8.

Badenhorst, F.P. 1992. *The lithostratigraphy of area 2115 B and D in the Central Zone of the Damara Orogen, Namibia: with emphasis on facies changes and regional correlations*. Unpubl. M.Sc. thesis, University of Port Elizabeth, 124pp.

Botha, P.J. 1978. *Die geologie in die omgewing van die benede-Omaruru-rivier, Suidwes-Afrika*. Unpubl. M.Sc. thesis, University Orange Free State, 157pp.

Brandt, R. 1983. *1:250.000 Geological Map of the area 2214. Walvis Bay* (unpubl.). Geol. Surv. S.W. Afr./ Namibia, Windhoek.

Brandt, R. 1985. Preliminary report on the stratigraphy of the Damara Sequence and the geology and geochemistry of Damaran granites in an area between Walvis Bay and Karibib. *Communs. geol. Surv. S. W.Afr./Namibia*, **1**, 31-43.

Brandt, R. 1987. A revised stratigraphy for the Abbabis Complex in the Abbabis Inlier, Namibia. *S. Afr. J. Geol.*, **90**, 314-323.

Bunting, F.J.L. 1977. *Geology of part of the central Damara belt around the Tumas River, South West Africa*. Unpubl. M.Sc. thesis, Univ. Rhodes, 168pp.

Gevers, T.W. 1931. *The fundamental complex of western Damaraland, SWA*. Unpubl. D.Sc. thesis, Univ. Cape Town, 163 pp.

Henry, G. 1992. *The sedimentary evolution of the Damara Sequence in the lower Khan River Valley, Namibia*. Ph.D. thesis, Univ. Witwatersrand, Johannesburg (Unpubl.), 217pp.

Henry, G., Stanistreet, I.G. and Maiden, K.J. 1986. Preliminary results of a sedimentological study of the Chuos Formation in the Central Zone of the Damara Orogen: Evidence for mass flow processes and glacial activity. *Communs. geol. Surv. S.W. Africa/Namibia*, **2**, 75-92.

Jacob, R.E. 1974. Geology and metamorphic petrology of part of the Damara Orogen along the lower Swakop River, South West Africa. *Bull. Precambr. Res. Unit, Univ. Cape Town*, **17**, 201pp.

Klein, J.A 1980. *The geology of areas 2115A&B (Southeastern Damaraland), with emphasis on the structural geology*. Unpublished report. Geol. Surv. Namibia, Windhoek.

Kröner, A. 1984. Dome structures and basement reactivation in the Pan-African Damara belt of Namibia, 191-206. *In*: Kröner, A and Greiling, R. (eds.), *Precambrian tectonics illustrated*. Schweizerbarth, Stuttgart, 419pp.

Marlow, A.G. 1981. *Remobilisation and primary uranium genesis in the Damaran Orogenic Belt, Namibia*. Ph.D. thesis (unpublished), University of Leeds, 277 pp.

Miller, RMcG. 1983. The Pan-African Damara Orogen of South West Africa/Namibia. *In*: Miller, RMcG. (ed.), *Evolution of the Damara Orogen of South West Africa/Namibi*a. Spec. Publ. geol. Soc. S. Afr., **11**, 431-515.

Smith, D.A.M. 1965. The geology of the area around the Khan and Swakop Rivers in South West Africa. *Mem. geol. Surv. S. Afr. (SWA series)*, **3**, 113pp. with geol. map 1:125 000.

Watson, N.I. 1982. *Regional geology of areas 2115C and 2115DC*. Unpublished report, geol. Surv. S.W. Afr./Namibia, Windhoek, 51 pp.

*Communs geol. Surv. Namibia, **11** (1996), 83-88*

A preliminary note on a revised subdivision and regional correlation of the Otavi Group 'based on glaciogenic diamictites and associated cap dolostones

K.-H. Hoffmann[1] and A.R. Prave[2*]

[1]*Geological Survey of Namibia, P.D.Box 2168, Windhoek, Namibia*

[2]*Department of Earth and Atmospheric Sciences, The City College, City University of New York, New York, NY10031, USA*

[*]*Present address: Department of Geology, University of St Andrews, St Andrews, Fife, KY 16 9ST, Scotland*

Introduction

The Otavi Group is a thick succession of Neoproterozoic carbonates exposed within the Otavi foreland fold belt of northern Namibia (Fig. 1). It overlies predominantly coarse-grained terrigenous siliciclastic and local volcanic rocks of the Nosib Group and is overlain by fine- to coarse-grained Mulden Group siliciclastic sediments (Hedberg, 1979; Guj, 1970). Lithostratigraphic subdivision and nomenclature presently in use for the Otavi Group (Fig. 2) is based on several decades of regional mapping, mainly in the Otavi Mountainland and eastern Kaokoveld (Fig. 1), and is the classification adopted formally by the South African Committee for Stratigraphy (SACS, 1980).

A key element of this stratigraphic classification is a glaciogenic diamictite horizon, the Chuos Formation, presumed to represent a single time-stratigraphic marker separating lower Otavi (Abenab Subgroup) from upper Otavi (Tsumeb Subgroup) rocks (Fig. 2). However recent field studies along the Fransfontein Ridge flanking the southern margin of the Kamanjab Inlier and within adjoining areas of the metamorphic Damara Belt (Swakop Group) (Fig. 1) have established the presence of two, stratigraphically and lithologically distinct, glacial diamictite intervals (Hoffmann, 1994; Prave and Hoffmann, 1995). The two diamictites are each capped by unique post-glacial dolostone and occupy distinct stratigraphic positions within the Otavi Group (Prave and Hoffmann, 1995). Here we present new field data to further constrain the stratigraphic position and correlation of the two diamictites and associated cap carbonates within the Otavi fold belt and, based on this evidence, propose a substantially revised subdivision and interbasinal correlation of the Otavi Group carbonate sequence.

Fransfontein Ridge

The Fransfontein Ridge comprises a well-exposed

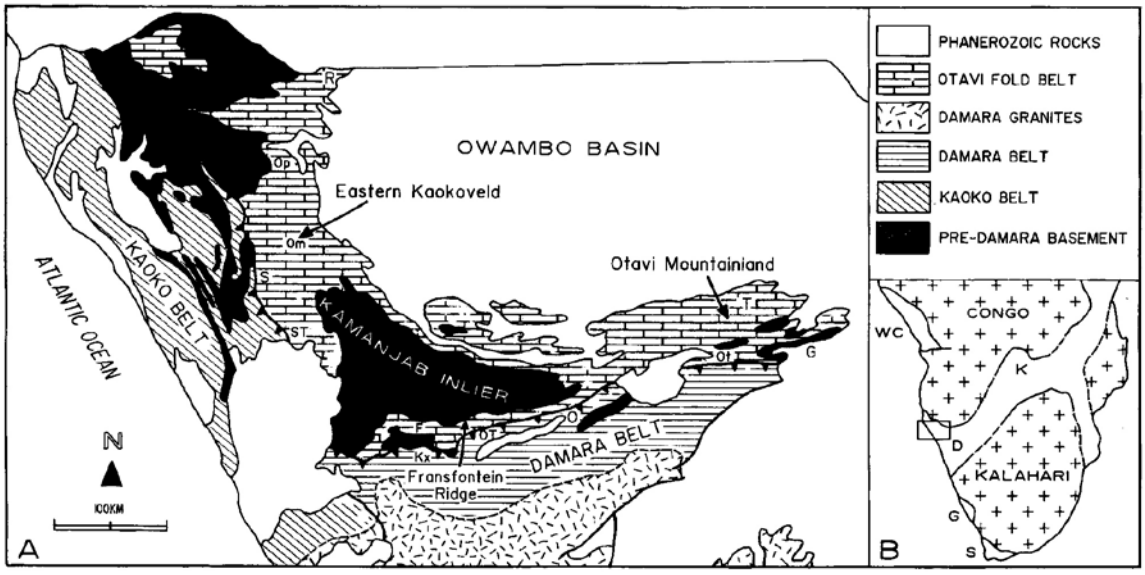

Figure 1: A. Sketch map of northern Namibia showing the distribution of the Otavi Group within the Otavi Mountainland, the north and south flanks of the Kamanjab Inlier and the eastern Kaokoveld (G - Grootfontein, T - Tsumeb, Ot - Otavi, Kx - Khorixas, F -Fransfontein, S - Sesfontein, Om - Ombambo, Op - Opuwa; OT - Outjo Thrust, ST - Sesfontein Thrust). **B.** Inset map showing Pan-African belts in central and southern Africa. D - Damara Belt, WC - West Congo Belt, G - Gariep Belt, S - Saldhania Belt, K - Katangan.

succession of Otavi Group carbonates along the southern flank of the Kamanjab Inlier between Outjo and Fransfontein village (Fig. 1). The lower diamictite occurs as locally preserved lenses, up to 80 m thick and 3.5 km in strike length, at the base of the Otavi succession on farms Malta 7 and Duurwater 66 (15 km E of Fransfontein), directly north of Fransfontein, and again on farms Bethanie 514 and Austerlitz 515 (70 km W of Fransfontein). The diamictite rests either directly on crystalline basement or, locally, on Nosib Group rocks (Fig. 3). It consists mostly of angular pebbles and boulders (up to 30 cm in diameter) of granite, gneiss, schist, quartzite and rare carbonate enclosed in a dark unsorted, iron-rich matrix. On the farm Malta, iron-formation and laminated mudstones interbedded with the diamictite contain dropstones which indicate glacial conditions of sedimentation (Prave and Hoffmann, 1995).

At the base of the Otavi carbonate succession is a prominent unit of dark grey, very finely laminated dolostone that varies from 15 to 30 m in thickness (Fig. 3). It is characterised by a complex lateral interfingering of wavy-parallel laminites, convoluted and slumped microbial laminites, and mm- to cm-thick finely graded beds. This dolostone invariably displays a sharp base where it caps the diamictite, or rests directly on Nosib Group rocks or basement. Upwards, it is conformably overlain by a heterolithic unit, 30 to 450 m thick, dominated by uniform light grey traction-bedded dolostone and subordinate variegated limestone and shale.

The upper glacial interval is composed of massive carbonate-clast diamictite developed at the base of the upper, main part of the Otavi succession (Fig. 3). It varies from a few metres up to 375 m in thickness and consists almost entirely of unsorted, highly angular clasts and blocks of dolostone and limestone in a fine-grained carbonate matrix. Previous workers inferred a non-glacial, sediment gravity-flow origin for the diamictite (Frets, 1969; Guj, 1974; Hedberg, 1979). However, the presence of well-preserved drops tones within the rare lenses of dolostone rhythmite enclosed by the diamictite and in a 5 to 10m thick interval of bedded dolostone present locally at the top of the diamictite, is unequivocal evidence of ice-rafting and, hence, glaciomarine sedimentation (Prave and Hoffmann, 1995). The diamictite pinches out on the western part of farm Kranspoort, about 30 km east of Fransfontein, and with the exception of a few local occurrences noted by Guj (1974), appears to be mostly absent eastward as far as Outjo. It is present in most places along the western extension of the Fransfontein Ridge and in the Bethanie area west of Khorixas (Frets, 1969).

The carbonate-clast diamictite is capped by a thin (3-25 m) light grey to cream or pink, laminated and slumped dolostone (Fig. 3). The basal contact defines a sharp, transgressive (flooding) surface whereas at the top it passes gradationally into a limestone-dolostone rhythmite unit, typically 30 to 50 m in thickness. The remainder of the succession consists mainly of light grey medium-bedded to laminated dolostone, with minor limestone rhythmites and shales, up to 1200 m in total thickness.

Together with the overlying limestone-dolostone rhythmite interval, the cap dolostone makes an excellent, continuous marker bed. Where the diamictite is present, the cap dolostone averages only a few metres in thickness and typically consists of the characteristic thinly bedded to laminated or slumped, cream or pink lithofacies. Where the diamictite is absent, or very thin and impersistent (such as at Bothashof, 35 km east of Fransfontein), the cap is thicker, by as much as 25 m, and grades laterally into a light-grey dolostone which contains enigmatic, but highly distinctive, subvertical tubular structures (from a few centimetres to

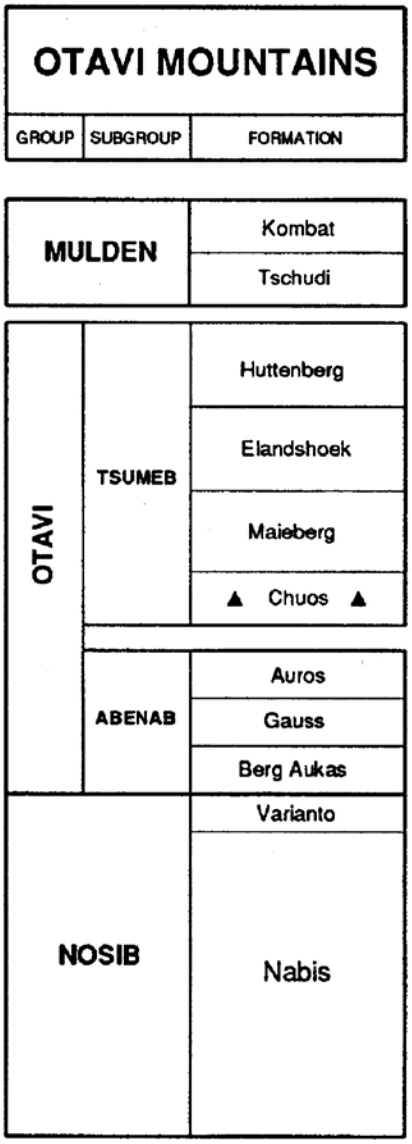

Figure 2: Lithostratigraphic subdivision and nomenclature of the Otavi Group in the Otavi Mountainland, after the South African Committee for Stratigraphy (SACS, 1980).

several decimetres in length and up to 15 mm in diameter) filled with quartz and dolomite spar. On detailed 1:25 000 scale exploration company maps of an area half-way between Fransfontein and Outjo (Thirion, 1969), this unit has been equated with a lithologically identical dolomite marker bed, "the quartz-cluster dolomite", at the top of the Abenab Subgroup in the Otavi Mountains.

Otavi Mountainland

In the Otavi Mountainland, the lower glacial interval is represented by local "diamictite and associated iron-formation of the upper Nosib Varianto Formation (Figs. 2 and 3). The diamictite attains a maximum thickness of 130 m where it unconformably overlies Nabis Formation (lower Nosib Group) feldspathic quartzite and conglomerate in the central and western Otavi Mountainland, but is absent in the southern and eastern Otavi Mountains. It consists of massive or crudely stratified diamictite containing dispersed, rounded, pebble- to boulder-sized basement clasts derived from the unconformably underlying Nabis Formation. The matrix is typically dark, feldspathic to iron-rich muddy sandstone. Lenticular intervals of laminated iron-formation have been observed to contain isolated drops tones

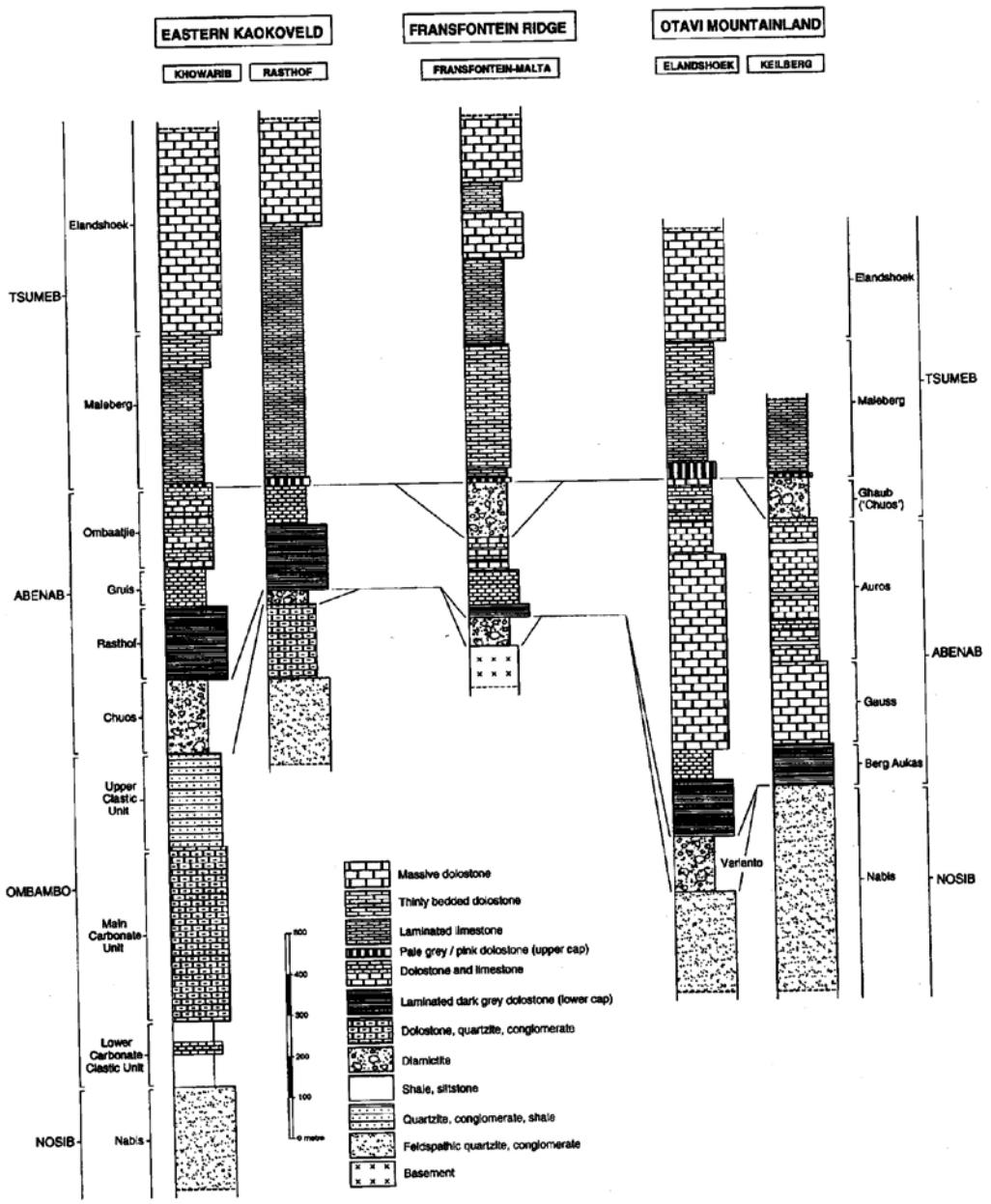

Figure 3: Generalised composite stratigraphic sections of the lower to middle Otavi Group in parts of eastern Kaokoveld, the south flank of Kamanjab Inlier and the Otavi Mountainland. Sections compiled from Hedberg (1979); Beukes (1986); King (1994); A.R. Prave and K.H. Hoffmann (unpubl. data); P.F. Hoffman (pers. comm. 1995).

and provide clear evidence for a glacial origin of the diamictite.

The overlying Abenab Subgroup consists upward of the Berg Aukas, Gauss and Auros Formations (Figs. 2 and 3). The base of this subgroup is a sharp, unconformable contact above which follows medium grey, very finely parallel laminated and mm-thick graded dolostone. This dolostone shows widespread small-scale convolute bedding and slumping, identical to the dark laminated basal dolomite of the Otavi succession along the Fransfontein Ridge. The upper part of the Berg Aukas and the overlying Gauss and Auros Formations amount to as much as 730 m in thickness and comprise a succession of shoaling cycles made up of grey traction-bedded dolostone, microbial laminites and stromatolitic and oolitic beds (Beukes, 1986; King, 1994).

The upper glacial interval recognised in the Otavi Mountains is the 'Otavi tillite', or 'Chuos Formation' (Fig. 2), which marks the base of the upper Otavi Tsumeb Subgroup. A maximum thickness of approximately 2000 m has been reported from the western and southern Otavi Mountainlands (Grobler, 1961), whereas it is thin or absent in most of the eastern Otavi Mountains. It consists of variously shaped, mixed carbonate and basement clasts in an orange-brown weathering carbonate-rich (dolarenitic to micritic) matrix.

A sharp transgressive surface separates the diamictite from a light coloured dolostone unit at the base of the overlying Maieberg Formation (Fig. 3). The basal dolostone displays the same lateral facies change as the thin dolostone which caps the carbonate diamictite along the Fransfontein Ridge. Where the diamictite is present, the dolostone is buff- to pink-coloured, thinly bedded to laminated and locally slumped, on average a few metres in thickness (e.g. Keilberg section in Fig. 3). In areas where the diamictite is absent (e.g Elandshoek section in Fig. 3), it is up to 40 metres thick, takes on a generally light grey colour and contains the same quartz-dolomite filled tubular structures observed on Bothashof near Fransfontein. Field evidence reveals that this unit is equivalent to a regional marker known as the 'quartz-cluster dolomite' and included as the uppermost unit in the Auros Formation of the upper Abenab Subgroup (SACS, 1980; Beukes, 1986; King, 1994). This unit was described in detail by Hegenberger (1987) who interpreted the tube structures as possible gas- or fluid-escape features.

The remainder of the Maieberg Formation comprises several hundred metres of uniform limestone-marl rhythmite passing upward into thinly bedded and

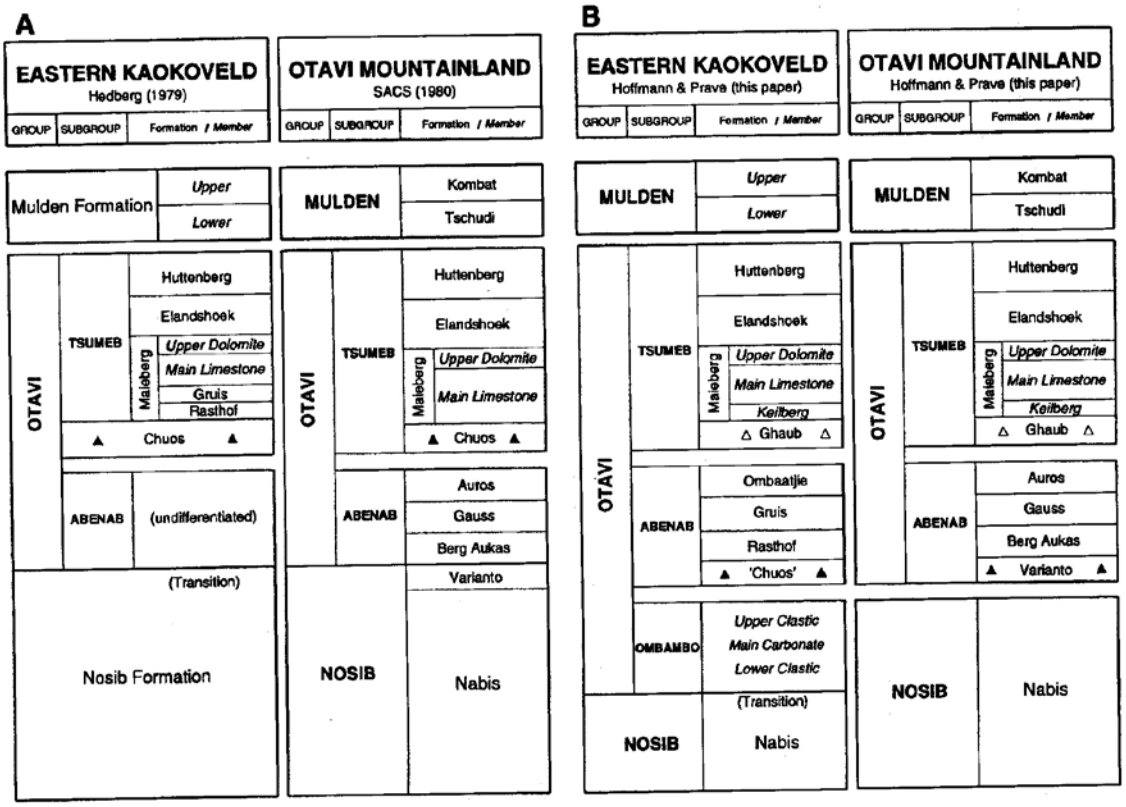

Figure 4: A. Lithostratigraphic subdivision and correlation of the Otavi Group in the Otavi Mountainland and the eastern Kaokoveld by SACS (1980) and Hedberg (1979). Two additional informal units of the Maieberg Formation in the Kaokoveld by Hedberg (1979), the local arkosic carbonate member and the arenaceous member, have been omitted for clarity. **B.** Proposed new lithostratigraphic subdivision and correlation of the Otavi Group.

laminated dolostone (Fig. 3). These are overlain by the monotonous succession of grey, traction-bedded, commonly cherty and stromatolitic, dolostones of the Elandshoek and Huttenberg Formations.

Eastern Kaokoveld

In the eastern Kaokoveld, the lower glacial interval is represented by the thick (up to several hundred metres) and laterally continuous diamictite (Fig. 3) mapped as 'Chuos Formation' by Guj (1970), Hedberg (1979) and Hoffman *et al.* (1994) (Fig. 4A). In contrast, the upper glacial interval is only very locally present, in the form of thin lenses (generally less than a few metres) recognised only recently through detailed mapping (P.F. Hoffman, A.R. Prave and Hu Guowei - unpublished data).

The lower interval ('Chuos') is made up of massive to crudely stratified diamictite with clasts (up to several metres in size) derived from older carbonate rocks and basement, set in a typically iron-rich matrix. It unconformably overlies lower Otavi Group strata consisting of carbonates and fine to coarse grained siliciclastics. A total thickness in excess of 2000 m is present in the Ombambo area south of Opuwa (Hedberg, 1979). This sequence follows conformably on Nosib Group quartzites (up to 1250 m thick) with no evidence for an intervening unconformity (Guj, 1970; Hedberg, 1979; Hoffman *et al.*, 1974). Based on mapping by P.P. Hoffman, Hu Guowei and one of the present authors (ARP), it consists of a lower fine-grained clastic-carbonate unit, a middle or main carbonate unit of mainly well-bedded dolostone and minor limestone, and an upper clastic unit (Fig. 3).

Resting with an invariably sharp contact on the lower diamictite is a dark grey, finely flat -laminated dolostone, less than two metres thick, and up to 200 m of slumped, microbial laminated, and traction-bedded dark to medium grey dolostone (Fig. 3). This unit, named the Rasthof Member and included by Hedberg (1979) as a local facies unit in the Maieberg Formation (Fig. 4A), is a continuous marker horizon throughout the eastern Kaokoveld. However, in contrast to Hedberg (1979), we regard this unit as identical to the finely laminated dark basal dolostone of the Berg Aukas Formation and the basal Otavi Group in the Fransfontein Ridge.

Above the Rasthof Member, the Gruis Member (Fig. 3) consists of very light-coloured (buff and pink) laminated and medium bedded, cherty dolostones, up to several tens of metres in thickness (Hedberg, 1979). In the Khowarib area, the Gruis Member is followed by grey to dark grey, laminated to nodular limestone and traction-bedded dolostone and limestone, up to 200 m thick, named the Ombaatjie Member by P.P. Hoffman (*pers. comm.* 1995).

A thin (typically less than several tens of metres) laminated, buff-coloured cap dolostone with abundant quartz-dolomite filled tubular structures sharply overlies the Ombaatjie Member and patchily preserved, thin (upper) diamictite lenses. The cap dolostone is the stratigraphic equivalent of the light-coloured, pink, laminated and grey tubular (or 'quartz-cluster') dolostone described above from the Fransfontein Ridge and the Otavi Mountainland. It passes upwards into pink and grey limestone laminites and rhythmites, and thinly bedded dolostones, of the main and upper Maieberg Formation respectively. These are followed by the thick dolostone succession of the Elandshoek Formation.

Proposed stratigraphic revision of the Otavi Group

Two distinct stratigraphic couplets, each consisting of diamictite and cap dolostone, are recognised throughout the Otavi foreland in northern Namibia. The lower couplet consists of iron-rich diamictite, dominated by basement-derived clasts, sharply overlain by dark grey, finely laminated dolostone. The upper couplet is a carbonate-matrix diamictite, dominated by carbonate clasts, sharply overlain by light-coloured carbonate that changes laterally from thin buff or pink, laminated and slumped, dolostone to thicker light grey dolomite characterised by quartz-dolomite filled tubular structures. Both the lower and upper diamictite vary greatly in thickness and are absent from large areas. In contrast, the cap dolostones both define regionally persistent stratigraphic markers recognizable throughout the Otavi fold belt. Furthermore, stable isotope studies in progress have revealed that the two cap units have distinct carbon isotope signatures (Kaufman *et al.*, 1996; A.R. Prave and M.J.Kennedy, unpublished data)

Correlation of the two diamictites and associated cap dolostone units presented here requires a substantially revised lithostratigraphic subdivision and correlation of lower and middle Otavi Group units, as follows:

1. The local Varianto Formation of the Otavi Mountainland, previously included in the upper Nosib Group (Fig. 4A), is stratigraphically equivalent to the thick and regionally extensive, main diamictite mapped in the past as 'Chuos Formation' in the eastern Kaokoveld (Fig. 4B). Both units are separated from underlying rocks by a regional unconformity and should therefore be included in the lower Otavi Abenab Subgroup.
2. Dark grey, finely laminated cap dolostone of the basal Berg Aukas Formation is lithologically correlative to the Rasthof cap dolostone in the eastern Kaokoveld (Fig. 4B). This implies that the Rasthof and Gruis Members (including the newly defined Ombaatjie Member of P.F. Hoffman, *pers. comm.* 1995), which Hedberg (1979) interpreted as local facies members of the lower Maieberg Formation (Fig. 4A), are in fact stratigraphic equivalents of the Abenab Subgroup.
3. The thick succession of mixed carbonates and siliciclastics, which follows conformably on

Nosib Group rocks in eastern Kaokoveld and which has been traditionally correlated with the Abenab Subgroup in the Otavi Mountainland (Fig. 4A), is an entirely older marine carbonate sequence for which the name Ombambo Subgroup is proposed (Fig. 4B). Rocks equivalent to the Ombambo Subgroup appear to be entirely absent from both the northern and southern flanks of the Kamanjab Inlier, as well as from the Otavi Mountainland.

4. The well-known carbonate clast-rich diamictite, the 'Otavi tillite' - or Chuos Formation in the nomenclature of SACS (1980) and other stratigraphers (Fig. 4A) developed at the base of the Tsumeb Subgroup in the Otavi Mountains and along the Fransfontein Ridge, is renamed the Ghaub Formation (Fig. 4B) after the farm Ghaub 47 near the area from which it was first described by Le Roex (1941). It is absent, with few local exceptions, throughout most of the eastern Kaokoveld.
5. The Maieberg Formation of the lower Tsumeb Subgroup comprises three units, consisting of the basal light grey to buff or pink cap dolostone overlying the Ghaub Formation, a main limestone member and an upper dolomite member (Fig. 4B). The name 'Keilberg Member' is proposed for the basal Maieberg Formation cap dolostone which incorporates the so-called 'quartz-cluster dolomite' formerly mapped as part of the uppermost Auros Formation.

Acknowledgements

We thank P.F. Hoffman and M.J. Kennedy for discussions in the field. Bridget Allison and Simon Cloete are thanked for help with preparation of the diagrams. Critical comments by N.J. Beukes, P.B. Groenewald and W. Hegenberger helped to improve the manuscript. Support for A.R.P. through a National Science Foundation grant (No. EAR-9406586) is acknowledged.

References

Beukes, N.J. 1986. *A field introduction to the geology of the Otavi Mountainland, northern Namibia. Workshop on Precambrian carbonate sedimentology*. Tsumeb Corp. Ltd., Tsumeb, 30 pp.

Frets, D.C. 1969. Geology and strncture of the Huab-Welwitschia area, South West Africa. *Bull. Precambr. Res. Unit, Univ. Cape Town*, **5**, 235 pp.

Grobler, N.J. 1961. *The geology of the. western Otavi Mountainland, South West Africa.* M.Sc. thesis (unpubl.), Univ. Orange Free State, 199 pp.

Guj, P. 1970. The Damara mobile belt in the south-western Kaokoveld, South West Africa. *Bull. Precambr. Res. Unit, Univ. Cape Town*, **18**, 168 pp.

Guj, P. 1974. A revision of the Damara stratigraphy along the southern margin of the Kamanjab inlier, South West Africa. *Bull. Precambr. Res. Unit, Univ. Cape Town*, **15**, 167-176.

Hedberg, R.M. 1979. Stratigraphy of the Ovamboland Basin, South West Africa. *Bull. Precambr. Res. Unit, Univ. Cape Town*, **24**, 325 pp.

Hegenberger, W. 1987. Gas escape structures in Precambrian peritidal carbonate rocks. *Communs. geol. Surv. S.W. Afr./Namibia*, **3**, 49-55.

Hoffmann, K.H. 1994. New constraints on the timing of continental breakup and collision in the Damara belt. Abstr. vol., *Proterozoic Crustal and Metallogenic Evolution*. Geol. Soc. and Geol. Surv. of Namibia, Windhoek, p.30.

Hoffman, P.F., Swart, R., Freyer, E.E. and Hu Guowei. 1994. Damara orogen of northwest Namibia. *Excursion 1, Proterozoic Crustal and Metallogenic Evolution*. Geol. Soc. and Geol. Surv. of Namibia, Windhoek, 55 pp.

Kaufman, A.J., Hoffman, P.P. and Bowring, S.A 1996. The carbon isotopic record of Neoproterozoic glaciations in continuous carbonate sequences, Otavi Group, Namibia. *Geol. Soc. Am., Abstracts with Program*, **28**, 219.

King, C.H.M. 1994. Carbonates and mineral deposits of the Otavi Mountainland. *Excursion 4. Proterozoic Crustal and Metallogenic Evolution*. Geol. Soc. and Geol. Surv. of Namibia, Windhoek, 40 pp.

Le Roex, H.D. 1941. A tillite in the Otavi mountains, S.W.A. *Trans. geol. Soc. S. Afr.*, **44**, 207-218.

Prave, A.R and Hoffmann, K.H. 1995. Unequivocal evidence for two Neoproterozoic glaciations in the Damara succession of Namibia. *Geol. Soc. Am., Abstr. with Program*, **27**, 380.

South African Committee for Stratigraphy (SACS). 1980. Stratigraphy of South Africa. Kent, L.E., (Comp.); Part 1. Lithostratigraphy of the Republic of South Africa, South West Africa/Namibia, and the Republics of Bophutatswana, Transkei and Venda. *Handb. geol. Surv. S. Afr.*, **8**, 690 pp.

Thirion, N.C. 1969. *Geological map of the area west of Ouijo, scale 1:25 000*. Unpubl. grant report M46/3/130, Tsumeb Corporation Ltd., 10 pp.

COMMUNICATIONS OF THE GEOLOGICAL SURVEY OF NAMIBIA

GUIDELINES FOR CONTRIBUTORS

The main purpose of Communications is to provide a means for the rapid dissemination of information gathered by Geological Survey personnel and Survey funded researchers. Communications is published annually and distributed to institutions and universities worldwide. It is also available for sale to mining companies and the public.

General

1. Manuscripts should preferably be written in English.

2. Papers and reports should be limited to a maximum of 5 000 words. A short abstract, of less than 200 words, should be provided.

3. Short geological notes, not exceeding 1000 words, may also be submitted. Notes do not require an abstract.

4. **Three copies** (original and two photocopies) of the manuscript, including Tables, Figures and Figure captions, should be provided. The text should be typed using double or one-and-a-half spacing, on A4 paper, with wide margms.

5. The entire manuscript should be paginated starting with the title page and indent the first line of each para-graph.

6. Papers will be reviewed by both internal and external referees; reports will be reviewed by internal referees. In addition to this, manuscripts from Survey funded students should be critically reviewed by their supervisors before submission. It is the responsibility of the supervisor, not the referees, to ensure that a high standard is maintained.

7. Final submissions of refereed manuscripts should be in the form of a single good quality printout in a non-proportional font (e.g. Courier) **and** accompanied by text files on 5.25- or 3.5-inch (low/high density) computer disks (see details below).

8. Galley proofs will be sent to authors for final checking. Authors should restrict changes to correcting of printer's errors. The corrected galley proofs, marked in **blue** (typographical errors) and **red** (author's errors), must be returned to the Geological Survey within **10 days** of receipt.

Text

1. A recent issue of Communications should be consulted for the general style and format to be adopted. Useful information may also be obtained from "Guide to the Preparation of Papers for Publication by the Geological Society of South Africa", *Trans. geol. Soc. S. Afr.*

2. The format and sequence of headings are as follows:

   a. Bold upper and lower case, centred.

   b. Free-standing italics, centred.

   c. Italics, above the line and at the margin.

   d. Italics, indented in the line.

If further subdivision is needed, numerals or letters of the alphabet (lower case) should be used.

3. Only words to be set in italics should be underlined. No material should be typewritten in italics unless also submitted as a text file (see point 5).

4. An alphabetical list of all references should follow the text, with a format as follows:

Gevers, T.W. and Frommurze, H.F. 1929. The tin-bearing pegmatites of the Erongo Area, South-West Africa. *Trans. geol. Soc. S. Afr*., **32**, 111-149.

Blignault, H.J. 1977. *Structural-metamorphic imprint on part of the Namaqua Mobile Belt in South West Africa*. Ph.D. thesis (unpubl.), Univ. Cape Town, 197 pp.

"Guide to the preparation of Papers for Publication by the Geological Society of South Africa" provides a list of preferred abbreviations for names of periodicals, otherwise give the periodical name in full.

5. Text files may be written in any format that can be read by **Xerox Ventura Publisher** (version 2) software, namely **ASCII** (including 8-bit ASCII), **Wordstar** (versions 3.3, 3.4,4.0,5.0), **WS** (versions 4.0, 5.0), **MS-Word** (versions 3.1, 4.0), **WordPerfect** (versions 4.1, 4.2 and 5.0), **XyWrite** (std II and III files), **Xerox Writer** (version 2.0), **Multimate** (version 3.31), and **DCA**.

Illustrations

1. Captions to Figures should be provided as a separate list. All illustrations and photographs are termed Figures, and are referred to as Fig. or Figs in the text.

2. Headings for Tables should appear above the Table.

3. Originals (or high quality copies) of diagrams are required, drafted in black pen on tracing film. A bar scale should be included where necessary and all lettering must be a minimum height of 1 mm after reduction. Glossy black and white photographs only can be accepted.

4. Diagrams and photographs will be printed to either single column (8 cm) or double column (16.5 cm) width. They should therefore be provided at this size, or of dimensions which can be conveniently reduced to the correct size. Maps should be either A4 or A3 size.

5. Figure numbers and author's name should be printed in pencil on the back of all Figures.

6. Location of Figures and Tables in the text should be indicated in pencil in the left hand margin.

7. All illustrations should be given separately, not pasted on pages.

8. Illustrations (except photographs) may, in addition, be submitted in one or more of the following industry standard graphics formats: GEM, CGM, DXF, HPGL, Lotus 1-2-3 (PIC), Macintosh PICT, Macintosh Paint, PC Paintbrush (PCX), Postscript (EPS), TIFF, Video Show, and MS-Windows. For technical reasons it is important that good quality hard copies be included of all graphics.

COMMUNICATIONS OF THE GEOLOGICAL SURVEY OF NAMIBIA

VOLUME 11 **CONTENTS** **1996**

RESEARCH PAPERS

REPORT

NOTE